
Physiological, molecular and biochemical
characterization of rodent extraocular muscles:
Implications for Duchenne Muscular Dystrophy

I n a u g u r a l d i s s e r t a t i o n

zur

Erlangung des akademischen Grades eines

Doktors der Naturwissenschaften

der

Mathematisch-Naturwissenschaftlichen Fakultät

der

Ernst-Moritz-Arndt-Universität Greifswald

vorgelegt von

Ulrike Zeiger

geboren am 11. März 1977

in Erlangen

Greifswald, 04. Mai 2011

Dekan: Prof. Dr. Klaus Fesser

1. Gutachter: Prof. Dr. H. Brinkmeier (Institut für Pathophysiologie, Universität Greifswald)
2. Gutachter: Prof. Dr. R. Wiesner (Institut für vegetative Physiologie, Universität Köln)

Tag der Promotion: 4. Oktober 2011

TABLE OF CONTENTS

ABBREVIATIONS.....	7
1. INTRODUCTION.....	11
1.1 The Extraocular Muscles (EOMs).....	11
1.2 Duchenne muscular dystrophy (DMD).....	18
1.2.1 Clinical & molecular background of DMD	18
1.2.2 Pathogenesis of DMD	20
1.4 Calcium homeostasis in normal and dystrophic muscle	23
1.4.1 Excitation-contraction (E-C) coupling.....	23
1.4.2 Store-operated calcium entry: role of TRP channels, Orai and STIM.....	25
1.4.2.1 The TRP superfamily of cation channels.....	25
1.4.2.2 Orai and STIM proteins	28
1.4.3 Dysregulated calcium homeostasis in DMD.....	29
1.3 Potential sparing mechanisms in EOM.....	31
1.4 Aim of the study	34
2. MATERIALS AND METHODS	35
2.1 Materials	35
2.1.1 Chemicals.....	35
2.1.2 Reagents.....	36
2.1.2 Consumables	38
2.1.3 Equipment & Devices.....	39
2.1.4 Animals	40
2.1.5 Solutions and buffers for SDS-Page and Western blotting.....	40
2.1.7 Solutions for immunohisto- and cytochemistry	42
2.1.8 Primary antibodies	43
2.1.9 Secondary antibodies and nucleic acid (nuclear) stain	43
2.1.10 Solutions for cell culture of primary myoblasts.....	43
2.1.11 Solutions for calcium imaging	44

2.1.12 Molecular biology kits & reagents.....	45
2.1.12.1 Molecular biology kits	45
2.1.12.2 Reverse Transcription (RT) reaction mixes.....	45
2.1.12.3 Primers and Probes	47
2.1.12.4 SYBR Green reaction	49
2.1.12.5 TaqMan reaction	49
2.1.13 Software and Databases.....	53
2.2 Methods.....	54
2.2.1 Tissue dissection	54
2.2.2 Tissue preservation	55
2.2.3 Western blotting.....	55
2.2.3.1 Sample preparation for Western blotting.....	56
2.2.3.2 Determination of protein concentration	56
2.2.3.3 SDS Page electrophoresis	57
2.2.3.4 Protein transfer (blotting).....	58
2.2.3.5 Protein detection	59
2.2.3.6 Stripping of blot membranes.....	60
2.2.3.7 Protein quantification using densitometry	61
2.2.4 Immunohisto- and cytochemistry	61
2.2.4.1 Preparation of cryosections.....	61
2.2.4.2 Staining of cryosections.....	61
2.2.4.3 Staining of cultured myoblasts and myotubes	62
2.2.4.4 Mounting of slides	62
2.2.5 Cell culture.....	63
2.2.5.1 Acid washed cover slips	63
2.2.5.2 Collagen I-coated cell culture dishes	63
2.2.5.3 Isolation of myoblasts.....	63
2.2.5.4 Culture of primary myoblasts	64
2.2.5 Intracellular calcium measurements (calcium imaging).....	64
2.2.6.1 Calcium imaging in myotubes	64
2.2.6.2 Analysis of calcium imaging experiments.....	65

2.2.7 RNA isolation and quantification	65
2.2.8 Reverse transcription	66
2.2.9 Quantitative PCR (qPCR).....	67
2.2.9.1 SYBR Green based qPCR.....	68
2.2.9.2 Primer design for SYBR Green qPCR.....	68
2.2.9.3 SYBR Green qPCR analysis: deltadelta Ct-method	69
2.2.9.4 TaqMan Assay based qPCR	69
2.2.9.5 TaqMan Assay analysis: absolute quantification	70
2.2.10 Statistical analyses	70
3. RESULTS	71
3.1 Calcium handling properties in rat EOM	71
3.1.1 Expression of myogenic markers in EOM myotubes	71
3.1.2 Calcium buffering in EOM and TA myotubes	73
3.1.3 mRNA expression levels of calcium handling proteins in EOM.....	76
3.1.4 Protein expression of calcium handling proteins in EOM.....	79
3.1.5 Immunohistochemistry of calcium handling proteins.....	83
3.2 Molecular components of the calcium homeostasis in normal and mdx mouse EOM	85
3.2.1 Protein expression of calcium handling proteins.....	85
3.2.2 Expression of TRP channel proteins in EOMs	88
3.2.2.1 mRNA expression of TRPC channels	88
3.2.2.2 Protein expression of TRPC1 and TRPC3.....	89
3.2.2.3 mRNA expression of TRPV channels	90
3.2.2.4 Protein expression of TRPV4	90
3.2.2.5 mRNA expression of TRPM channels.....	91
3.2.3 Expression of Orai1 and STIM1	93
3.2.3.1 mRNA expression of Orai1 and Stim1	93
3.2.3.2 Protein expression of Orai1 and STIM1	93
4. DISCUSSION	95
4.1 Calcium buffering in rat EOM	95

4.2 Calcium buffering in mouse EOM 99

4.3 Model of the superior calcium homeostasis in EOM..... 100

4.3 Expression of TRP channels, Orai and STIM in normal mouse muscle including EOM 101

4.4 Expression of calcium handling proteins and channels in mdx muscle: Implications for DMD 107

4.5 Therapeutic interventions targeting calcium homeostasis in DMD 111

5. SUMMARY 114

6. REFERENCES..... 116

ACKNOWLEDGEMENTS 138

Abbreviations

~	about
#	number
10 x	10 times concentrated solution
1 x	normal strength solution
ATPase	adenosine triphosphatase
AU	arbitrary units
Bp	base pair
Ca ²⁺	calcium
CaCl ₂	calcium chloride
CALM	calmodulin
CAMKII	Ca ²⁺ /calmodulin dependent kinase II
CASQ	calsequestrin
Cat#	catalog number
cDNA	complementary DNA
DHPR	dihydropyridine receptor
DI water	deionized water
DMEM	Dulbecco's Modified Eagle Medium
DNA	desoxyribonucleic acid
DTT	dithiotreitol
E-C	excitation-contraction
ECL	enhanced chemiluminescence
EDTA	ethylenediaminetetraacetic acid
EGTA	ethylene glycol tetraacetic acid
EOM	extraocular muscle

ER	endoplasmatic reticulum
FBS	fetal bovine serum
FGF	fibroblast growth factor
FW	forward
GAPDH	Glyceraldehyde 3-phosphate dehydrogenase
h	hour
H ₂ O	water
HCl	hydro chloric acid
HEPES	4-(2-hydroxyethyl)-1-piperazineethanesulfonic acid
HRP	horse radish peroxidase
IgG	immunoglobulin G
kDa	kiloDalton
M	Molar (mol/l)
mg	milligram
µg	microgram
µl	microliter
µM	micromolar (µmol/l)
Milli-Q water	ultrapure laboratory grade water
min	minute
miRNA	microRNA
ml	milliliter
mm	millimeter
mM	millimolar (mmol/l)
mRNA	messenger RNA
Na ⁺	sodium
NaCl	sodium chloride

nM	nanomolar (nmol/l)
NCX1/Slc8a1	sodium-calcium exchanger
nm	nanometer
NTC	non-template control
°C	degrees Celsius
oN	over night
PARV	parvalbumin
PBS	phosphate buffered saline
Pen/Strep	Penicillin/Streptomycin
PKA	protein kinase A
PLN	phospholamban
PMCA	plasmamembrane Ca ²⁺ ATPase
PVDF	polyvinylidene fluoride
qPCR	quantitative polymerase chain reaction
RGN	regucalcin
RNA	ribonucleic acid
ROS	reactive oxygen species
rpm	revolutions per minute
RT	reverse transcription
RV	reverse
RYR	ryanodine receptor
s	second or seconds
SD	standard deviation
SEM	standard error of the mean
SDS	sodium dodecyl sulfate
SERCA	sarcoplasmic reticulum Ca ²⁺ ATPase

SLN	sarcolipin
SR	sarcoplasmic reticulum
SRL	sarcalumenin
STIM	stromal interaction molecule
Std	standard
SOCE	store-operated Ca ²⁺ entry
TA	tibialis anterior
TBS	Tris buffered saline
TBST	Tris buffered saline Tween
temp.	temperature
TIF(F)	tagged image file format
TNNC	troponin C
TRP	transient receptor potential

1. Introduction

1.1 The Extraocular Muscles (EOMs)

The EOMs are responsible for the eye movements. They are fundamentally distinct from other skeletal muscle, which is reflected on many levels, such as functionality, anatomy as well as in their molecular make-up. The EOMs have even been termed as having a unique muscle allotype or muscle class (Hoh and Hughes, 1988; Hoh, 1989). The currently recognized allotypes are limb/diaphragm, masticatory and extraocular muscles (Hoh, 1989; Porter and Baker, 1996). These allotypes share some traits of skeletal muscle, but differ from one another in numerous important aspects that relate to their unique functions.

The EOMs are comprised of six muscles arranged around the eyeball in three functional pairs of agonist and antagonist to perform the voluntary and reflex eye movements. The reflex movements depend on the optokinetic and vestibular reflexes that help to stabilize the images on the retina during head and body movements. The EOMs also control saccades and smoothpursuit movements that help to track and focus on new objects, while vergence movements are important for binocular vision, such as in mammals with frontally placed eyes (Porter et al., 1995; Spencer and Porter, 2005). These various movements (e.g. saccades are very fast eye movements, whereas vergence movements require slow and precise muscle activity) demand a high degree of acuity, coordination and a wide dynamic range of functionality. This functional diversity requires high specialization of the EOMs as a muscle group. The six EOMs are: the four recti (rectus medialis, rectus lateralis, rectus superior and rectus inferior) and the two obliques (superior oblique and inferior oblique) (Fig. 1.1). The six extraocular muscles are attached to the eye ball (globe) such that each muscle forms an agonist-antagonist pair with the opposing muscle. The lateral and medial rectus cause the eye to look left and right (abduction, away from the nose and adduction, toward the nose) respectively, whereas the main actions of the superior and inferior recti are to control up- and downward gaze (elevation and depression). The superior and inferior obliques primarily coordinate in- and extorsion of the eye (when the top of the eye moves toward the nose or away from the nose, respectively) and as a secondary action contribute to adduction and abduction in combination with the recti muscles (Bron et al., 1997). The levator palpebrae superioris is also considered an extraocular muscle but does not share all allotype specific

features of the other six EOMs. The levator is responsible for moving the eye lid and is not attached to the eyeball (Bron et al., 1997).

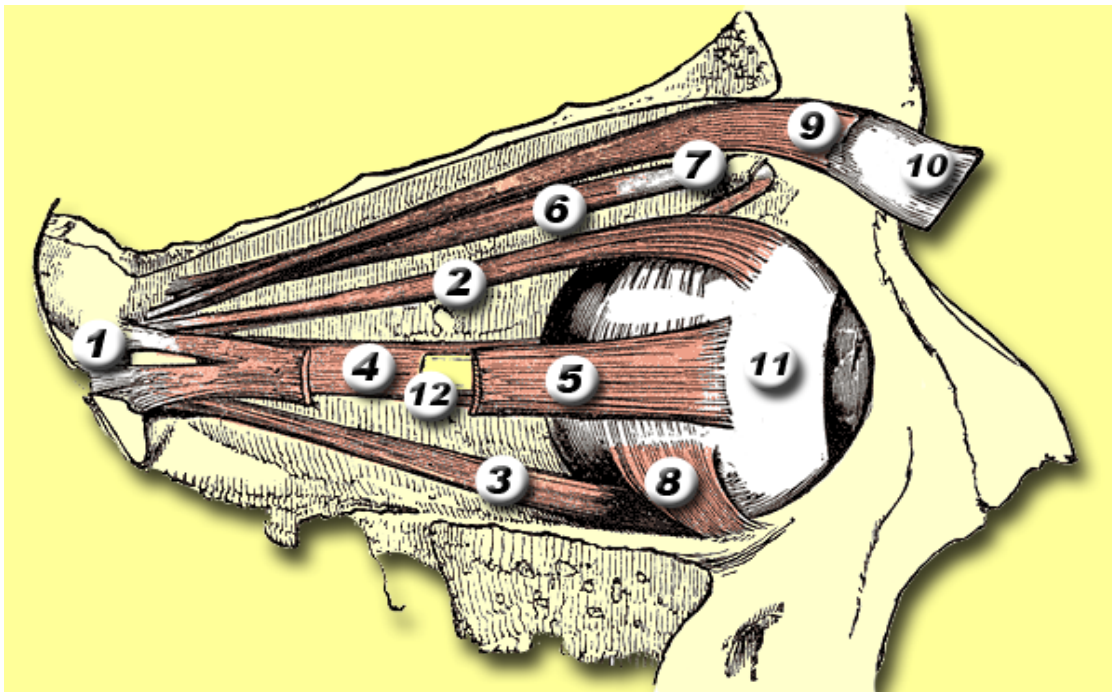


Fig. 1.1: Schematic of the right eye depicting the localization of the extraocular muscles relative to the eye ball: 1 = Annulus tendineus communis, 2 = Superior rectus muscle, 3 = Inferior rectus muscle, 4 = Medial rectus muscle, 5 = Lateral rectus muscle, 6 = Superior oblique muscle, 7 = Trochlea of superior oblique, 8 = Inferior oblique muscle, 9 = Levator palpebrae superioris muscle, 10 = Eyelid, 11 = Eyeball, 12 = Optic nerve (Schematic: Wikipedia and Gray's Anatomy 20th US Edition).

The anatomical origin of the EOMs is a portion of a tendinous ring, the annulus of Zinn or annulus tendineus communis, which originates from the optic foramen at the back of the orbit. The EOMs insert at or slightly proximal of the equator of the eye ball. Only the inferior oblique arises from the maxillary bone in the medial wall of the orbit. In addition, the superior oblique is deflected by the trochlea, a fibrocartilaginous loop at the medial wall of the orbit on its path from the annulus of Zinn to its insertion site on the eyeball (Fig. 1.1) (Bron et al., 1997; Porter et al., 1995).

Anatomically, EOMs are compartmentalized into two layers: the inner global layer (GL), which is the part of the muscle adjacent to the globe, and the outer orbital layer (OL), which is the part of the muscle neighboring the bony orbit (Kato, 1938). These two layers are morphologically different and they are thought to be functionally distinct (Budak et al., 2004; Demer, 2002). The global layer spans the full muscle length while the orbital layer ends

before the global layer becomes tendinous (Felder et al., 2005). The OL encases the GL roughly in a C-shape. Within both layers the fiber sizes vary much more compared with other skeletal muscle. The fibers are also more loosely arranged, especially in the OL, which generally has smaller fibers than the GL (Mayr, 1971). Characteristic of adult EOMs, especially of the orbital layer is its continuous expression of genes associated with developing muscle, for instance embryonic myosin heavy chain (MyHC) (Jacoby et al., 1990; Wieczorek et al., 1985), the fetal acetylcholine receptor and neural cell adhesion molecule (Fraterman et al., 2006; McLoon and Wirtschafter, 1996), which is typically expressed in newly formed myotubes. In addition, the expression of cardiac protein isoforms in EOMs, such as α -cardiac MyHC and cardiac/slow troponin C (TNNC1) are another hallmark of EOMs. This may be part of their functional specialization as EOMs show typical cardiac properties, such as high endurance and continuous activation. Particularly, in the OL the high mitochondrial content and oxidative enzyme activities in combination with higher vascularity enable continuous activation and high fatigue resistance (Demer et al., 2000; Mayr, 1971; Oh et al., 2001; Scott and Collins, 1973).

Whether a skeletal muscle is qualified as a slow or fast muscle is largely determined by its composition of fiber-types. Typically four different fiber-types are distinguished, mainly according to MyHC expression, myosin ATPase activity and fatigue resistance. The slow fibers express the type 1 MyHC and have a high number of mitochondria. Due to their reliance on oxidative energy metabolism, slow fibers have the highest endurance. There are three fast fiber types that express the fast MyHCs, 2A, 2X/2D and 2B. Fibers that express MyHC 2A are relatively fatigue-resistant because of their relative abundance of mitochondria and mixed use of oxidative-glycolytic metabolism. 2B fibers rely solely on glycolytic metabolism and are fast-fatigable. Finally, type 2X/2D are fast fibers and have features that are intermediate between 2A and 2B (Brooke and Kaiser, 1970; Burke, 1981; Schiaffino et al., 2007). Of note, human and rodent fiber types differ in their expression of fast MyHC in that the fasted human fiber type expresses MyHC 2X, while MyHC 2B is not expressed in human fibers. This has to be taken into account when inferring results from mouse studies (Schiaffino et al., 2007).

The EOMs have six different fiber types. None of these fiber-types fit the fiber-type classification of regular skeletal muscles, but EOM fibers feature variations of the classical skeletal muscle fiber-types. EOMs virtually express all known MyHC, including the

embryonic MyHC and an eom-specific MyHC (Wieczorek et al., 1985). This also entails hybrid fibers that express two or more MyHCs in one fiber. For example, in OL fibers embryonic MyHC is expressed around the innervation zone toward the center of the fiber, while eom-specific MyHC is found in the periphery (Rubinstein et al., 2004). The EOM fiber-types are distinguished regarding their location and innervation pattern in addition to their myosin ATPase staining pattern, MyHC expression and color (Porter et al., 1995). The innervation of EOM fibers shows two patterns. In addition to the typical singly innervated fibers (SIF) of mammalian muscle, where one fiber forms only a single synapse with one motoneuron, some EOM fibers are multiply innervated fibers (MIF). A MIF fiber has several synapses along its length, which resembles the more primitive fibers of amphibian and avian skeletal muscle (Hess and Pilar, 1963; Mayr, 1971). These fibers also express a slow MyHC and exhibit rather tonic than twitch contraction characteristics and are called slow-tonic or slow non-twitch fibers (Bormioli et al., 1980; Hess and Pilar, 1963; Lynch et al., 1994; Rossi et al., 2009a). Both layers of the EOMs contain SIFs and MIFs. While the OL has two fiber-types (orbital SIFs and orbital MIFs), the global layer has four fiber-types (global MIFs, global white SIFs, global intermediate SIFs and global red SIFs) (Porter et al., 1995). As the nomenclature indicates, the fibers in each layer are distinct from each other. Orbital MIFs comprise about 20% of the OL fibers and express, as mentioned above, fast-twitch embryonic MyHC in the mid-belly region and slow MyHC toward the end, which confers different contractile properties within the same fiber. The remaining 80% of the OL fibers are orbital SIFs and are thought to be twitch fibers expressing embryonic and the eom-specific MyHC. The three SIF fiber types of the global layer somewhat resemble the three fast twitch fiber types of regular skeletal muscle as they largely express the respective MyHC as indicated by their name but show variations in mitochondrial content and histochemical profile (Mayr, 1971; Porter et al., 1995). The global red SIFs and the global white SIFs each make up about one third, while the global intermediate make up about one fourth of the GL. Lastly, the global MIFs comprise the remaining 10% of the GL fibers expressing slow MyHC and probably α -cardiac MyHC. Their ultrastructural profile with large distances between SR and contractile apparatus indicates resemblance of slow-tonic fibers such as seen in amphibians but their role in the GL of a very fast muscle is not clear (Porter et al., 1995; Spencer and Porter, 2005).

The expression of the whole range of MyHC in various combinations in EOM provides a fiber-type pattern that together with multiple and single innervations enables the wide dynamic range of different contractions needed for the complex and various eye movements. Functional measurements allowed further insight into the physiological properties the EOMs. Due to their low force production and low twitch/tetanic tension ratio of about 0.13, EOMs have been reported as being ultrafast and fatigue resistant but weak muscles (Close and Luff, 1974; Frueh et al., 1994). Limb muscles typically produce higher forces with twitch/tetanus tension ratios of 0.2-0.5 (Burke, 1981). Moreover, EOMs receive motoneuronal input of up to 600 Hz, whereas other skeletal muscles receive only up to 125 Hz (Asmussen and Gaunitz, 1981; Burke, 1981). In addition, EOMs feature some of the smallest motor units with 10-20 fibers per motor neuron (Asmussen, 1978; Asmussen and Gaunitz, 1981), which allows very fine and precise movements. In contrast, regular skeletal muscles have motor units sizes of 100-2000 fibers per motor neuron (Burke, 1981). Contributing to the high fatigue resistance in EOMs is their unusually high number of mitochondria, whose distribution, number and morphology varies between the fiber-types (Mayr, 1971; Spencer and Porter, 2005).

Anatomically and developmentally, EOM belong to the cranio-facial lineage of muscles. They do not develop from the somites as other skeletal muscles; instead, EOM precursor cells arise from the non-somitic head mesoderm and migrate to the preocular regions where muscle premordia form around the developing eye (von Scheven et al., 2006). Similarly, EOMs are not innervated by somatic motoneurons, but by three cranial nerves; the trochlearis (IV), oculomotor (III) and abducens (VI) nerve (Bron et al., 1997; Porter et al., 1995).

All these features demonstrate the morphological as well as functional complexity of the EOMs. A comparison of key differences between extraocular and other skeletal muscle are summarized in Table 1.1.

In recent years, researchers have begun to explore the distinctiveness of EOM on the molecular level. Several groups have worked on deciphering the molecular makeup of rodent and human EOMs using Gene Chip based genome wide expression profiling and proteomic approaches (Fischer et al., 2005; Fischer et al., 2002; Fraterman et al., 2007a; Fraterman et al., 2007b; Khanna et al., 2004; Porter et al., 2001a). Comparison of the superfast EOM with the fast limb muscles tibialis anterior (TA), extensor digitorum longus (EDL) or gastrocnemicus revealed considerable differences on the gene expression level. Unique

features of glucose metabolism, content of mitochondrial enzymes as well as the expression of uncommon isoforms, such as cardiac and developmental genes in EOM have been described (Farh et al., 2005; Fischer et al., 2005; Fischer et al., 2002; Khanna et al., 2003; Porter et al., 2001a). For instance, EOM express genes supporting production of energy based on blood glucose and oxidative phosphorylation, whereas fast muscles usually rely on glycogen as a source of energy (Fischer et al., 2002; Porter et al., 2001a).

Trait	Limb allotype	Extraocular muscle allotype
Fiber types	I, IIA, IIB, IIC, IIX(D); type composition is muscle dependent	Peculiar to allotype, full range of properties except for slow twitch; all types in each muscle.
Fiber diameter (μm)	35-75	20-50
Innervation pattern	Single	Single and multiple
Adult fiber myosin types	I, IIA, IIB, IIX(D)	Most known isoforms, including cardiac, developmental and tissue specific.
Embryonic origin	Somitic, paraxial mesoderm	Somitomeric mesoderm
Mode of contraction	Twitch	Twitch and tonic
Contraction properties:		
Time to peak (ms)	12.6 (extensor digitorum), 37.6 (soleus)	4.4
One-half relaxation time (ms)	8.7 (extensor digitorum), 54.8 (soleus)	4.8
Twitch-tetanic tension ratio	0.20	0.13
Fatigue resistance	Variable	Moderate to extremely high
Motor unit size (fibers/motor neuron)	100-2000	13-20
Motor neuron types	Alpha and gamma, bimodal size distribution	Alpha only, unimodal size distribution
Acetylcholine receptor type	Adult	Adult and embryonic
Maximum motor neuron discharge rates (Hz):		
Phasic	125	> 600
Sustained	50	> 200
Motor system strategy	Division of labor with role-specific muscle	Capability for all movement types in single muscles
Stretch reflex	Important features	Absent
Proprioceptors	Muscle spindles and tendon organs	Palisade endings >> spindles > tendon organs

Table 1.1: Comparison of key differences between extraocular and other skeletal muscles (Table reproduced from Porter and Baker, 1996).

Particular insight was gained when the gene expression of the OL and GL were compared on the transcript level. Marked differences became evident supporting the notion of different functional properties of the two layers (Budak et al., 2004; Khanna et al., 2004). Based in part on the expression of slow/cardiac isoforms, such as α -cardiac MyHC, the OL is thought to be functionally slower but of higher endurance compared to the GL (Spencer and Porter, 2005).

Proteomic analysis using mass-spectrometry revealed differences in the expression of sarcomeric proteins. Protein expression studies showed that also on the protein level two muscle allotypes could be differentiated (Fraterman et al., 2006; Fraterman et al., 2007b). One of these studies revealed up-regulation of proteins connected to the Z-band of the sarcomere suggesting particular reinforcement of sarcomeric structures in EOM (Fraterman et al., 2007b).

To complement the studies on the transcript and proteomic level recently mircoRNA (miRNA) specific microarray chips were used to describe the miRNA expression pattern of EOMs relative to limb muscle (Zeiger and Khurana, 2010). miRNAs are a novel class of small non-coding regulatory RNAs that provide a new mechanism of transcriptional regulation (Ambros, 2004). miRNAs are 18-24 nucleotides long and bind to the 3'UTRs (Brennecke et al., 2005) of messenger RNAs (mRNAs) resulting in suppression of translation or degradation of the mRNA and reduced protein levels (Bartel, 2004). Differential expression of miRNAs has been reported to play a role in many disease processes, including muscular dystrophy, therefore offering new potential therapeutic targets (Eisenberg et al., 2007). In EOM, significant differences of miRNA expression compared to the fast TA muscle were found, particularly within the muscle-specific miRNAs, suggesting that different muscle-types are defined by a certain miRNA signature even regarding the tissue-specific miRNAs (Zeiger and Khurana, 2010).

Another most striking hallmark of EOM is their differential involvement in a number of diseases. EOMs are primarily affected in Myasthenia gravis, Grave's disease (thyroid myopathy), oculopharyngeal muscular dystrophy and mitochondrial myopathies (Bahn and Heufelder, 1993; Kaminski and Ruff, 1997). On the other hand EOMs are preferentially spared in muscular dystrophies like Duchenne Muscular Dystrophy (DMD), limb girdle muscular dystrophy (LGMD) and congenital muscular dystrophy (CMD), while other skeletal

muscles are severely affected (Kaminski et al., 1992; Porter and Karathanasis, 1998; Porter et al., 2001b). The sparing of EOMs has most intensively been studied in DMD. The EOMs remain functional throughout the disease process and do not present the classical patterns of necrosis and fibrosis seen in most other skeletal muscles affected by neuromuscular diseases (Kaminski et al., 1992; Karpati et al., 1988; Khurana et al., 1995).

1.2 Duchenne muscular dystrophy (DMD)

1.2.1 Clinical & molecular background of DMD

DMD is a hereditary muscle wasting disease clinically characterized by progressive muscle weakness. Mutations in the dystrophin gene result in deficiency of the protein product dystrophin causing DMD. With an incidence of approximately 1 in 3.500 male newborns DMD is one of the most common fatal X-linked hereditary diseases (Emery and Muntoni, 2003). The disease is usually first diagnosed at age 2-5 years and death normally occurs in the late teens up to late twenties as a result of respiratory or cardiac failure (Emery and Muntoni, 2003). Besides massively elevated serum creatine kinase levels, a prominent clinical sign is the pseudo-hypertrophy of calf muscles (Fig. 1.2).



Fig. 1.2: Duchenne's original case, showing marked calf enlargement and lumbar lordosis (from Duchenne, 1868, p.8) (Caption and Image reproduced from Emery and Muntoni, 2003).

In the early phase of the disease necrotic and regenerative processes seem to be balanced, which later shifts toward necrosis due to exhaustion of the regenerative capacity. The muscle tissue is progressively replaced by fibrotic tissue, which manifests in pseudo-hypertrophy of the muscle (Emery and Muntoni, 2003).

Eventually all skeletal muscles are affected in DMD but for unclear reasons fast muscles seem to be earlier affected than slow muscles (Minetti et al., 1991; Webster et al., 1988). There is no clear pattern, which would predict susceptibility to damage according to fiber-type composition of the individual muscle. Histologically, a muscle biopsy of a DMD patient shows variation in fiber size, clusters of necrotic fibers, central nuclei in regenerating fibers, fibrosis, and inflammatory infiltration of the tissue by macrophages and other immune cells (Gorospe et al., 1994; McDouall et al., 1990). The few muscle groups that are fully or partially spared throughout the disease process are the laryngeal muscles (Marques et al., 2007; Smythe, 2009), the striated muscles of the sphincters and the extraocular muscles (Caress et al., 1996; Khurana et al., 1995). Wheelchair bound DMD patients have normal extraocular muscle motility as demonstrated by infrared oculography (Kaminski et al., 2002).

To date the disease is incurable and only a few treatment options are available for patients. Corticosteroids are believed to dampen inflammation in the muscle and prolong ambulation of patients for one or two more years before becoming wheel-chair bound (Manzur et al., 2008). In addition, mechanical long-term ventilation has been shown to improve life expectancy into the mid or late twenties (Gibson, 2001). A number of new treatment options, including gene therapeutic approaches, are currently explored and a few promising agents are now in clinical trials. Anti-sense mediated exon skipping and forced read-through of premature stop-codons (PTC124) would restore the expression of a truncated but functional dystrophin or sufficient levels of full length dystrophin, respectively (Kinali et al., 2009; van Deutekom et al., 2007; Welch et al., 2007). However, not all patients would benefit from these treatments because only certain mutations can be successfully targeted by those treatments. In addition, hurdles like side-effects, high drug costs, applicability to a larger group of patients and approval are still to be overcome and the search for new potential therapeutic targets is ongoing (Aartsma-Rus et al., 2010).

Several animal models are available to researchers to study DMD including a golden retriever dog model (GRMD), a cat model (hypertrophic feline muscular dystrophy, HFMD),

zebrafish, *C. elegans* and *Drosophila* models (Allamand and Campbell, 2000). However, most commonly used is the mdx mouse (Bulfield et al., 1984), which carries a natural mutation in the dystrophin gene that creates a premature stop codon in exon 23 (Sicinski et al., 1989) and therefore lacks the dystrophin protein. In contrast to DMD patients, the mouse shows a milder phenotype with relatively mildly impaired muscle function and an almost normal lifespan. The milder phenotype of the mdx mouse has been attributed to its greater capacity to regenerate (Coulton et al., 1988; Torres and Duchen, 1987). Nevertheless, mdx mice exhibit high CK levels and show a similar histopathology, especially in the diaphragm, which makes them a good model to study the disease and potential treatment options (Bulfield et al., 1984; Stedman et al., 1991). The golden retriever dog model resembles the human phenotype better; however its usage is limited due to high costs and variations in clinical presentation within one litter and is usually used for highly promising studies (Cooper et al., 1988).

1.2.2 Pathogenesis of DMD

Dystrophin is located just underneath the sarcolemma of the muscle cell as part of the dystrophin glycoprotein complex (DGC). Its N-terminus binds to cytoskeletal actin and its C-terminus binds to β -dystroglycan, which is integral to the membrane. On the extracellular side β -dystroglycan binds to laminin $\alpha 2$ (Fig. 1.3) (Ervasti and Sonnemann, 2008). The loss of dystrophin results in the loss of several components of the DGC, such as the dystroglycans, sarcoglycans and $\alpha 1$ - and β -syntrophins (Brenman et al., 1995; Ervasti et al., 1990; Matsumura and Campbell, 1994; Ohlendieck and Campbell, 1991). One major role of dystrophin is to link the cytoskeleton to the extracellular matrix (Campbell and Kahl, 1989; Matsumura and Campbell, 1994). This interaction stabilizes the membrane during excitation-contraction cycles of muscle activity (Moens et al., 1993; Petrof et al., 1993). When dystrophin is lost, eccentric contractions damage the muscle such that less force is produced and the sarcolemma becomes leaky allowing movement of membrane-impermeant molecules across the membrane (Matsuda et al., 1995; Moens et al., 1993).

Another important role of dystrophin is its interaction with signaling and channel proteins (Ervasti and Sonnemann, 2008). The proper positioning of these molecules seems to be important for muscle function. For example nitric oxide synthase (NOS), which is bound

to α -syntrophin (Fig. 1.3) is lost in DMD and restoration of NOS to the DGC ameliorated muscle pathology in mdx mice (Tidball and Wehling-Henricks, 2004). Recently, the interaction of α 1-syntrophin with mechanosensitive cation channels has been suggested to play a role in mdx pathology (Vandebrouck et al., 2007). The exact processes leading to muscle damage in DMD are still unclear and many hypotheses are being discussed (Deconinck and Dan, 2007); but it is widely accepted that an elevation of intracellular calcium (Ca^{2+}) levels contributes to the pathogenesis (Gillis, 1999).

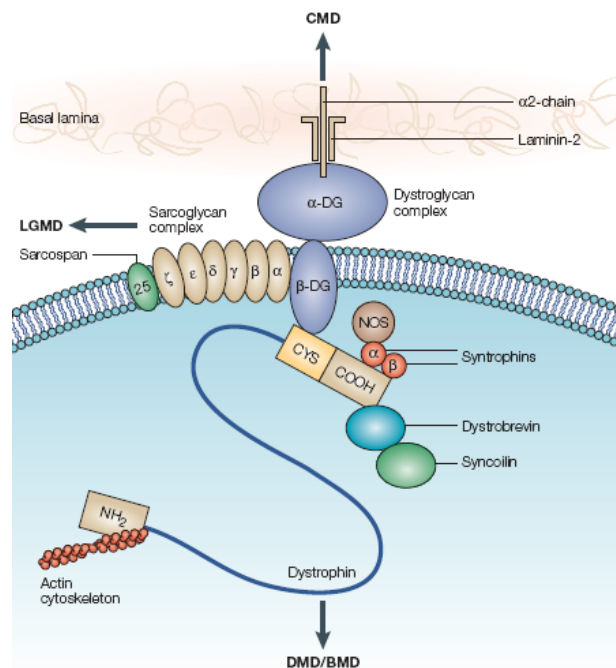


Fig. 1.3: The Dystrophin-Glycoprotein Complex. The N-terminus of dystrophin binds to actin of the cytoskeletal network, while the C-terminus binds the dystroglycan complex, which in turn associates with the transmembrane sarcoglycans. The C-terminus of dystrophin further acts as scaffold for proteins such as syntrophins, dystrobrevin, syncoilin and nitric oxide synthase (NOS). Laminin- α 2 connects the dystroglycans with the extracellular matrix. Loss of dystrophin leads to Duchenne or its milder form Becker muscular dystrophy. Loss of delta or gamma Sarcoglycan causes Limb Girdle Muscular Dystrophy (LGMD) and loss of laminin- α 2 causes congenital muscular dystrophy (CMD) (Schematic reproduced from Khurana and Davies, 2003).

Two hypotheses as to how this elevation of Ca^{2+} is taking place are currently being discussed: (I) Sarcolemmal integrity is compromised and the fragile membrane is more susceptible to activity induced tears or micro lesions through which membrane-impermeant molecule can cross and extracellular Ca^{2+} can enter. (II) Dysregulated mechanosensitive or

Ca^{2+} leak channels are activated during muscle activity allowing increased influx of Ca^{2+} . Both processes can cause un-physiologically high intracellular Ca^{2+} levels, followed by a dysregulation of the Ca^{2+} homeostasis (Gillis, 1999; Hopf et al., 1996).

In support of an abnormal Ca^{2+} homeostasis, early studies found the total Ca^{2+} content of dystrophic muscle to be increased in muscle from DMD and other myopathy patients (Bodensteiner and Engel, 1978; Emery and Burt, 1980). Whether resting Ca^{2+} is elevated in DMD and mdx muscle is under debate. Several studies reported normal levels (Collet et al., 1999; Gailly et al., 1993a; Han et al., 2006; Head, 1993; Pressmar et al., 1994) others report elevated levels (Hopf et al., 1996; Turner et al., 1988; Tutdibi et al., 1999). Others suggested that elevated Ca^{2+} is localized underneath the sarcolemma (Mallouk et al., 2000; Robert et al., 2001; Turner et al., 1991). Dysregulated and/or up-regulated Ca^{2+} channels in mdx myofibers or myotubes have been suggested to account for increased Ca^{2+} levels. Increased Ca^{2+} influx through Ca^{2+} leak channels, stretch-activated channels, mechanosensitive channels, insulin-like growth factor (IGF1) activated channels or store-operated channels (SOC) has been reported (Alderton and Steinhardt, 2000; Boittin et al., 2006; Franco-Obregon and Lansman, 1994; Franco and Lansman, 1990; Hopf et al., 1996; Iwata et al., 2003; Yeung et al., 2005). There is strong evidence that Ca^{2+} levels rise in dystrophin-deficient muscles that are subjected to mechanical stress, such as cycles of contraction or exposure to hypo-osmotic solutions (Imbert et al., 1996; Leijendekker et al., 1996; Yeung et al., 2005). Elevated Ca^{2+} levels result in Ca^{2+} overload of mitochondria and activation of Ca^{2+} dependent proteases, such as calpains that cause further breakdown of membrane components and other proteins resulting in the necrosis and fibrosis of the muscle cells (Kuznetsov et al., 1998; Robert et al., 2001; Spencer et al., 1995; Turner et al., 1988). In the early phases of DMD, in an attempt to compensate for the damage, the muscle undergoes cycles of regeneration and degeneration until the pool of satellite cells (muscle specific stem cells) is exhausted and the necrotic events predominate causing the debilitating course of the disease (Schmalbruch, 1984).

1.4 Calcium homeostasis in normal and dystrophic muscle

Ca^{2+} regulates a myriad of processes in the cell as a second messenger and is therefore spatially and temporally tightly regulated. A number of different Ca^{2+} handling proteins help maintain the Ca^{2+} homeostasis of the cell. Ca^{2+} is critical for the main function of muscle driving contraction by mediating E-C coupling. A second function of Ca^{2+} signaling is to modulate gene expression in muscle cells. This occurs via the activation of Ca^{2+} /calmodulin (CALM), which in turn stimulates downstream pathways, such as the calcineurin/nuclear factor of activated T-cells (NFAT) and Ca^{2+} /calmodulin dependent kinase II (CAMKII)/histone deacetylase (HDAC) pathways altering the activity of slow/oxidative programs (Schiaffino et al., 2007). In this way Ca^{2+} signaling is translated to adapt muscle properties to changing demand such as exercise. In the following, E-C coupling, store-operated Ca^{2+} entry (SOCE) and other Ca^{2+} influx mechanisms that are involved in the muscle Ca^{2+} homeostasis will be highlighted.

1.4.1 Excitation-contraction (E-C) coupling

E-C coupling is the process that converts an electrical stimulus into muscle contraction. The arrival of an action potential at the neuromuscular endplate junction depolarizes the transverse (T)-tubules of the plasma membrane of the muscle (sarcolemma) and triggers the interaction of the dihydropyridine receptor (DHPR) and the ryanodine receptor (RYR), which in turn releases Ca^{2+} from the intracellular sarcoplasmic reticulum (SR) Ca^{2+} stores. The resulting transiently elevated Ca^{2+} levels in the cytoplasm activate contraction of the muscle. Ca^{2+} binds to tropomyosin and troponin (e.g. troponin C) initiating movement of the myofilaments actin and myosin, which appears as muscle contraction. This action is terminated when Ca^{2+} is cleared from the cytoplasm by pumps situated in the SR (sarcoplasmic Ca^{2+} ATPase: SERCA) and to a lesser extent by the plasma membrane (plasma membrane Ca^{2+} ATPase: PMCA) and the $\text{Na}^+/\text{Ca}^{2+}$ exchanger (NCX) (Fig. 1.4) (Rossi and Dirksen, 2006).

During E-C coupling, cytosolic proteins, such as S100 and parvalbumin (PARV) help to buffer Ca^{2+} and in case of PARV also regulate the speed of relaxation (Heizmann et al., 1982). Inside the sarcoplasmic reticulum calsequestrin (CASQ) and sarcalumenin (SRL) are

high capacity Ca^{2+} storage proteins that are involved in regulating the amount of releasable Ca^{2+} (Leberer et al., 1989; MacLennan and Wong, 1971).

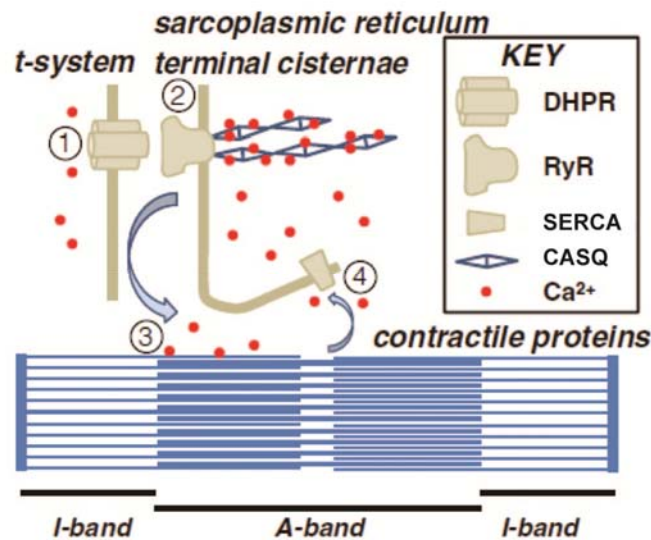


Fig. 1.4. The steps in E-C coupling of skeletal muscle. Depicted is a schematic of a sarcomere and the terminal cisternae formed by the SR adjacent to the T-system (T-tubules). An action potential depolarizes the T-tubules, which causes the DHPR to activate the RYR (step 1), which in turn releases Ca^{2+} from the SR (step 2). The Ca^{2+} in the cytosol binds to the contractile proteins (myofilaments) initiating contraction (step 3). The SR pump (SERCA) resequesters Ca^{2+} into the SR, where it is bound again by calsequestrin (CASQ) concluding the E-C coupling cycle (step 4) (Schematic reproduced from Launikonis et al., 2010).

Fast and slow/cardiac muscles express different isoforms of CASQ and SERCA; CASQ1 and SERCA1 are typically found in fast muscle, whereas CASQ2 and SERCA2 are typically found in cardiac and slow muscle (Murphy et al., 2008). An important regulator of the SERCA pumps is phospholamban (PLN), which is active depending on its phosphorylation status at two distinct sites (Simmerman et al., 1986). The serine 16 (Ser16) residue can be phosphorylated by protein kinase A (PKA), while the threonine 17 (Thr17) residue is phosphorylated by CAMKII. Phosphorylated PLN increases the activity of SERCA, whereas dephospho-PLN inhibits SERCA activity. How PLN regulates SERCA has mainly been studied on the SERCA2 isoform in heart muscle but PLN can also act on SERCA1 *in vitro* (Toyofuku et al., 1993). The main Ca^{2+} turnover during E-C coupling occurs between the SR and the cytosol with the myofilaments. The proteins involved in this turnover determine the speed of muscle contraction (Rossi and Dirksen, 2006).

1.4.2 Store-operated calcium entry: role of TRP channels, Orai and STIM

Although, muscle contraction can be sustained for some time without presence of extracellular Ca^{2+} , in the long run Ca^{2+} influx into muscle cells plays an important role for E-C coupling (Kurebayashi and Ogawa, 2001; Launikonis and Rios, 2007; Stiber et al., 2008a). This Ca^{2+} influx from the extracellular space into the cell is triggered in response to intracellular Ca^{2+} store depletion, such as the ER or the SR, and is called store-operated Ca^{2+} entry (SOCE). In non-excitabile cells (e.g. immune cells) the importance of SOCE during sustained Ca^{2+} signaling has been appreciated for a long time (Parekh and Putney, 2005). More recently, the role of SOCE has become apparent in skeletal muscle. During repetitive contraction cycles, over time the SR is depleted of Ca^{2+} . SOCE enables Ca^{2+} entry from the extracellular space to replenish Ca^{2+} in the SR to prepare for subsequent contractions. Furthermore, SOCE seems to play a role in muscle development and remodeling (Stiber et al., 2008a). As molecular entities of SOCE the proteins Orai and STIM and members of the transient receptor potential channel (TRP) superfamily have been implicated (Worley et al., 2007).

1.4.2.1 The TRP superfamily of cation channels

The TRP superfamily of cation channels consists of six structurally related subfamilies divided into two groups (Venkatachalam and Montell, 2007). Group 1 contains the subfamilies TRPC, TRPV, TRPM and TRPA. Group 2 contains TRPP and TRPML, which are distantly related to group 1 members (Montell, 2005; Montell et al., 2002). The TRP channels are non-voltage gated channels and display a wide range of ion selectivity. Some are selective for Ca^{2+} , Na^+ or Mg^{2+} or are non-selective cation channels. Their function is equally diverse ranging from regulation of Ca^{2+} and Mg^{2+} homeostasis, neuronal function or vascular tone to mediating sensory transduction of cold, heat, mechanical, osmotic or noxious stimuli (Beech et al., 2004; Clapham, 2003; Clapham et al., 2001; Montell et al., 2002). TRP channels are expressed ubiquitously. In skeletal muscle however, only members of the TRPC, TRPV and TRPM channel subfamilies were detected (Kunert-Keil et al., 2006). An expression study showed the highest levels of TRP channels in brain and kidney, while the expression levels in muscle were moderate with predominant expression of TRPC3, TRPC1, TRPC6, TRPM7, TRPM3 and TRPM4 (Kunert-Keil et al., 2006). TRP channels form

tetramers and can operate in homo- and heteromeric associations, which likely results in a large variation of functional properties (Venkatachalam and Montell, 2007).

The TRPC channel subfamily comprises seven members TRPC1-7, with TRPC2 being a pseudogene in humans (Montell, 2005). TRPC channels are non-selective, Ca^{2+} permeable channels. TRPC1, TRPC3, TRPC4 and TRPC6 are expressed in skeletal muscle (Krüger et al., 2008; Kunert-Keil et al., 2006; Vandebrouck et al., 2002), of which TRPC1 is the best characterized channel. It has been shown to be located at the sarcolemma by several studies (Stiber et al., 2008a; Vandebrouck et al., 2002); however this has been challenged by a report showing predominant expression in the SR (Berbey et al., 2009). In support of sarcolemmal localization are reports about the association of TRPC1 with several proteins that may influence or regulate channel function. TRPC1 association with the DGC has been suggested via interaction with $\alpha 1$ -syntrophin (Vandebrouck et al., 2007). In addition binding to caveolin-3 may be responsible for targeting TRPC1 to the sarcolemma where it may be regulated by src kinase (Gervasio et al., 2008). These interactions may also play a role in muscular dystrophy (Gervasio et al., 2008). Furthermore, TRPC1 can be activated by store depletion and/or membrane stretch in muscle fibers and the role this might play in muscle disease is currently being explored (Gervasio et al., 2008; Maroto et al., 2005; Vandebrouck et al., 2007). The transient up-regulation of TRPC1 during myoblast differentiation and fusion suggests a role of TRPC1 mediated Ca^{2+} entry in myogenesis, development and regeneration (Formigli et al., 2009; Louis et al., 2008).

Another channel of the TRPC family that has been studied in muscle is TRPC3. In contrast to TRPC1, immunohistological localization suggested that TRPC3 expression in skeletal muscle is located intracellularly rather than at the sarcolemma (Krüger et al., 2008; Vandebrouck et al., 2002). TRPC3 is thought to associate with the triadic proteins CASQ, Triadin and Junctophilin and be located in the T-tubules. It functionally couples to RYR1, regulating SR Ca^{2+} release, which suggests a function in EC-coupling (Lee et al., 2006; Woo et al., 2008). Moreover, TRPC3 has also been implicated with store-operated Ca^{2+} entry and seems to play an important role in differentiation of skeletal myoblasts (Lee et al., 2006; Santillan et al., 2004; Woo et al., 2010). TRPC3 has also been implicated with Ca^{2+} influx during neuromuscular activity that couples to the calcineurin/NFAT pathway altering gene regulation (Rosenberg et al., 2004). Of the remaining TRPC channels, TRPC5 and TRPC7 are not expressed in muscle, while TRPC4 and TRPC6 have been suggested to be expressed

at the sarcolemma and have been implicated with a potential role in SOCE but their role in muscle has not been further explored (Vandebrouck et al., 2002; Yuan et al., 2007). However, issues with TRP antibodies (e.g. TRPC4) have been raised, therefore the specificity of the antibodies used for expression analyses should be established (Flockerzi et al., 2005; Tajeddine et al., 2010).

Most of the TRPC channels (TRPC1, TRPC3, TRPC4, TRPC5 and TRPC6) have been implicated with SOCE, of which TRPC1 is the best characterized channel (Yuan et al., 2007). In muscle robust SOCE via TRPC channel, probably TRPC1 or C4 has been observed in dystrophic myofibers (Gervasio et al., 2008; Vandebrouck et al., 2002).

Cation channels of the TRPV channel subfamily (TRPV1-V6) function in the sensation of cold, heat or changes in osmolarity and are often polymodally activated (TRPV2-4). Two members of the TRPV channel subfamily, TRPV2 and TRPV4, show consistent expression in skeletal muscle (Krüger et al., 2008; Kunert-Keil et al., 2006) and their role in muscle is starting to be elucidated (Iwata et al., 2009; Pritschow et al., 2010; Zanou et al., 2009). TRPV2 and TRPV4 are Ca^{2+} permeable nonselective cation channels that belong to the functional group of “osmo-mechano-TRPs” (Liedtke, 2007). TRPV4 is expressed at the sarcolemma, while TRPV2 is located intracellularly and translocates to the surface membrane upon stimulation and in dystrophic muscle (Iwata et al., 2003). TRPV4 has been implicated with a role in muscle fatigue, while TRPV2 seems to be involved in abnormal Ca^{2+} influx in muscular dystrophy (Iwata et al., 2009; Zanou et al., 2009). Relevant expression levels or function of TRPV1, TRPV3, TRPV5 and TRPV6 in muscle have not been reported yet.

The TRPM subfamily consists of members TRPM1-8. TRPM channels serve functions ranging from cold sensation (TRPM8) to Mg^{2+} transport (TRPM7 and TRPM8) and enzymatic activity in addition to their channel activity (TRPM2, TRPM6 and TRPM7) (Montell et al., 2002). TRPM7 shows the highest overall expression of all TRP channel subtypes in muscle (Kunert-Keil et al., 2006). It is a non-selective cation channel that is important for cellular Mg^{2+} homeostasis (Fleig and Penner, 2004). Along with TRPM7, TRPM4, a Ca^{2+} activated channel that is permeable to Na^+ and K^+ , has been consistently found in skeletal muscle but the function of these channels in muscle has not been explored yet (Krüger et al., 2008; Kunert-Keil et al., 2006; Vennekens and Nilius, 2007).

1.4.2.2 Orai and STIM proteins

Recently, the Orai and STIM proteins have been identified as the molecular components of Ca^{2+} release activated Ca^{2+} current, I_{CRAC} , a type of SOCE current (Liou et al., 2005; Soboloff et al., 2006b; Venkatachalam et al., 2002; Zhang et al., 2005a). I_{CRAC} has been well studied in non-excitabile cells, such as immune cells, and is notable for its high selectivity for Ca^{2+} (Parekh and Putney, 2005; Salido et al., 2009; Venkatachalam et al., 2002). Orai1 is a sarcolemmal channel protein mediating this highly Ca^{2+} selective store-operated current (Vig et al., 2006). The isoforms Orai2 and Orai3 are less well characterized and differ from Orai1 in their ability to conduct SOCE and differential sensitivity to different concentrations of 2-aminoethoxydiphenyl borate (2-APB) (Roberts-Thomson et al., 2010). 2-APB can also activate and alter the ion selectivity of Orai3 independent of store depletion (Roberts-Thomson et al., 2010; Varnai et al., 2009). STIM1 is a transmembrane protein localized mainly in the intracellular compartments, the endoplasmic reticulum (ER) or the sarcoplasmic reticulum (SR) (Liou et al., 2005). STIM1 contains a luminal EF-hand domain that binds Ca^{2+} and acts as a Ca^{2+} sensor (Liou et al., 2005). In non-muscle cells, upon Ca^{2+} depletion of the ER STIM1 oligomerizes into tetramers, clusters into punctae and translocates within the ER membrane into close vicinity of Orai1 (Liou et al., 2005). Interaction of STIM1 and Orai1 tetramers activates SOCE (Deng et al., 2009; Penna et al., 2008). The isoform STIM2 is 70% homologous to STIM1 and both proteins can activate SOCE (Brandman et al., 2007); STIM2 can also act in an inhibitory fashion, and is believed to play a role in the maintenance of basal cytosolic Ca^{2+} (Brandman et al., 2007; Johnstone et al., 2010; Parvez et al., 2008; Soboloff et al., 2006a).

The role of SOCE mediated by Orai1 and STIM1 in muscle is starting to be understood (Edwards et al., 2010b; Lyfenko and Dirksen, 2008; Stiber et al., 2008a; Stiber et al., 2008b). Recent work in myoblasts showed that both STIM1 and STIM2 are required for SOCE during differentiation and E-C coupling (Darbellay et al., 2010). It has been shown that SOCE in skeletal muscle takes place between the junctional membranes of the T-tubules and the SR (Launikonis et al., 2010; Lee et al., 2006). SOCE in skeletal muscle requires Orai1 and STIM1 and is rapidly activated and deactivated (Edwards et al., 2010b; Lyfenko and Dirksen, 2008). In muscle cells STIM1 is preferentially located in the sarcoplasmic membrane, possibly in close proximity to the sarcolemma of the T-tubules and Orai1 (Edwards et al.,

2010b; Stiber et al., 2008a). Since Ca^{2+} turnover in muscle cells is much faster than in non-excitable cells it has been suggested that the close proximity of STIM1/Orai1 facilitate more rapid interaction between the two proteins than in non-excitable cells (Edwards et al., 2010b; Liou et al., 2007; Lyfenko and Dirksen, 2008; Stiber et al., 2008a). The role of SOCE in skeletal muscle is further underscored by the development of a perinatally fatal skeletal myopathy in mice lacking functional STIM1 (Stiber et al., 2008a) and patients with Orai1 deficiency exhibiting skeletal myopathy (McCarl et al., 2009).

In addition, the dynamic formation of ternary complexes of TRPC1 with Orai1 and STIM1 upon store depletion has been reported in non-muscle cells suggesting cooperation of these proteins in mediating Ca^{2+} influx (Ong et al., 2007; Salido et al., 2009). However, details about the specific function of each component and how the association between TRPC1 and Orai1 could occur are still to be elucidated. Besides interacting with Orai1, STIM1 has been proposed to regulate SOCE mediated by all TRPC channels, except TRPC7, by either binding directly to TRPC1, TRPC2, TRPC4 and TRPC5 or indirectly via heteromultimerization of TRPC1 with TRPC3 and TRPC4 with TRPC6 suggesting STIM1 as the “universal” regulator of SOCE (Salido et al., 2009; Yuan et al., 2007).

1.4.3 Dysregulated calcium homeostasis in DMD

Elevated Ca^{2+} levels in DMD activate proteases, such as calpains, which leads to proteolysis and alteration of the activity of Ca^{2+} leak channels resulting in further Ca^{2+} influx (Alderton and Steinhardt, 2000). As a result, the expression and function of several Ca^{2+} buffering proteins and channels is impaired in mdx mice. Ca^{2+} buffering proteins in the SR, such as calsequestrin-like proteins, calsequestrin and sarcalumenin, are reduced in muscles of mdx mice combined with decreased Ca^{2+} binding capacity (Culligan et al., 2002; Doran et al., 2004; Dowling et al., 2004). Regucalcin, a cytosolic Ca^{2+} binding protein is decreased in mdx diaphragm (Doran et al., 2006). CALM and CASQ are expressed at lower levels in several mdx muscles (Pertille et al.), while PARV is dysregulated in various muscles (Gailly et al., 1993b; Rouger et al., 2002).

In addition to the reduction of Ca^{2+} buffering proteins, several Ca^{2+} channel types have been implicated with the dysregulation of Ca^{2+} in mdx/DMD muscle. In mdx myotubes and

fibers increased Ca^{2+} influx has been observed through different types of channels, such as mechanosensitive channels (Franco-Obregon and Lansman, 1994; Yeung et al., 2005), store-operated channels (Stiber et al., 2008a; Vandebrouck et al., 2002), Ca^{2+} leak channels (Alderton and Steinhardt, 2000) or growth factor-regulated channels (Alderton and Steinhardt, 2000). Several studies demonstrated that mechanosensitive Ca^{2+} channels in mdx muscle fibers and myotubes have a greater open probability causing increased Ca^{2+} influx at rest (Franco-Obregon and Lansman, 1994; Franco and Lansman, 1990). However, there is evidence that increased intracellular Ca^{2+} in mdx/DMD fibers and myotubes depends on contractile activity (Imbert et al., 1995; Turner et al., 1993). Since, mdx muscle is particularly sensitive to stretch-induced damage, mechano- or stretch-sensitive channels have been investigated as possible mediators of increased Ca^{2+} influx and found to show increased activity in mdx fibers (Alderton and Steinhardt, 2000; Petrof et al., 1993).

Streptomycin and gadolinium (Gd^{2+}) were able to block activity induced Ca^{2+} influx through mechanosensitive channels thereby ameliorating muscle pathology in mdx (Whitehead et al., 2006; Yeung et al., 2005). As candidates for this stretch-activated abnormal Ca^{2+} influx in mdx mice members of the TRPC and TRPV channel families, primarily TRPC1 and TRPV2, have been investigated (Iwata et al., 2009; Vandebrouck et al., 2002; Zanou et al., 2009). Dominant-negative inhibition of TRPV2 mediated Ca^{2+} influx ameliorated dystrophic pathology in mdx mice and protected muscle from eccentric contraction induced damage (Iwata et al., 2009, Zanou et al., 2009). Another study suggested stretch-/or store-dependent regulation of overly active TRPC1 channels in mdx fibers and demonstrated the inhibition of these channels by Src kinase and reactive oxygen species (ROS) inhibitors (Gervasio et al., 2008).

Furthermore, increased Ca^{2+} influx in mdx fibers, triggered by store depletion (SOCE), has been suggested to be mediated by TRPC1 and/or TRPC4 (Boittin et al., 2006; Vandebrouck et al., 2002). Antisense nucleotides against TRPC1 and TRPC4 diminished increased SOCE in mdx fibers (Vandebrouck et al., 2002). Moreover, SOCE was shown to be under the control of abnormally high levels of phospholipase A2 in mdx fibers, which were repressed by specific inhibitors (Boittin et al., 2006).

Besides the potential involvement of TRPC channels the proteins Orai1 and STIM1 have recently been implicated in increased Ca^{2+} influx triggered by store depletion. Edwards et al

reported increased expression of Orai1/STIM1 associated with enhanced SOCE in mdx mice (Edwards et al., 2010a). In addition, the loss of dystrophin may cause malfunctioning of channels by interaction with scaffolding proteins. For instance, the loss of dystrophin leads to dysregulation of TRPC1 and increased Ca^{2+} influx possibly due to secondary loss of its association with α 1-syntrophin, a member of the DGC complex (Sabourin et al., 2009; Vandebrouck et al., 2007). In the same way the loss of the channel scaffolding protein Homer1 causes skeletal myopathy, which may be caused by dysfunctional regulation of TRPC1 (Stiber et al., 2008b). An indirect approach demonstrated possible involvement of TRPC channels by showing that increased Ca^{2+} influx through overexpressed TRPC3 channels is sufficient to induce muscular dystrophy (Millay et al., 2009). In summary, several lines of evidence support the hypothesis that Ca^{2+} influx contributes to the pathogenesis DMD and that members of the transient receptor channel (TRP) family, e.g. TRPC1 and TRPV2, and/or the proteins Orai1 and STIM1 are candidates for mediating increased Ca^{2+} influx in DMD and mdx muscle. Overall, these findings demonstrate that several components of the Ca^{2+} homeostasis in dystrophic muscles are dysregulated providing candidate Ca^{2+} handling proteins to be further explored as potential therapeutic targets.

1.3 Potential sparing mechanisms in EOM

A multitude of mechanisms have been discussed in the literature as to why EOMs are not affected by mutations that cause dystrophic muscle damage, such as in DMD (Andrade et al., 2000; Porter and Baker, 1996). The sparing of EOM may be explained by expression of alternative proteins that could compensate for the lost proteins or functional and metabolic characteristics could be protective of the consequences of the primary defect. In the following, allotype specific mechanisms potentially responsible for the sparing of EOM will be introduced.

Upregulation of utrophin (Utrn): Increased expression of Utrn, a homologue of dystrophin, in EOM has been suggested to mediate the sparing of EOM by preserving sarcolemmal integrity. Utrn is able to replace dystrophin and reestablish the DGC complex and muscle function (Deconinck et al., 1997; Tinsley et al., 1996). It is normally restricted to neuromuscular and myotendinous junctions but is up-regulated and expressed at the sarcolemma in regenerating myofibers of dystrophic muscle. Increased levels of Utrn in mdx

or DMD EOM have been reported by several studies (Lewis and Ohlendieck, 2010; Matsumura et al., 1992; Porter et al., 1998), while others did not find any difference (Khurana et al., 1995). A detailed report by Porter and co-workers found sarcolemmal Utrn levels up-regulated in only three fiber types of mdx EOM (the two orbital layer fibers-types and one fiber type in the global layer) restoring the DGC in those fibers but not in the other three fiber types (Porter et al., 2003a). Interestingly, the histological sparing of the EOMs is lost in the utrnl/mdx double knockout mouse, however the three fiber types that expressed sarcolemmal Utrn in the mdx mouse were still spared in the dys/utrnl double knockout (Porter et al., 2003a). Therefore, Utrn up-regulation and the retention of the DGC cannot account for the sparing of mdx EOM.

Preserved sarcolemmal integrity: Loss of sarcolemmal integrity is thought to contribute to the pathogenesis of dystrophic muscles (Petrof et al., 1993; Weller et al., 1990). The sarcolemma of EOM may experience less damaging contractions compared with other skeletal muscles. This may be mediated by the small caliber of EOM myofibers, since large muscle fibers are more susceptible to dystrophic damage than smaller fibers (Karpati et al., 1988). In addition, EOMs experience discharge rates that are an order of magnitude higher than that of most skeletal muscles and cover a wide dynamic range of movements including very rapid saccades. Indeed, saccades are thought to apply considerable strain on the eye muscles (Spencer and Porter, 2005). EOMs remain spared, in spite of being fast and highly active muscles, which confers higher susceptibility to membrane damage in regular skeletal muscles (Karpati and Carpenter, 1986; Webster et al., 1988).

Increased free radical scavenging capacity: The high numbers of mitochondria combined with increased superoxide dismutase expression in EOM convey enhanced capacity of free radical scavenging (Felder et al., 2005; Ragusa et al., 1996). This may be advantageous during the inflammatory process of muscular dystrophy, which is associated with increased oxidative stress (Hunter and Mohamed, 1986; Mechler et al., 1984). However, several studies showed that enhanced free radical scavenging capacity is not responsible for their sparing in mdx mice (Ragusa et al., 1997; Ragusa et al., 1996; Wehling et al., 1998).

Enhanced regenerative capacity: The high number of satellite/stem cells and increased regenerative capacity could facilitate more active and more effective regeneration contributing to the sparing of EOM. EOM contain a large number of side population stem

cells, a subfraction of immature stem cells thought to contribute to muscle regeneration (Pacheco-Pinedo et al., 2009). Other studies showed increased numbers of activated satellite cells, the muscle specific stem cell, based on the expression of specific markers and continuous BrdU incorporation in uninjured muscle (McLoon and Wirtschafter, 2003; McLoon and Wirtschafter, 2002).

Enhanced Ca^{2+} homeostasis: Compared to limb muscles, EOM exhibit a number of characteristics predicting differences in their ability to buffer Ca^{2+} that would in part, provide mechanistic explanation of their unique patho-physiological properties. The fast twitch properties of EOM require a quick turnover of Ca^{2+} , which is supported by a large SR, high Ca^{2+} ATPase content and abundant mitochondria (Andrade et al., 2005; Felder et al., 2005; Kjellgren et al., 2003; Mayr, 1971; Porter and Karathanasis, 1998). This enhanced Ca^{2+} homeostasis of EOM has been proposed to play a role in the sparing of EOMs. Expression patterns of SERCA isoforms in EOMs are more complex and differ widely from those typical of limb muscles (Jacoby and Ko, 1993; Kjellgren et al., 2003). Several expression profiles implied that mRNA for proteins involved in Ca^{2+} homeostasis, such as S100a, PLN and SRL were up-regulated in EOM as compared to TA (Fischer et al., 2005; Fischer et al., 2002; Fraterman et al., 2007b; Khanna et al., 2004). Moreover, EOMs from DMD patients and animal models, such as mdx mice and dystrophic dogs lack dystrophic calcification seen in dystrophin-deficient limb muscles when treated with drugs that cause pathological increase in intracellular Ca^{2+} levels, such as the Ca^{2+} ionophore A23187 and the SERCA blocker cyclopiazonic acid. Moreover, EOMs demonstrated higher resistance to the anesthetic bupivacaine, which causes a rise in intracellular Ca^{2+} (Porter et al., 1988). This implies that EOMs are more resistant to pharmacologically elevated Ca^{2+} levels (Khurana et al., 1995). Another factor contributing to this superior Ca^{2+} homeostasis is the greater number of mitochondria of EOM compared to limb muscles, which are capable of quickly taking up a considerable amount of Ca^{2+} (Andrade et al., 2005; Fischer et al., 2002).

1.4 Aim of the study

The EOMs are a unique muscle allotype featuring characteristics that distinguish them from other skeletal muscle. Interestingly, they are enigmatically spared in DMD. While all other skeletal muscles deteriorate the EOMs remain morphologically and functionally healthy (Kaminski et al., 1992; Khurana et al., 1995).

The goal of this study is to characterize the spared EOM in the context of DMD pathology. By studying a spared muscle group it is hoped to reveal potentially protective mechanisms that occur in the spared muscle in the course of the disease. This may help to identify new therapeutic targets to be explored in subsequent studies. The reasons for the preferential sparing of EOM remain elusive. In the pathogenesis of DMD elevated Ca^{2+} levels are believed to be an early event and it has been shown that EOMs are protected from pharmacologically induced Ca^{2+} damage (Khurana et al., 1995; Porter et al., 1988). Moreover, the functional properties of superfast muscles, like the EOMs, imply very efficient Ca^{2+} turnover to maintain high frequency twitch contractions. However, so far the knowledge about the Ca^{2+} homeostasis in EOMs remains fragmentary and molecular and physiological details are lacking. Based on these points we hypothesize that EOMs are endowed with a superior Ca^{2+} homeostasis that enables them to remain protected from elevated Ca^{2+} level that might otherwise damage the muscle. To test this hypothesis we propose the following aims:

1) In the first aim the Ca^{2+} homeostasis of rodent EOMs (rats and mice) will be characterized and compared with the fast skeletal limb muscle, the TA-Tibialis anterior. Information about expression patterns of key Ca^{2+} handling proteins and their mRNAs will be obtained using biochemical and molecular methods, such as western blotting and qPCR. Furthermore, Fura-2 based Ca^{2+} measurements will be used to examine Ca^{2+} handling and buffering properties of primary cell cultures of EOM myotubes compared with TA myotubes.

2) The second aim will extend the investigations of the first aim based on recent reports about expression and function of Ca^{2+} channels of the TRP superfamily and the proteins Orai and STIM in skeletal muscle and their implications in the dysregulation of the Ca^{2+} homeostasis in DMD. The mRNA expression of TRPC, TRPV, TRPM and Orai and STIM proteins will be investigated in EOM compared with TA. Furthermore, the expression of selected members of these proteins group will be further explored on the transcript and protein level in EOM and TA tissue from mdx mice.

2. Materials and Methods

Whenever variations of materials or methods were used at the University of Pennsylvania (UPenn) or University of Greifswald (EMAU) it is indicated using the respective abbreviation of the university.

2.1 Materials

For conducting the experiments and analyzing the results the following materials and reagents were used.

2.1.1 Chemicals

<u>Chemical</u>	<u>Company</u>	<u>Cat#</u>
β -Mercaptoethanol	Sigma	M3148
Calcium chloride	Sigma	C1016
2-Methylbutane	Sigma	M32631
Bromphenol blue	Sigma	B3269
EDTA 0.5 M pH 8	Gibco	4284
EDTA (powder)	Sigma	431788
EGTA	Sigma	E3889
Ethanol 200 proof	Decon Laboratories	2701
Glacial acetic acid	Sigma	695084
Glucose	Sigma	158968
Glycerol	Invitrogen	15515-011
Glycine	Bio-Rad	161-0718
Hydrochloric acid (36 - 38%)	Sigma	H1758
HEPES acid	Sigma	H4034
Isopentane (2-methylbutane)	Sigma	M32631
Mannitol	Sigma	240184
Methanol	Sigma	M1775
Magnesium chloride	Sigma	M-8266
Non-fat dry milk	LabScientific	M0841
Paraformaldehyde	Sigma	P6148

Pluronic acid F127	Sigma	P2443
Potassium chloride	Sigma	P9541
SDS 10%	Gibco	1762
Sodium chloride	Sigma	S9888
Sodium HEPES	Sigma	H3784
Sodium hydroxide	Sigma	221465
Tris	Bio-Rad	161-0719
Tris-hydrochloride (powder)	Invitrogen	15506-017
Tris-hydrochloride (solution)	Sigma	88438
Triton X-100	Sigma	X-100
Trizma Base	Sigma	T06066

2.1.2 Reagents

<u>Reagent</u>	<u>Company</u>	<u>Cat#</u>
Antioxidant	Invitrogen	NP0005
BCP	MRC	BP151
Bio-Rad running buffer (10 x)	Bio-Rad	161-0732
Bovine serum albumin standard (conc. 1.44 mg/ml)	Bio-Rad	500-0007
Collagen 1	Sigma	C8919
Collagenase 4	Worthington Biochemical Corp.	4188
Complete Phosphatase Inhibitor Cocktail Tablets	Roche	1169749800
DC Assay Kit	Bio-Rad	500-0116
Dispase	Worthington Biochemical Corp.	2104
DMEM high glucose 4.5 mg/ml	Gibco	11965084
ECL Detection SuperSignal West Pico chemiluminescent substrate	ThermoScientific	34080
Fetal bovine serum	Hyclone	SH30074
bFGF	Promega	G507A
Fungizone	Invitrogen	15290018
Fura-2 AM 20 x 50 µg	Molecular Probes/Invitrogen	F1221

Gelcode Blue Stain Reagent	ThermoScientific	24590
Gel Mount Aqueous mounting medium	Sigma	F4680
Goat serum	ThermoScientific	31872
Ham's F10	Gibco	11550043
Horse serum	Invitrogen	16050122
Igepal CA-630	Sigma	I8896
Ionomylin calcium salt	Sigma	58168
L-Glutamine 100 x	Gibco/Invitrogen	25030081
Nuclease free water (10 x 50 ml)	Ambion	AM9937
Nupage Antioxidant	Invitrogen	NP0005
Nupage LDS sample buffer (4 x)	Invitrogen	NP0007
Nupage MES Running buffer (20 x)	Invitrogen	NP0002
Nupage MOPS Running buffer (20 x)	Invitrogen	NP0001
Nupage Reducing reagent (10 x)	Invitrogen	NP0004
O.C.T. tissue freezing medium	FisherScientific	15-183-13
PBS (w/o Ca ²⁺ and Mg ²⁺) (DPBS)	Invitrogen	11965084
Penicillin (10000 units) / Streptomycin (10 mg/ ml)	Invitrogen	15140122
PhosSTOP Phosphatase Inhibitor	Roche	04 906 845 001
Ponceau S	Sigma	P7170
PVDF membranes:		
- Immobilon P pore size 0.45 µm	Millipore	IPVH00010
- Immobilon PSQ pore size 0.2 µm	Millipore	ISE0920
Protein markers:		
- Precision Plus Kaleidoscope	Bio-Rad	161-0375
- Novex Sharp Protein Standard	Invitrogen	LC5800
Precast Gels:		
- 4-12 % Bis-Tris Gels (15 wells)	Invitrogen	0011971-0450
- 7.5 % Tris-HCl Gels	Bio-Rad	161-1100
Power SYBR Green	Applied Biosystems	4367659
Protease inhibitor Complete Mini	Roche	11 836 153 001
Restore Stripping Buffer	Thermo Fisher	21059

RNAlater	Ambion	AM7020
Rnase H	Invitrogen	18021014
Sterile Water (DEPC-treated)	Fisher	BP561
Sylgard 184/Silicone Elastomer	Swiss Composite	3097358-0503
TaqMan Universal Master Mix	Applied Biosystems	4304437
Trizol Reagent	Invitrogen	15596-026
Tween 20	Bio-Rad	170-6531

2.1.2 Consumables

<u>Consumable</u>	<u>Company</u>	<u>Cat#</u>
0.2 ml flat top PCR tubes	Molecular BioProducts	3412
0.5 ml tubes	USA Scientific	1605-4400
1.5 ml Eppendorf tubes	USA Scientific	1615-5510
60 mm cell culture dish	Corning	3295
100 mm cell culture petri dish	Greiner	P7612
100 mm round bottom culture tubes	USA Scientific	1485-0810
12 mm glass cover slips	FisherScientific	12-545-82
15 ml tubes	Corning	430790
384-well plates	Applied Biosystems	4309849
4-well Multiplates	Nunc	176740
50 ml tubes	Corning	430897
6-well plates Cellstar	Greiner	657160
75 mm round bottom culture tubes	USA Scientific	1450-0810
8-well chamber slides	Nunc	177445
96-well plates	Applied Biosystems	4306737
Aluminum foil heavy duty	Reynolds	624
Cell strainers 100 μ m	BD Biosciences	352360
Cell strainers 40 μ m	BD Biosciences	352340
Cover slips for staining	Fisher Scientific	12-545C
Glass petri dish	FisherScientific	08-747D
ImmEdge Pen	Vector Labs	H-4000
Optical adhesive film (MicroAmp)	Applied Biosystems	4311971

Parafilm	American National Can	01852-AB
Plastic wrap	FisherScientific	22-305654
RNAase ZAP	Ambion	AM9780
Scalpel No.21	Feather	GF12975-21
Serological pipets, 5 ml	Greiner BIO-ONE	608180
Serological pipets, 10 ml	Greiner BIO-ONE	607180
Serological pipets, 25 ml	Greiner BIO-ONE	760180
Stericup 1 l, 250 ml	Millipore	SCHV U11 RE
Steriflip, 50 ml	Millipore	SCGP00525
Styrofoam cups	CVS pharmacy	
Whatman paper	Invitrogen	LC2010

2.1.3 Equipment & Devices

<u>Equipment/Device</u>	<u>Company</u>
AB15 pH meter	Accumet
ABI Prism 7900HT	Applied Biosystems
Balance 602-S	Mettler Toledo
Balance AB104-S	Mettler Toledo
BioPhotometer 6131	Eppendorf
Cary 50 UV/Vis Spectrometer	Varian Analytical Instruments
Charge-coupled device (CCD) camera	Photon Technologies International
Cryostat Microm HM 500	Microm International
Diaphot Microscope	Nikon
Dissections instruments	F.S.T. fine science tools
Eppendorf Centrifuge 5415D	Eppendorf
Eppendorf centrifuge 5430R	Eppendorf
Fisher Vortex Genie	Fisher Scientific
Fujiimager Fuji LAS-3000	FujiFilm Medical Solutions
GeneQuantPro spectrophotometer	Amersham Pharmacia Biotech
Hofer EPS2A200 Power Supply	Hofer
MagnaFire CCD camera	Olympus
Mighty Small II SE250/SE260	Hofer

Milli-Q Biocell	Millipore
Mini Trans-Blot Cell system	Bio-Rad
NanoDrop 1000	Thermo Scientific
Olympus BX51 Fluorescence Microscope	Olympus
Peltier Thermal Cycler PTC-200	Applied Biosystems
Polytron	Brinkmann Instruments
Power Pac HC	Bio-Rad
PowerPac HC	Bio-Rad
Shaker Orbit 1000	Labnet International
Speedmill P12 homogenizer	Analytikjena
Stereomicroscope	Olympus
TaqMan 5700 Sequence Detection System	Applied Biosystems
Thermomixer	Eppendorf
Tissue Raptor	Biospec Products
Wild Heerbrugg M5 Stereomicroscope	Wild Heerbrugg

2.1.4 Animals

Animals were accommodated at the animal facility of the University of Pennsylvania (UPenn) and the Ernst-Moritz-Arndt University of Greifswald (EMAU) in accordance with the guidelines of animal use and welfare of the respected university. Adult Sprague Dawley rats were obtained from Charles River Laboratories (USA) and bred at the animal facility of UPenn to obtain pups of the desired age. C57Bl/10ScSn/J and C57Bl/10ScSn-Dmd^{mdx}/J mice were obtained from Jackson Laboratories, USA (UPenn) or were bred at EMAU, originally obtained from Charles River Wiga GmbH, Sulzfeld, Germany.

2.1.5 Solutions and buffers for SDS-Page and Western blotting

TNEC lysis buffer:

50 mM Tris-HCL pH 8.0 (1 M stock solution)	2.5 ml
150 mM NaCl (4 M stock solution)	1.88 ml
1% Igepal	0.5 ml

2 mM EDTA (0.5 M stock solution)	0.2 ml
Protease inhibitor	1 cocktail tablet/50 ml
PhosStop phosphatase inhibitor	1 cocktail tablet/10 ml

The reagents were dissolved in a final volume of 50 ml in Milli-Q water, aliquoted and frozen at -20 °C. The volumes are referring to the stock solutions. Protease and phosphatase inhibitor tablets were added just before use according to the buffer volume used.

10 x Transfer buffer:

0.25 M Trizma Base	30.3 g
1.92 M Glycine	144 g

The chemicals were dissolved in 1 l of Milli-Q water, pH should be 8.3 and was not adjusted.

1 x Transfer buffer for calmodulin western blot:

100 ml of the 10 x transfer buffer were diluted in 900 ml of DI-water and 2 mM CaCl₂ were added.

10 x TBS:

0.5 M Tris	60.5 g
1.5 M NaCl	87.6 g

The chemicals were dissolved in 1 l Milli-Q water and the solution was filtered using a 1 l Stericup.

1 x TBST:

100 ml of 10 x TBS were diluted in 900 ml of Milli-Q water and pH was adjusted to 7.4 with concentrated HCl. Finally, 1 ml of Tween 20 was added to a final concentration of 0.1 %.

Milk/TBST blocking solutions:

5 % non-fat dry milk in 1 x TBST
1 % non-fat dry milk in 1 x TBST

The solutions were made up freshly and stirred for at least one hour before use and stored at 4 °C for up to two days. For detection of TRPV4 and Orai1 the 5 % milk/TBST solution was centrifuged at 7000 rpm for 10 min and the supernatant was used for blocking.

2 x SDS sample loading buffer:

0.25 mM Tris/HCl pH 6.8

20 % Glycerol

10 % β -Mercaptoethanol

2 % SDS

0.1 % Bromophenol blue

Chemicals were dissolved in Milli-Q water and stored at 4 °C.

20 x MOPS or MES running buffer and 10 x Bio-Rad running buffer:

1 x running buffer were prepared using DI-water.

Fixation solution for gels run with MOPS or MES buffer:

(see GelCode Blue Stain Reagent Instructions)

50 % methanol

7 % glacial acetic acid

Chemicals were mixed in DI-water and the solution was stored at RT for up to 4 weeks.

2.1.7 Solutions for immunohisto- and cytochemistry**4 % Paraformaldehyde:**

4 g paraformaldehyde were dissolved in 50 ml 1 x PBS and heated under stirring to 54 °C until turbidity started to clear. Concentrated NaOH was slowly added until solution was completely clear. The solution was allowed to reach room temperature. The pH was adjusted to 7.4 and the solution was filtered using a stericup with 0.2 μ m pore size.

0.05 % Triton X-100/PBS:

0.05 % Triton X-100 was added to 1 x PBS, vortexed and stored at 4 °C up to one week.

Blocking solution 10 % goat serum/PBS:

10 % goat serum was added to 1 x PBS and stored at 4 °C up to one week.

2.1.8 Primary antibodies

Antibody	Host	Company	Cataloge #
Anti-SERCA1	mouse monoclonal	Affinity Bioreagents (now ThermoScientific)	MA3-919
Anti-SERCA2	mouse monoclonal	Affinity Bioreagents (now ThermoScientific)	MA3-912
Anti-CASQ	rabbit polyclonal	Affinity Bioreagents (now ThermoScientific)	PA 1-913
Anti-CALM	rabbit polyclonal	Affinity Bioreagents (now ThermoScientific)	MA3-918
Anti-CAMKIIB	mouse monoclonal	Abnova	H00000816-M02
Anti-PLN	mouse monoclonal	Affinity Bioreagents (now ThermoScientific)	MA3-922
Anti-PLN-Phospho-Ser16	rabbit polyclonal	Badrilla, UK	A010-12
Anti-PLN-Phospho-Thr17	rabbit polyclonal	Badrilla, UK	A010-13
Anti-FYXD (Phospholemman)	rabbit polyclonal	Abcam	ab76597
Anti-ORAI1 (CT)	rabbit polyclonal	ProSci Incorporated	4281
Anti-STIM1	rabbit polyclonal	ProSci Incorporated	4119
Anti-TRPC1	rabbit polyclonal	Alomone Labs	ACC-016
Anti-TRPC3	rabbit polyclonal	Alomone Labs	ACC-010
Anti-TRPV4	rabbit polyclonal	Alomone Labs	ACC-034
Anti-Desmin	mouse monoclonal	Sigma	D1033
Anti-Myogenin	mouse monoclonal	IMGENEX	IMG-131
Anti-alpha-Actinin	mouse monoclonal	Sigma	A7811

Table 2.1: List of primary antibodies used in this thesis.

2.1.9 Secondary antibodies and nucleic acid (nuclear) stain

Goat anti-mouse-IgG HRP-conjugated antibody, Jackson ImmunoResearch, 115-035-003

Goat anti-rabbit-IgG HRP-conjugated antibody, Jackson ImmunoResearch, 111-035-003

Goat anti-mouse-IgG Alexa-Fluor-546-conjugated antibody, Molecular Probes, A-11003

Goat anti-rabbit-IgG Alexa-Fluor-546-conjugated antibody, Molecular Probes, A-11010

Nuclear stain Hoechst 33342, Sigma, B2261

2.1.10 Solutions for cell culture of primary myoblasts

Enzyme mix:

10 mg/ml Collagenase 4

2.4 U/ml Dispase

5 mM CaCl₂ in 1 x PBS

Growth medium:

Ham's F10 medium
20 % FBS
1 % Pen/Strep
1 % fungizone
5 ng/ml FGF

Differentiation medium:

Ham's F10/DMEM medium 1:1
5 % horse serum
1 % Pen/Strep

2.1.11 Solutions for calcium imaging**Isotonic solution:**

105 mM NaCl
4.5 mM KCl
2.8 mM Na HEPES
7.2 mM HEPES acid
1.3 mM CaCl₂
0.5 mM MgCl₂
5 mM glucose
75 mM mannitol

The chemicals were dissolved in 1 l of MilliQ-water, the pH was adjusted to 7.4 and filtered using a 1 l Stericup.

Isotonic solution containing 300 nM free Ca²⁺:

Isotonic solution containing
820 μM Ca²⁺
1 mM EGTA

Minimum calibration solution:

Isotonic solution containing
10 mM EGTA
5 μ M ionomycin
pH 8

Maximum calibration solution:

Isotonic solution containing
5 μ M ionomycin
pH 8

High K⁺ solution:

Isotonic solution containing
50 mM KCl
60 mM NaCl

Fura-2 mix:

10 μ M Fura-2 AM
20 % pluronic acid F127

2.1.12 Molecular biology kits & reagents**2.1.12.1 Molecular biology kits**

RNeasy Mini Kit	Qiagen, cat #74104
RNeasy Fibrous Tissue Mini Kit	Qiagen, cat #74704
RNase-free DNase Set	Qiagen, cat #79254
SuperScript First-Strand Synthesis System for RT-PCR	Invitrogen, cat # 11904-018
TaqMan Gold RT-PCR Kit	Applied Biosystems, cat# N808-0234

2.1.12.2 Reverse Transcription (RT) reaction mixes**Superscript First Strand Synthesis:**

1 x reaction mix:

Up to 5 µg RNA	n µl
10 mM dNTP mix	1 µl
Oligo(dT)12-18 Primers	1 µl
Nuclease-free water	to 10 µl

After incubation at 65 °C for 5 min followed by > 1 min chilling on ice, 9 µl of the following mix was added:

10 x RT buffer	2 µl
25 mM MgCl ₂	4 µl
0.1 M DTT	2 µl
RnaseOUT Recombinant RNase Inhibitor	1 µl

After incubation for 2 min at 42 °C, 1 µl of reverse transcriptase was added and the reaction was continued for 50 min at 42 °C followed by 15 min at 70 °C. The reaction was finished by addition of 1 µl of RNase H and incubation at 37 °C for 20 min.

TaqMan Gold RT-PCR:**1x reaction mix:**

10 x RT buffer	10 µl
25 mM MgCl ₂	22 µl
2 mM dNTP mix	20 µl
RNase Inhibitor	2 µl
Random hexamers	5 µl
Reverse transcriptase	2.7 µl
RNA	400 ng
Nuclease-free water	to 100 µl

Thermal cycling program:

25 °C 10 min	Hexamer incubation
37 °C 60 min	Reverse transcription
95 °C 5 min	Enzyme inactivation
4 °C ∞	Cooling

2.1.12.3 Primers and Probes

Primers for SYBR Green quantitative polymerase chain reaction (qPCR):

Gene	Accession number	Amplicon size	Sequence 5' - 3'
Atp2a1	NM_017290	101 bp	FW: GCTCGGAACTATCTGGAGGGA RV: GGCACAAGGGCTGGTACTTC
Atp2a2	NM_058213.1	102 bp	FW: GGGAGAACATCTGGCTCGTG RV: GCGGTGTGATCTGGAAAATGA
Atp2b1	NM_053311	101 bp	FW: GTAGTGGCCGTGATTGTTCGC RV: AGCGTGTCCATGATGAGGTTG
Atp2b4	NM_001005871	101 bp	FW: ACAAGCCCCTGATCTCTCGC RV: CAGTTTGTGCCAGCAAAGAC
Cacna1s	L04684.1	101 bp	FW: CCCCTGTCATGGCTAACCAA RV: GCCTGGGTTCTGAGGGAAGTC
Calmodulin 1	NM_031969	102 bp	FW: AATCCGTGAGGCATTCCGAG RV: TCTGTTAGCTTTTCCCCGAGG
Calsequestrin1	XM_001063867	103 bp	FW: GACTTCCCACTGCTGGTCCC RV: TCCATATGCTGTCCGCATCC
Calsequestrin2	NM_017131	102 bp	FW: GGAGCATCAAAGACCCACCC RV: TTCTCCGCAAATGCCACAAT
Gapdh	NM_017008	195 bp	FW: CCATGGAGAAGGCTGGGG RV: CAAAGTTGTCATGGAT
Ncx1/Slc8a1	NM_019268	101 bp	FW: TTGTCGCTCTTGGAACCTCAG RV: GCTTCCGGTGACATTGCCTAT
Parvalbumin	NM_022499	103 bp	FW: CATTGAGGAGGATGAGCTGGG RV: CTTGTCTCCAGCAGCCATCAG
Phospholamban	NM_022707	105 bp	FW: GCTGAGCTCCCAGACTTCACA RV: TTGACAGCAGGCAGCCAAAC
Regucalcin	NM_031546	103 bp	FW: ACGTGACATGTGCCAGGGAT RV: GCAATTCCTTTGACCCCAAGA
Ryanodine Receptor 1	XM_341818	101 bp	FW: CAAGCGGAAGGTTCTGGACA RV: TGTGGGCTGTGATCTCCAGAG
S100a1	NM_001007636	101 bp	FW: AGAACCTGCTCCGACGTCAG RV: GGGCATGGAACACATTGATGA
Sarcalumenin	XM_220171	104 bp	FW: CCCACATCGAGAAAACCCTGA RV: GGGCTTGATGGATGTGTGGTA
Sarcolipin	NM_001013247	101 bp	FW: CAGGACGTGAAGACGAGCCA RV: CAGCTCCTGGGTAGACCGCT
Troponin C1	NM_001034105	101 bp	FW: TGTCGGATCTCTTCCGCATG RV: TTCCGTGATGGTCTCACCTGT
Troponin C2	NM_001037351	101 bp	FW: GCCATCATCGAGGAGGTGG RV: TTCCCTTTCGCATCCTCTTTC

Table 2.2: Primers used for SYBR Green qPCR: 100 μ M primer stock solutions were diluted 1:10 to obtain 10 μ M working mixes, which were stored at 4 $^{\circ}$ C for up to four weeks.

Primers for TaqMan Assay based qPCR:

Commercially available TaqMan Assays were obtained from Applied Biosystems.

Additional primer sets and probes were obtained from TIBMOL-BIOL.

Gene	Accession number	Amplicon size	Assay ID
TRPC1	NM_011643	130 bp	Mm00441975_m1
TRPC2	NM_011644	72 bp	Mm00441984_m1
TRPC5	NM_009428	105 bp	Mm00437183_m1
TRPC6	NM_13838	153 bp	Mm00443441_m1
TRPC7	NM_012035	23 bp	Mm00442606_m1
TRPV2	NM_011706	99 bp	Mm00449223_m1
TRPV3	NM_145099	56 bp	Mm00454996_m1
TRPV4	NM_022017	55 bp	Mm00499025_m1
TRPV6	NM_22413	58 bp	Mm00499069_m1
TRPM1	NM_018752	100 bp	Mm00450619_m1
TRPM5	NM_020277	65 bp	Mm00498453_m1
TRPM7	NM_021450	115 bp	Mm00457998_m1
TRPM8	NM_134252	88 bp	Mm00454566_m1
18S TaqMan ribosomal RNA control reagents			Part# 4308329

Table 2.3: List of TaqMan Assays used for qPCR obtained from Applied Biosystems.

Gene	Accession number	Fragment size	Sequence 5' - 3'
TRPC3	NM_019510	180 bp	FW: CCAAGCTGGCCAACATAGAG RV: GGCAAGTTTGACACGACTCA Probe: ACTCGGAGGAGGTGGAAGCCATTC
TRPC4	NM_016984	209 bp	FW: TGGAGTGGATGATATTACCG RV: CCACATGTCCCATGATTC Probe: TGTGATGAACCTTGTATCTGGCAACAA
TRPV1	XM_112546	321 bp	FW: GCATCTTCTACTTCAACTTCTTCGTC RV: CCACATACTCCTTGCGATGGC Probe: CAAACTCTTGAGGGATGGTCGCCTCT
TRPV5	XM_112633	281 bp	FW: CAAGAAGAAAAGAGGCTCGAC RV: AATGACTGTCACCAACTCCC Probe: CCGTACACATGTTTCGAGATAACACCATCA
TRPM2	NM_138301	187 bp	FW: CAGATCCCAACCTACATTGACG RV: GAAGGTGTAGTTGAACATGGCGA Probe: ACCAGTGCAGCCCCAATGGCA
TRPM3	NM_177341	157 bp	FW: CAAAGATGACATGCCCTATATGA RV: CTTTCTTCTGGATGATTCCT Probe: ATGAAGAGGACATGGAGCTAACAGCAA
TRPM4	NM_175130	176 bp	FW: CCCTGAGGATGGTGTGAGT RV: AGGAGCACTGGGATGTCAAT Probe: CTTCTTGGTGGATGATGGCACC
TRPM6	NM_153417	219 bp	FW: CCAGGTGCCGTAATAACA RV: CTCTTGTGGCTGCCTTAGGT Probe: CAGTTGAATGCAGAGCCAGGAGAAAC

Table 2.4. List of primers and probe sets used for qPCR obtained from TIBMOL-BIOL.

2.1.12.4 SYBR Green reaction

1x reaction:

Power SYBR Green Master Mix (10 x)	10 μ l
Primer FW	1 μ l
Primer RV	1 μ l
Template cDNA	5 ng
Nuclease-free water	to 8 μ l
	Total volume 20 μ l

A typical setup of a 384-well qPCR plate is shown in Fig. 2.3.

Thermal cycling conditions:

50 °C 2 min	Pre-incubation
95 °C 10 min	Polymerase activation
95 °C 15 sec	Melting
60 °C 1 min	Annealing/Elongation
→	Repeat 40 times

Melting curve conditions:

95 °C 15 sec	Melting
60 °C 20 sec	Annealing
95 °C 15 sec	Melting
4 °C ∞	Cooling

2.1.12.5 TaqMan reaction

1 x reaction:

TaqMan Universal Master Mix	10 μ l
TaqMan Primer Mix	2 μ l
Template cDNA	2 μ l
Nuclease-free water	6 μ l
	Total volume 20 μ l

20 x primer mixes from Applied Biosystems were diluted 1:1 before use. TIBMOB-BIOL primers (FW and RV) and probes were mixed according to individual molar ratios. Eight ng of template were used per reaction and the template for 18s reaction was diluted 1:500. Genes were run in duplicates and a typical setup of a 96-well qPCR plate is shown in Fig. 2.4.

Thermal cycling conditions:

50 °C 2 min	Pre-incubation
95 °C 10 min	Polymerase activation
95 °C 15 sec	Melting
60 °C 1 min	Annealing / Elongation
4 °C ∞	Cooling

	1	2	3	4	5	6	7	8	9	10	11	12	13	14	15	16	17	18	19	20	21	22	23	24
EOM 1 A	GAPDH	GAPDH	GAPDH	Serca1	Serca1	Serca1	Serca2	Serca2	Serca2	Casq1	Casq1	Casq1	Casq2	Casq2	Casq2	Pln	Pln	Pln	Tnnc1	Tnnc1	Tnnc1	Tnnc2	Tnnc2	Tnnc2
EOM 2 B	GAPDH	GAPDH	GAPDH	Serca1	Serca1	Serca1	Serca2	Serca2	Serca2	Casq1	Casq1	Casq1	Casq2	Casq2	Casq2	Pln	Pln	Pln	Tnnc1	Tnnc1	Tnnc1	Tnnc2	Tnnc2	Tnnc2
EOM 3 C	GAPDH	GAPDH	GAPDH	Serca1	Serca1	Serca1	Serca2	Serca2	Serca2	Casq1	Casq1	Casq1	Casq2	Casq2	Casq2	Pln	Pln	Pln	Tnnc1	Tnnc1	Tnnc1	Tnnc2	Tnnc2	Tnnc2
TA 1 D	GAPDH	GAPDH	GAPDH	Serca1	Serca1	Serca1	Serca2	Serca2	Serca2	Casq1	Casq1	Casq1	Casq2	Casq2	Casq2	Pln	Pln	Pln	Tnnc1	Tnnc1	Tnnc1	Tnnc2	Tnnc2	Tnnc2
TA 2 E	GAPDH	GAPDH	GAPDH	Serca1	Serca1	Serca1	Serca2	Serca2	Serca2	Casq1	Casq1	Casq1	Casq2	Casq2	Casq2	Pln	Pln	Pln	Tnnc1	Tnnc1	Tnnc1	Tnnc2	Tnnc2	Tnnc2
TA 3 F	GAPDH	GAPDH	GAPDH	Serca1	Serca1	Serca1	Serca2	Serca2	Serca2	Casq1	Casq1	Casq1	Casq2	Casq2	Casq2	Pln	Pln	Pln	Tnnc1	Tnnc1	Tnnc1	Tnnc2	Tnnc2	Tnnc2
EOM 1 G	Pmca1	Pmca1	Pmca1	Pmca4	Pmca4	Pmca4	Srl	Srl	Srl	NTC GAPDH	NTC GAPDH	NTC Tnnc1	NTC Tnnc1											
EOM 2 H	Pmca1	Pmca1	Pmca1	Pmca4	Pmca4	Pmca4	Srl	Srl	Srl	NTC Serca1	NTC Serca1	NTC Tnnc2	NTC Tnnc2											
EOM 3 I	Pmca1	Pmca1	Pmca1	Pmca4	Pmca4	Pmca4	Srl	Srl	Srl	NTC Serca2	NTC Serca2	NTC Pmca1	NTC Pmca1											
TA 1 J	Pmca1	Pmca1	Pmca1	Pmca4	Pmca4	Pmca4	Srl	Srl	Srl	NTC Pln	NTC Pln	NTC Pmca4	NTC Pmca4											
TA 2 K	Pmca1	Pmca1	Pmca1	Pmca4	Pmca4	Pmca4	Srl	Srl	Srl	NTC Casq1	NTC Casq1	NTC Srl	NTC Srl											
TA 3 L	Pmca1	Pmca1	Pmca1	Pmca4	Pmca4	Pmca4	Srl	Srl	Srl	NTC Casq1	NTC Casq1													

Figure 2.3. Plate set-up 324-well plate (UPenn).

	1	2	3	4	5	6	7	8	9	10	11	12
A	std1 10e6	std2 10e5	std3 10e4	std4 10e3	std5 10e2	EOM 1	EOM 2	EOM 3	EOM 4	EOM 5	EOM 6	EOM 7
B	Std1 10e6	std2 10e5	std3 10e4	std4 10e3	std5 10e2	EOM 1	EOM 2	EOM 3	EOM 4	EOM 5	EOM 6	EOM 7
C	EOM 8	EOM 9		EOM mdx 1	EOM mdx 2	EOM mdx 3	EOM mdx 4	EOM mdx 5	EOM mdx 6	EOM mdx 7	EOM mdx 8	EOM mdx 9
D	EOM 8	EOM 9		EOM mdx 1	EOM mdx 2	EOM mdx 3	EOM mdx 4	EOM mdx 5	EOM mdx 6	EOM mdx 7	EOM mdx 8	EOM mdx 9
E	std1 10e6	std2 10e5	std3 10e4	std4 10e3	std5 10e2	EOM 1	EOM 2	EOM 3	EOM 4	EOM 5	EOM 6	EOM 7
F	Std1 10e6	std2 10e5	std3 10e4	std4 10e3	std5 10e2	EOM 1	EOM 2	EOM 3	EOM 4	EOM 5	EOM 6	EOM 7
G	EOM 8	EOM 9		EOM mdx 1	EOM mdx 2	EOM mdx 3	EOM mdx 4	EOM mdx 5	EOM mdx 6	EOM mdx 7	EOM mdx 8	EOM mdx 9
H	EOM 8	EOM 9		EOM mdx 1	EOM mdx 2	EOM mdx 3	EOM mdx 4	EOM mdx 5	EOM mdx 6	EOM mdx 7	EOM mdx 8	EOM mdx 9

Gene 1

Gene 2

Figure 2.4: Plate set-up 96-well plate (EMAU).

2.1.13 Software and Databases

Microsoft Office 2007	Microsoft
Adobe Acrobat 9.0 Professional	Adobe
Adobe Photoshop 6.0	Adobe
Adobe Illustrator CS3	Adobe
GraphPad Prism 5.0	GraphPad Software
ImageJ	Wayne Rasband National Institutes of Health, USA http://rsb.info.nih.gov/ij
EndnoteX	Thompson
Primer Express 1.5	Applied Biosystems
7900 SDS v2.3	Applied Biosystems
SDS software 5700 Sequence Detection System	PE Applied Biosystems
NCBI (National Center for Biotechnology Information)	http://www.ncbi.nlm.nih.gov
Pubmed (National Library of Medicine)	http://www.ncbi.nlm.nih.gov/pubmed
REST 2005	http://www.gene-quantification.de/rest-2005.html
Felix spectroscopy software	Photon Technology International

2.2 Methods

Standard research protocols conducted in this thesis were performed using methods described by (Ausubel, 1999) or (Sambrook, 1989), unless otherwise stated.

2.2.1 Tissue dissection

Adult animals, Sprague Dawley rats, male and female 200 - 300 g or adult mice, 8 - 14 weeks of age, were sacrificed using CO₂ asphyxiation (UPenn) or by ether inhalation (EMAU). Muscles were dissected rapidly and conserved according to the subsequent application.

Sterile PBS was used to keep muscles moist during dissections of EOM and TA. EOM muscles were dissected by carefully removing the eyeball from the bony orbit with the muscles attached using a scalpel or scissors cutting alongside the bones. After the eyeball was dissected free from non-EOM orbital content (connective tissue and glandular tissue), it was pinned facing down in a PBS filled sylgard dish in such a way that the optic nerve was pointing upwards. After that the tissue surrounding the eye muscles was carefully removed using fine scissors until the four recti muscles were visible (Fig. 2.1 A). When individual muscles were required, e.g. for protein lysates or RNA isolation, individual rectus muscles were carefully dissected away from the eyeball starting near the optic nerve toward the proximal tendon (Fig. 2.1 B). TA muscles were dissected using standard methods by first removing the skin and connective tissue covering the muscle. Then the tendon was freed and cut and by holding the muscle by the tendon it was lifted off the bone releasing it from surrounding tissue using scissors.

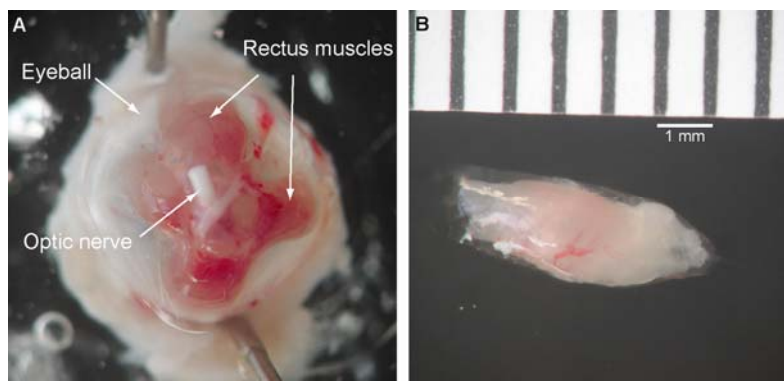


Fig. 2.1: Images of dissected rat EOMs. (A) The four rectus muscles still attached to the eyeball surrounding the optic nerve in the center. (B) Individual rectus muscle.

2.2.2 Tissue preservation

RNA isolation:

Individually dissected EOM recti muscles were pooled and TA muscles were immediately placed in RNAlater. The samples were kept at 4 °C over night before transfer to -20 °C for longterm storage. The table shows the amounts of RNA later used for the different muscle types/amounts:

Species	Muscle (#)	RNAlater (μl)
Rat	EOM (4 recti)	500
Rat	TA (1/4)	1000
Mouse	EOM (8 recti)	300
Mouse	TA (1)	500

Alternatively (at EMAU), harvested tissues were flash frozen in liquid nitrogen and stored at -80 °C until use for RNA isolations.

Western Blotting:

Individually dissected EOM recti muscles or TA muscle were placed in Eppendorf tubes, flash frozen in liquid nitrogen and stored at -80 °C.

Immunohistochemistry:

The eye balls of the animals were carefully dissected from the bony orbit. While the EOMs were still attached to the eyeball, the EOMs were freed of any connective and gland tissue. Eyeballs were placed lens down on labeled pieces of styrofoam, covered with OCT and frozen in isopentane cooled using liquid nitrogen for at least one minute. TA muscles were dissected from the animals, placed on styrofoam, covered with OCT and frozen in the same way. Samples were stored in 50 ml tubes at -80 °C.

2.2.3 Western blotting

Western blot analysis facilitates specific detection of proteins and a semi-quantitative estimation of protein levels. Proteins were immuno-detected after binding to a polyvinylidene fluoride (PVDF) membrane and visualized using enhanced chemoluminescence (ECL). Antigen structures of the target proteins were detected using specific primary antibodies.

Bound primary antibody was detected by a secondary antibody (goat anti-mouse-IgG or Goat anti-rabbit-IgG) conjugated with horseradish peroxidase (HRP). HRP catalyses the oxidation of luminol and the chemiluminescence signal can be detected as blackening of ECL-film, or as in this thesis the signal was detected digitally using a Fuji Imager.

2.2.3.1 Sample preparation for Western blotting

Crude whole muscle samples were prepared from flash frozen rat or mouse muscle samples using TNEC lysis buffer. The following buffer volumes were used for individual muscle preparations:

Species	Muscle (#)	TNEC lysis buffer (μ l)
Rat	EOM (4 recti)	400
Rat	TA (1/4)	1000
Mouse	EOM (8 recti)	200
Mouse	TA (1)	400

The samples were placed into 1.5 ml Eppendorf tubes with the lysis buffer and were briefly chopped with small dissection scissors into small pieces. Then the samples were transferred to 75 mm round bottom bacterial culture tubes (mouse muscle) or 100 mm round bottom bacterial culture tube (rat muscle). The samples were then homogenized using a Tissue Raptor (mouse muscle) or a Polytron (rat muscle) until no more clumps were visible. Homogenates were centrifuged at 4 °C for 20 min. The supernatant was aliquoted and stored at -80 °C.

2.2.3.2 Determination of protein concentration

The protein concentrations of the lysates were determined using the DC Assay (Bio-Rad), a colorimetric assay based on the Lowry method (Lowry et al., 1951). The following dilutions of a bovine serum albumin standard (stock solution 1.44 mg/ml) were used to generate a standard curve: 0.2, 0.5, 0.75, 1.0, 1.2 (mg/ml). The protocol was followed according to the manufacturer's protocol. The standards were treated in the same way as the samples. The protein samples were diluted 1:5 in Milli-Q water to a final volume of 20 μ l and

the reagent volumes were downscaled 1:5 accordingly. A blank was generated by adding 4 μ l TNEC lysis buffer to 16 μ l Milli-Q water. The working solution “reagent A’ ” was made up by adding 20 μ l of reagent S (DTT) to each ml of reagent A (alkaline copper tartrate solution). Then 100 μ l of reagent A’ were added to each sample and vortexed. 800 μ l of reagent B were added followed by immediate vortexing. After samples were incubated for 15 min at room temperature absorbance was measured at 750 nm using a Cary UV/Vis spectrometer.

2.2.3.3 SDS Page electrophoresis

SDS page electrophoresis (Laemmli, 1970) facilitates the separation of protein samples according to their electrophoretic mobility, which is determined by molecular weight and charge. A gel consists of a separating gel on top of which typically a low percentage (5 %) stacking gel is cast. The stacking gel condenses the proteins into a tight band before entering the separating gel. The percentage of the separating gel indicates its polyacrylamide content, which corresponds to its pore size and therefore the ability to separate proteins according to size. Higher percentage gels have smaller pores and are suitable for smaller proteins, whereas lower percentage gels have larger pores and are suitable for larger proteins. Gradient gels provide a gradient of pore size from large to small to separate a wide range of protein sizes. Protein samples are mixed with sample buffer, usually containing SDS and a reducing agent, such as β -mercaptoethanol to reduce disulfide bonds. SDS attaches to the protein giving it a uniform negative charge. Therefore, migration of the protein through the gel remains solely dependent on the size of the protein.

SDS page was performed using the NuPage precast gels (Invitrogen) for most proteins or the Bio-Rad precast gel system as described by the manufacturers.

Nupage gels:

Nupage gels were loaded with 10 - 75 μ g of protein per well and the samples were prepared as follows:

Sample	x μ l
Nupage LDS sample buffer (4 x)	2.5 μ l
Nupage reducing reagent (10 x)	1 μ l
Milli-Q water	to 6.5 μ l

For a 10 μ l reaction mix, the ingredients were combined, mixed and incubated at 70 °C for 10 min before loading on the gel. Volumes were upscaled when necessary.

4 - 12 % precast Bis/Tris gels were used either in combination with 1 x MES running buffer for PLN and CALM or in combination with 1 x MOPS running buffer for all other larger proteins.

Bio-Rad gels:

The Bio-Rad system (Mini-Trans-Blot cell system) was used to run 7.5 % precast Tris/HCl gels to separate CASQ1 and CASQ2. 75 μ g of protein were mixed with an equal volume of 2 x SDS sample loading buffer. The samples were heated to 95 °C for 5 min before loading on the gel.

All samples were briefly centrifuged to collect all material before loading on the gel. All gels were run under reducing conditions except for the PLN gels and unless indicated otherwise. The gels were run initially at 80 V for 30 min to condense the proteins in the stacking gel. The separation gel was run at 110 V for another 45 – 60 min depending on the desired running distance of the proteins. This was judged according to the separation of the standard or the progression of the lead dye.

2.2.3.4 Protein transfer (blotting)

Immediately after running the proteins on the gel they were transferred onto a PVDF membrane using electrophoresis. For the wet transfer of all proteins the Bio-Rad Mini Trans-Blot cell system was used. To set up the blotting sandwich in the gel-holder cassette, the hydrophobic PVDF membrane was hydrated and equilibrated by immersion in methanol for about 30 s followed by immersion in 1 x transfer buffer. Two Whatman papers and foam pads were soaked in transfer buffer. Then one Whatman paper was placed onto a foam pad followed by the gel and the equilibrated membrane. Lastly, the other Whatman paper and the

second foam pad were placed on top of the membrane. The gel-holder cassette was closed and placed in between the electrodes and the tank was filled with transfer buffer. The proteins were usually transferred onto Immobilon-P PVDF membranes for 1.25 h at 100 V. Small proteins, such as PLN and CALM, were transferred onto Immobilon-PSQ PVDF membranes with a smaller pore size for 50 min at 80 V. The transfer buffer for CALM also contained 2 mM CaCl_2 to enhance binding of CALM to the membrane (McKeon and Lyman, 1991). After the transfer the membrane was stained with Ponceau S for about 1 min to verify equal loading and efficient transfer (Fig. 2.2 A). Similarly, the gel was stained with GelCode blue stain reagent after fixation in 50 % MeOH/7 % glacial acetic acid for 15 min and washed twice in DI-water for 10 min each according to the manufacturer's instructions to verify efficient transfer of proteins (Fig. 2.2 B). Before protein detection the membrane was washed in 1 x TBST to remove the Ponceau S staining.

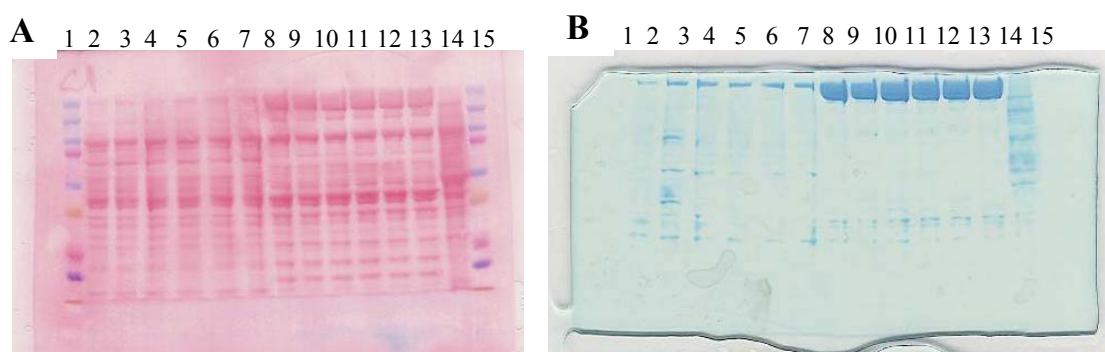


Fig. 2.2: Examples of a PVDF membrane and a protein gel after transfer. (A) Ponceau S stained membrane. (B) 4-12% Bis/Tris gel of the same run stained with GelCode (from left to right: lane 1 Marker, lanes 2-7 EOM, lanes 8-13 TA, lane 14 brain, lane 15 Marker).

2.2.3.5 Protein detection

Non-specific binding sites on the membrane were blocked using blocking solution (5 % non-fat dry milk in TBST) for 1 h at room temperature while shaking at 60 rpm or in case of TRPV4 and Orai1 over night at 4 °C. Primary antibodies were diluted in 1 % milk/TBST blocking solution and incubated either over night (oN) at 4 °C or for two hours at room temperature as follows:

Antibody	Dilution	Incubation
Anti-SERCA1	1:3000	oN or room temp.
Anti-SERCA2	1:1000	oN
Anti-CASQ	1:2500	oN
Anti-CALM	1:2000	oN
Anti-CAMKIIB	1:500	oN
Anti-PLN	1:1000	oN or room temp.
Anti-PLN-Phospho-Ser16	1:7000	oN or room temp.
Anti-PLN-Phospho-Thr17	1:7000	oN or room temp.
Anti-FYXD (Phospholemman)	1:1000	oN or room temp.
Anti-Orail (CT)	1:500	oN
Anti-STIM1	1:1000	oN or room temp.
Anti-TRPC1	1:750	oN
Anti-TRPC3	1:1000	oN or room temp.
Anti-TRPV4	1:750	oN

Table 2.5: List of dilutions and incubation times of primary antibodies used for western blotting.

After incubation with the primary antibody, blots were washed three times in 1 x TBST for 5 min each. The appropriate secondary antibody was diluted 1:15000 in 1 % milk/TBST blocking solution and incubated at room temperature for 1.5 h followed by three washes in 1 x TBST for 5 min each.

The blots were incubated for 2 min in ECL working solution. The chemiluminescence signal was detected using a LAS-3000 Fuji Imager. Images were saved and exported as TIF files and used for quantification.

2.2.3.6 Stripping of blot membranes

The membrane was washed in TBST twice for 5 min each before incubation with Restore Stripping buffer for 15 – 20 min. A dry membrane was re-wetted in methanol before washing in TBST. After incubation in stripping buffer the membrane was washed three times in TBST and blocked again in 5 % milk/TBST for 30 min. Then the membrane was ready again for reprobing.

2.2.3.7 Protein quantification using densitometry

The amount of protein was estimated by quantifying the protein bands densitometrically using ImageJ software. The image of each blot was saved in grayscale mode. A rectangular box was drawn around each protein band and kept the same for each protein and blot. The amount of protein represented by the gray value was measured in arbitrary units (AU).

2.2.4 Immunohisto- and cytochemistry

Immunostaining facilitates the detection of specific antigens in frozen or paraffin-embedded tissue sections. In this thesis fluorochrome (Alexa-Fluor) conjugated secondary antibodies were used to detect and visualize the primary antibodies bound to the specific antigen of interest in frozen sections. Illumination of the sample with a specific wavelength of light causes the fluorochrome to emit light of a different specific wavelength. Positive staining was visualized using a fluorescence microscope Olympus BX51 equipped with a MagnaFire CCD camera to take images.

2.2.4.1 Preparation of cryosections

Frozen muscles in OCT (see 2.2.2) were placed inside the cryostat and allowed to equilibrate to $-20\text{ }^{\circ}\text{C}$ for about 15 min. The samples were removed from the piece of styrofoam and frozen onto the specimen chuck with the help of OCT. Twelve μm thick frozen sections of EOM and TA tissue were prepared and stored at $-80\text{ }^{\circ}\text{C}$ until needed.

2.2.4.2 Staining of cryosections

While sections were allowed to thaw, circles were drawn around the sections using an ImmEdge pen to create a hydrophobic barrier to retain the incubation solutions on the sections. The sections were then fixed with 4 % paraformaldehyde for 5 min followed by 3 washes in 1 x PBS for 5 min each. Then sections were permeabilized with 0.05 % Triton-X100/PBS for 5 min. After 3 washes in 1 x PBS for 2 min each, sections were blocked with 10 % goat serum/PBS for 30 min at room temperature. Incubation with the respective

primary antibody followed over night at 4 °C or at room temperature as indicated in the table below. Sections were washed again 3 times for 5 min each with 1 x PBS and incubation with the appropriate secondary antibodies followed. Goat anti-mouse-Alexa-Fluor-546 or goat anti-rabbit-Alexa-Fluor-546 were used at a dilution of 1:500.

Antibody	Dilution	Incubation
Anti-SERCA1	1:500	oN or room temp.
Anti-SERCA2	1:100	oN or room temp.
Anti-CASQ	1:250	oN
Anti-PLN	1:100	oN or room temp.

2.2.4.3 Staining of cultured myoblasts and myotubes

Myoblasts or myotubes were stained similar to the procedure described in 2.2.3.2. After the cells were fixed in 4 % paraformaldehyde for 3 min they were washed two times for 5 min in 1 x PBS. Cells were then permeabilized using 0.05 % Triton X-100/PBS for 5 min, washed again and blocked in 10% goat serum/PBS for 30 min at room temperature. The incubation with antibodies for desmin, myogenin or alpha-actinin was done over night at 4 °C or at room temperature as indicated in the table below. This was followed by 3 washes with 1 x PBS and incubation with goat-anti-mouse-Alexa-Fluor-546. The nucleic acid stain Hoechst 33342 was added to the secondary antibody at a concentration of 1:20000.

Antibody	Dilution	Incubation
Anti-Desmin	1:50	oN
Anti-Myogenin	1:100	oN
Anti-Alpha-Actinin	1:200	room temp.

2.2.4.4 Mounting of slides

After incubation with the antibodies slides with either cells or tissue were washed again three times in 1 x PBS followed by Milli-Q water. Coverslips were mounted on the slides using Gel Mount Aqueous mounting medium. Slides were stored in the dark at 4 °C until microscopy.

2.2.5 Cell culture

2.2.5.1 Acid washed cover slips

Cover slips were heated in 1 M HCl in a beaker to 50 - 60 °C for 4 - 6 hours. After cooling to room temperature cover slips were washed extensively in Milli-Q water. Coverslips were then rinsed with 95 % ethanol and left to dry on a sheet of Whatman paper in the cell culture hood. Lastly, cover slips were sterilized by UV irradiation for 30 min.

2.2.5.2 Collagen I-coated cell culture dishes

Cell culture dishes or coverslips were covered in 0.01 % Collagen I working solution for > 1 hour at room temperature. Excess fluid was removed and saved for repeated usage. The dishes were allowed to dry and UV sterilized before they were wrapped in aluminium foil and stored at 4 °C for up to 4 weeks. Before cells were plated, dishes were rinsed with sterile water.

2.2.5.3 Isolation of myoblasts

Primary myoblasts were generated based on the methods of Rando et al (Rando and Blau, 1994). Freshly dissected EOM and TA muscles from 8 - 12 day old rat pups were liberated from connective tissue under a stereo microscope. Then a few drops of enzyme mix (1:1 mix of 10 mg/ml collagenase IV and 2.4 U/ml dispase) were added and the muscles were minced to a fine slurry using a scalpel. After transferring the minced muscle into 50 ml tubes 2 ml of enzyme mix was added and the digest was incubated for 45 min at 37 °C. During the incubation the mix was triturated for 10 times every 15 min using a 15 ml serological pipet. The digest was stopped by adding 20 ml of growth medium followed by passing the cell-suspensions through 100 µm and 70 µm cell strainers. The cell-suspension was centrifuged at 2000 rpm for 5 min, the supernatant was discarded and the cells were resuspended in 3 ml growth medium.

2.2.5.4 Culture of primary myoblasts

Cells were preplated for 45 min on uncoated petri dishes to reduce the number of fibroblasts. Unattached cells were transferred to collagen I-coated 60 mm cell culture dish and were allowed to proliferate in growth medium until reaching ~ 70 % confluence. The cells were split by adding cold PBS to the cells, which were then mechanical dislodged by knocking the dish against a table top. This procedure preferentially released myoblasts and fibroblasts remained attached to the dish. The cells were then plated on 12 mm collagen I coated glass cover slips. Formation of multinucleated myotubes was initialized using differentiation medium. For immunocytochemistry cells were plated on 8-well chamber slides and differentiated. Myotubes used for Ca^{2+} imaging and immunostaining were allowed to differentiate for 2 – 3 days until mainly unbranched tubes with occasionally spontaneous twitching activity was observed.

2.2.5 Intracellular calcium measurements (calcium imaging)

Ca^{2+} imaging facilitates the measurement of changes in intracellular (cytoplasmic) Ca^{2+} levels (Ca^{2+} transients) with the help of a Ca^{2+} sensitive dye (Fura-2) that is loaded into the cells. Fura-2 is a UV excitable fluorescent Ca^{2+} indicator. The excitation maximum shifts from 380 nm when no Ca^{2+} is bound to 340 nm upon Ca^{2+} binding, while the light emission is unchanged at about 510 nm. This allows for ratiometric measurements involving the calculation of a 340/380 ratio.

2.2.6.1 Calcium imaging in myotubes

Myotubes were loaded with 10 μM Fura-2 AM and 2 % pluronic F-127 for 30 min at room temperature. The cells were rinsed and maintained in Fura-2-free isotonic solution for 30 min to allow for complete de-esterification before data acquisition at room temperature began. Coverslips were mounted in a flow chamber on an inverted microscope and visualized with a 20X objective. Myotubes of similar size were selected for measurements and a region of interest was drawn around the cells. The field was alternately excited at 340 and 380 nm with a scanning monochromator, and the fluorescence emitted > 520 nm from the region of interest was imaged with a CCD camera. Cells were perfused with isotonic solution at the

start of Ca^{2+} imaging experiments. For assessment of intracellular Ca^{2+} changes, cells were permeabilized with 5 μM ionomycin during perfusion with extracellular solution containing 300 nM Ca^{2+} or perfusion with extracellular solution containing 60 mM KCl and 50 mM NaCl without ionomycin. Calibration was performed separately on each cell after the experiment using standard techniques (Zhang et al., 2005b); cells were perfused with a Ca^{2+} -free solution containing 5 mM EGTA and 5 μM ionomycin (R_{\min}) followed by a high- Ca^{2+} solution (R_{\max}) with 5 μM .

The 340 and 380 traces and 340/380-ratio were recorded and analyzed using Felix software (Photon Technology International).

2.2.6.2 Analysis of calcium imaging experiments

The 340/380-ratio was converted to Ca^{2+} concentration $[\text{Ca}^{2+}]_i$ using the method of Grynkiewicz (Grynkiewicz et al., 1985) with the following formula:

$$[\text{Ca}^{2+}]_i = Kd \cdot [(R-R_{\min})/(R_{\max}-R)] \cdot (S_f/S_b)$$

R is the ratio of the 340/380 nm fluorescence signal. R_{\max} is the 340/380 ratio in the presence of Ca^{2+} -saturated dye. R_{\min} is the 340/380 ratio in Ca^{2+} free buffer containing 5 mM EGTA, and S_f/S_b is the ratio of the fluorescence at 380 nm measured in Ca^{2+} -free buffer (S_f) and in a Ca^{2+} oversaturated solution (S_b).

The peak Ca^{2+} values were determined by subtracting the baseline from the maximum levels. The “decay 0.5” value denotes the time needed for the Ca^{2+} to decay from peak to half peak size and were measured as indicated in Fig. 3.1.2.1A and C. Data were statistically analysed using a Student’s t-test with $p < 0.05$ considered statistically significant. To correlate cell size with the corresponding Ca^{2+} peak (see Fig. 3.1.2.2), the cell length and width were measured using ImageJ and the cell size was calculated using an approximation of two cones abutting at the base to represent the spindle shaped cell.

2.2.7 RNA isolation and quantification

For isolating RNA a modified protocol of the Guanidinium thiocyanate-phenol-chloroform extraction method (Chomczynski and Sacchi, 1987) in combination with a column-based RNA purification method (RNeasy Mini Kit) was used.

Tissue preserved in RNAlater was placed into appropriate volumes of Trizol Reagent as indicated in the table below and homogenized using either a Polytron for rat muscle or a Tissue Raptor for mouse muscle by increasing the speed to half maximum for 2 - 3 times until no more clumps were visible.

Species	Muscle (#)	TriReagent (μ l)
Rat	EOM (4 recti)	400
Rat	TA (1/4)	1000
Mouse	EOM (8 recti)	300
Mouse	TA (1)	500

The solutions were transferred to Eppendorf tubes and 100 μ l of the phase separation reagent BCP per 1 ml Trizol Reagent solution was added and vigorously shaken until the solution became homogenous. The mix was incubated for 5 min at room temperature. Afterwards the tubes were centrifuged for 10 min at 12000 rpm at 4 °C. After centrifugation three distinct phases were visible. The upper aqueous phase contained the RNA and was carefully removed without disturbing the interphase and transferred into a fresh tube. The RNA in the aqueous phase was precipitated with an equal volume of 70 % ethanol. This mix was loaded onto a column of the RNeasy Mini Kit and the RNA was further purified according to the manufacturer's instructions including an on-column DNaseI digest to remove DNA. The RNA was eluted in 30 - 40 μ l of RNase free water, aliquoted on ice and stored at - 80 °C.

At EMAU the RNeasy Mini Kit for fibrous tissue in combination with a speed mill homogenizer was used according to the manufacturer's protocol to isolate RNA from cryo-preserved tissue.

The RNA concentration was quantified in 2 μ l of the sample on a NanoDrop 1000 (UPenn) or in a 1:50 dilution on a UV/Vis spectrometer (EMAU). Water was used as blank.

2.2.8 Reverse transcription

Reverse transcription allows the synthesis of complementary DNA (cDNA) from total RNA or mRNA with the help of a reverse transcriptase (RT), which is an RNA-dependent DNA polymerase that synthesizes DNA from single-stranded RNA.

For SYBR-Green qPCR up to 5 µg of RNA was reverse transcribed using the Superscript II First Strand Synthesis kit using Oligo(dT) Primers according to the manufacturer's instructions. To ensure uniform reverse transcription equal amounts of RNA were reverse transcribed for all samples that were compared. Total mRNA was incubated with a mix of dNTPs and Oligo(dT) for 5 min at 65 °C to allow annealing of the primers. After placing the tubes on ice for 1 min, 9 µl of the reaction mix were added and incubated at 42 °C for 2 min. Elongation occurred after 1 µl of SuperScript II RT was added and incubated for 50 min at 42 °C. The reaction was terminated at 70 °C for 15 min and residual RNA was destroyed by incubating the reaction mix with 1 µl of RNase H for 20 min at 37 °C. cDNA was stored long-term at -20 °C and short-term at 4 °C.

RT-PCR used for qPCR at EMAU was performed using the TaqMan Gold reverse transcription kit. 100 ng of RNA were reverse transcribed using random hexamers in a 25 µl total reaction volume according to manufacturer's protocol.

2.2.9 Quantitative PCR (qPCR)

PCR facilitates the amplification of DNA-Fragments in vitro. The standard method has been used without major modifications since 1985 (Saiki et al., 1985). In contrast to standard PCR, which is analyzed at the end-point of the reaction, real-time PCR, also called quantitative real-time PCR or quantitative (qPCR) facilitates the quantification of a target gene by monitoring the amplification rate of the amplicon throughout the reaction. The PCR product is detected by fluorescent labeling after each amplification cycle. Here, two common methods were used: 1. SYBR Green chemistry intercalates into double-stranded DNA 2. TaqMan Assays contain a fluorescent sequence specific reporter probe that hybridizes to the correct product. For quantification the exact time point of threshold cycle (Ct) is selected as soon as fluorescence is detected above background levels. The Ct-values are used to calculate the initial amount of the target gene. The later the Ct-value is reached in the reaction the less target gene mRNA was initially contained in the sample. Depending on the method used, the quantity can be expressed as the absolute copy number or as a ratio relative to a calibrator. The calibrator can be an untreated control or a sample, whose expression is set to one and expression levels of all other samples are expressed relative to the calibrator. All expression levels are usually normalized against a reference gene or endogenous control (also called

housekeeping gene). The expression levels of the reference gene should be the same in all samples and should remain constant under the experimental conditions compared. A difference of < 1 between the reference gene Ct values of sample (EOM) vs. calibrator (TA) is acceptable.

The standard PCR temperature protocol of the manufacturer (Applied Biosystems) was used for all qPCR reactions:

The enzyme was activated by heating at 95 °C for 10 min. For 40 cycles a two-step PCR procedure was used with a denaturation step at 95 °C for 15 s and annealing and extension at 60 °C for 60 s. The fluorescent intensity of the reporter label was normalized to the rhodamine derivate ROX as a passive reference label contained in the MasterMix solution. The system generated a kinetic amplification plot based upon the normalized fluorescence.

2.2.9.1 SYBR Green based qPCR

SYBR Green based qPCR was used to determine expression levels of Ca^{2+} genes in rat tissue and myotubes. Glyceraldehyde 3-phosphate dehydrogenase (Gapdh) was used as reference gene. Each reaction (well) contained 10 – 20 ng of template and the final primer concentration was 500 nM. In non-template controls (NTC) water was used instead of cDNA. Reactions were run in triplicates on 384-well plates on a 7900HT ABI-Prism Real-Time instrument. An example plate set is shown in Fig. (Fig. 2.3). A melting curve program was performed after qPCR amplification was finished. During this final step the temperature was gradually raised, while the change in fluorescence was measured. Analysis of the derivative melting curve confirmed proper primer performance, when a single peak at the correct melting temperature of the amplicon for each primer pair was present.

2.2.9.2 Primer design for SYBR Green qPCR

Primers used for SYBR Green qPCR were designed using Primer Express version 1.5 across exon-exon boundaries toward the 3' end, where possible, to optimize detection of transcripts after reverse transcription with Oligo-dT primers. The parameter settings were as follows: amplicon length 100 - 200 bp, melting temperature 59 - 61 °C, “optimal primers

only”, primer length 18 - 40 bp; primer pairs were blasted (BLAST <http://blast.ncbi.nlm.nih.gov/Blast.cgi>) to ensure specific binding.

2.2.9.3 SYBR Green qPCR analysis: deltadelta Ct-method

The deltadelta Ct-method ($\Delta\Delta C_t$) or so-called relative quantification was used to analyse SYBR Green based qPCR. The $\Delta\Delta C_t$ -method enables relative quantification of mRNA or miRNA levels without knowing exact copy numbers. The C_t -values of the target genes and the calibrator are normalized to the reference gene (see above). The relative expression levels (ratio) between a target and the calibrator relative to a reference gene are calculated as follows:

$$\Delta C_t = C_t \text{ target gene} - C_t \text{ reference gene}$$

$$\Delta C_t = C_t \text{ calibrator gene} - C_t \text{ reference gene}$$

$$\Delta\Delta C_t = \Delta C_t \text{ target gene} - \Delta C_t \text{ calibrator gene}$$

$$\text{Ratio} = 2^{-\Delta\Delta C_t}$$

SYBR Green data were analysed using SDS 3.2 software and REST 2005. Primer specificity was confirmed by melting curve analysis as mentioned above. Mean fold-changes (EOM vs. TA) of three independent experiments and samples for each muscle type were calculated. Expression differences, also called fold-changes, were calculated by REST 2005 employing the $\Delta\Delta C_t$ method with normalization against the reference gene Gapdh and TA as calibrator. Statistical significance of differences in fold-changes was analyzed using the software program REST 2005, which employs randomized statistical testing with $p < 0.05$ considered significant.

2.2.9.4 TaqMan Assay based qPCR

TaqMan Assay based qPCR was used to quantify mRNA levels of the TRP channels and the genes Orai1 and Stim1. The expression levels were analyzed using absolute quantification of the target genes. This was facilitated by using a plasmid standard curve containing the target sequence with known copy numbers. The copy numbers of the plasmid standard curves ranged from 10^2 to 10^6 copies. 18s rRNA served as reference gene. Each reaction contained 8

ng of template cDNA. Reactions were run in duplicates on 96- well plates on a TaqMan 5700 Sequence Detection System. An example of a plate setup is shown in Fig 2.4.

2.2.9.5 TaqMan Assay analysis: absolute quantification

The absolute copy number of a target gene mRNA was obtained as follows. For each sample the copy numbers of each gene and the reference gene 18s were calculated from the standard curves that were run in parallel with the samples. The copy numbers of the target genes were calculated from the standard curve and expressed relative to the copy numbers of the reference gene 18s. The copy numbers of each gene were then normalized against the copy numbers of 18s for each sample and statistically analyzed using GraphPad Prism 5, with $p < 0.05$ considered significant.

2.2.10 Statistical analyses

For all statistical analyses, except the analyses of the SYBR Green qPCR data, the software GraphPad Prism 5 was used. Data were analyzed using an unpaired two-tailed t-test testing the null hypothesis that the means of two normally distributed populations are equal. For the analysis of the SYBR Green qPCR the software program Rest 2005 was used. This program uses randomization and bootstrapping techniques with up to 50000 iterations to estimate up- or down-regulation of gene expression from the Ct-values. As results ratios \pm SEM and a p-value are given to specify expression differences. For all statistical analyses a p-value of < 0.05 was considered statistically significant.

3. Results

3.1 Calcium handling properties in rat EOM

3.1.1 Expression of myogenic markers in EOM myotubes

To test whether the EOM and TA primary cultured cells to be used for Ca^{2+} imaging expressed myogenic markers, the cells were stained immunohistochemically using specific antibodies. Primary cells from EOM and TA were morphologically similar (Fig. 3.1). However, undifferentiated EOM myoblasts proliferated somewhat faster and tended to form slightly longer myotubes than TA myoblast (observation not quantified). Spontaneous twitching in the myotubes demonstrated that the essential components of the muscle cells contractile apparatus was preserved in culture, which was confirmed by positive α -actinin staining, a sarcomeric marker (Fig. 3.2). Further characterization of the cell cultures showed that undifferentiated myoblasts stained positive with an antibody against the early muscle marker desmin (Fig. 3.2), whereas differentiated myotubes stained positive with the differentiation marker myogenin and the nucleic stain Hoechst 33342 showing multinucleated myotubes (Fig. 3.2). This demonstrated that the cultured cells retained myogenic character and were able to form multinucleated myotubes (Fig. 3.1 and 3.2).

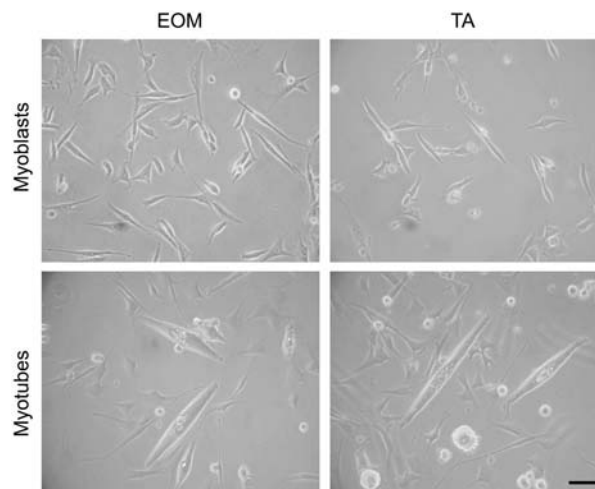


Fig. 3.1: Light microscopic images of cultured myoblasts and differentiated myotubes derived from EOM and TA. Cultured cells showed similar morphology. Scale bar = 100 μm .

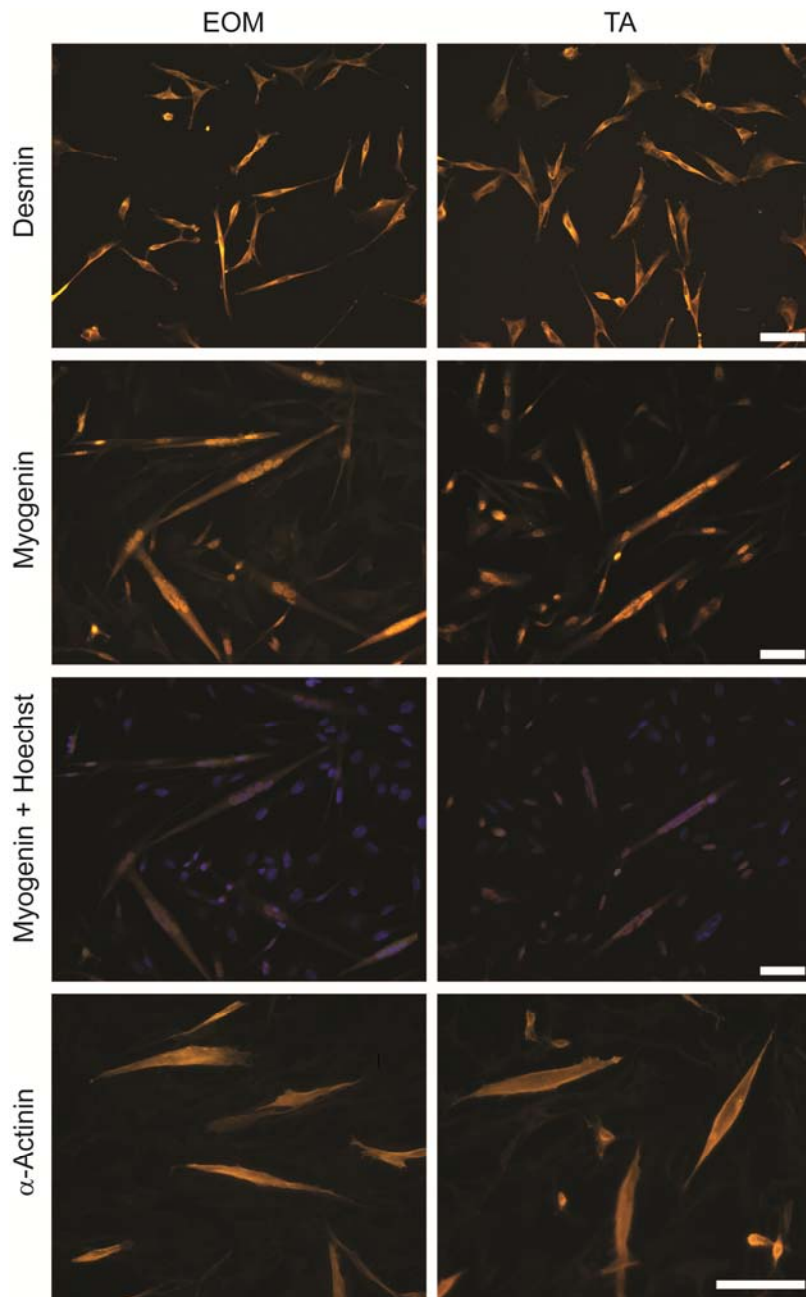


Fig. 3.2: Cultured primary EOM and TA myoblasts and myotubes stained for myogenic markers. Myoblasts stained for desmin (top panel). Differentiated myotubes stained for myogenin; the overlay with Hoechst 33342 staining shows localization of myogenin to the nuclei (middle panels). Differentiated myotubes stained for α -actinin indicated that sarcomeric structures were present (bottom panel). Scale bar = 100 μ m.

3.1.2 Calcium buffering in EOM and TA myotubes

To test the hypothesis that EOM are better able to buffer high intracellular Ca^{2+} levels, we used Fura-2 based ratiometric imaging to measure Ca^{2+} inside individual cultured primary EOM and TA myotubes (single cell imaging). Myotubes were loaded with Fura-2 at room temperature for 30 min followed by equilibration and de-esterification in isotonic solution for another 15 - 20 min until baseline level signals were stable. Moderate and similar baseline levels of 92.5 ± 9.1 nM in EOM and 90.4 ± 5.0 nM Ca^{2+} in TA confirmed that the signal originated predominantly from the cytoplasm and implied that the ability to control resting Ca^{2+} levels were similar in both cell types.

After reaching stable baseline levels, the cells were perfused with an extracellular solution containing 5 μM of the Ca^{2+} ionophore ionomycin and 300 nM Ca^{2+} . The lowered Ca^{2+} concentration (300 nM instead of 1.3 mM, which is similar to extracellular Ca^{2+} concentrations) of the perfusion solution was chosen to prevent myotube contraction. These reactive irreversible myotube hyper-contractions were observed in trial experiments using perfusion solutions containing up to 1.3 mM Ca^{2+} . Exposure to the solution containing 5 μM ionomycin and 300 nM Ca^{2+} led to a rapid rise in intracellular Ca^{2+} levels (Fig. 3.3 A) surpassing 300 nM Ca^{2+} . This rise in Ca^{2+} was considerably higher in EOM myotubes than in TA, with peak levels of 2.37 ± 1.8 μM in EOM compared with 1.14 ± 0.23 μM in TA ($p < 0.01$; Fig. 3.3 A). The decay time was quantified by defining decay 0.5 as the time needed for the Ca^{2+} levels to decrease by 50 % after reaching the peak. This decay was significantly faster in EOM myotubes, with levels taking only 56.6 ± 6.1 s to fall by half. This contrasts with TA cells, where the reduction took nearly twice as long (105.5 ± 19.4 s, $p < 0.05$; Fig. 3.3 C, D). Peak-size did not correlate with the size of the myotube, demonstrating that intrinsic cellular properties depending on the EOM vs. TA allototype rather than size per se mediated the differences (Fig. 3.4). This quantification confirms that EOM released more Ca^{2+} upon stimulation and that this excessive Ca^{2+} is buffered more effectively in EOM than in TA myotubes.

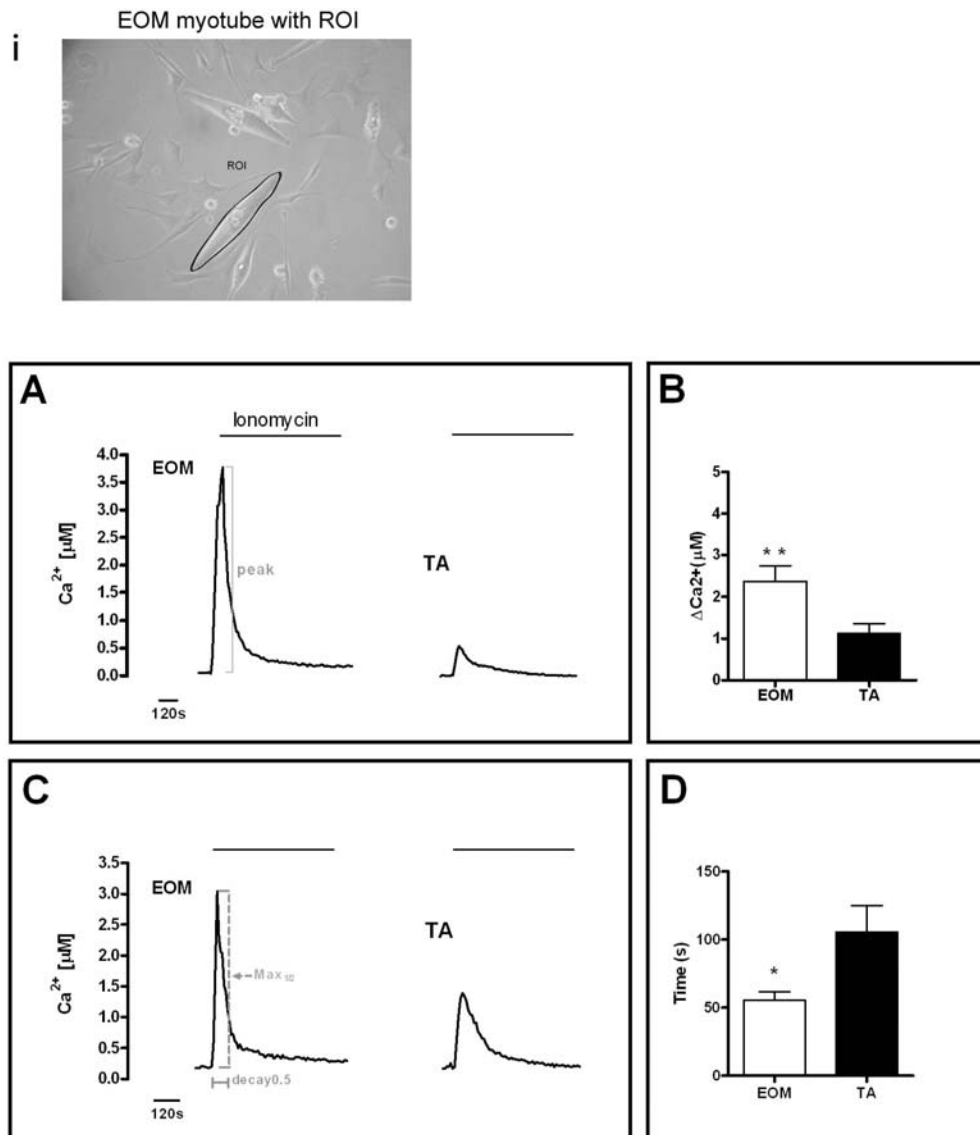


Fig. 3.3: Intracellular Ca^{2+} measurements in myotubes. Panel **i** shows the region of interest (ROI) on an EOM myotube from where the signal was recorded. Representative Ca^{2+} traces are shown for perfusion experiments of Fura-2 loaded myotubes with an extracellular solution containing 300 nM Ca^{2+} and 5 μM ionomycin. EOM myotubes showed a 2.0-fold larger maximum peak size (**A**, **B**), a 1.9-fold faster decay 0.5 time (**C**, **D**). Representative positions of the parameters measured are illustrated in **A** & **C**. Data are depicted as bar graphs showing significant differences in the evaluated parameters (**B**, **D**) (Mean \pm SEM, * $p < 0.05$, ** $p < 0.01$).

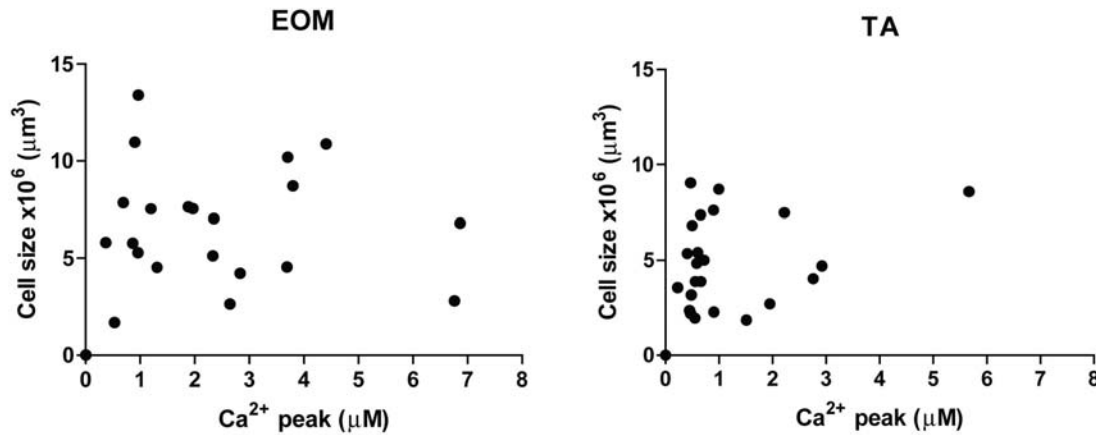


Fig. 3.4: Correlation of Ca^{2+} peak and cell size in EOM and TA myotubes. To correlate cell size with the corresponding Ca^{2+} peak, the cell size was calculated using an approximation of two cones abutting at the base to represent the spindle shaped cell. Ca^{2+} peak and cell size did not correlate in EOM or TA myotubes.

To independently validate these results we evaluated if similar responses were obtained by inducing membrane depolarization with high extracellular K^+ (60 mM K^+). High K^+ stimulation leads to E-C coupling and triggers immediate Ca^{2+} release from the SR (Melzer et al., 1995). EOM and TA myotubes were stimulated for 30 s with high K^+ . In accordance with the previous observations Ca^{2+} peaks recorded from EOM were significantly higher than the peaks recorded from TA myotubes (1.5 ± 0.3 vs. 0.77 ± 0.1 nM, $p < 0.05$; Fig. 3.5 A, B), likely reflecting a larger amount of Ca^{2+} released from the SR in EOM. The noted decay 0.5-rate in EOM was much faster than the decay rate with ionomycin but not significantly faster than in TA (14.9 ± 1.8 vs. 13.1 ± 1.6 s; Fig. 3.5 D). Nonetheless, EOM myotubes re-sequestered a larger amount of Ca^{2+} from the cytosol than TA myotubes within the same time period. These results further support the idea of a larger Ca^{2+} release in EOMs and more efficient elimination of Ca^{2+} from the cytoplasm.

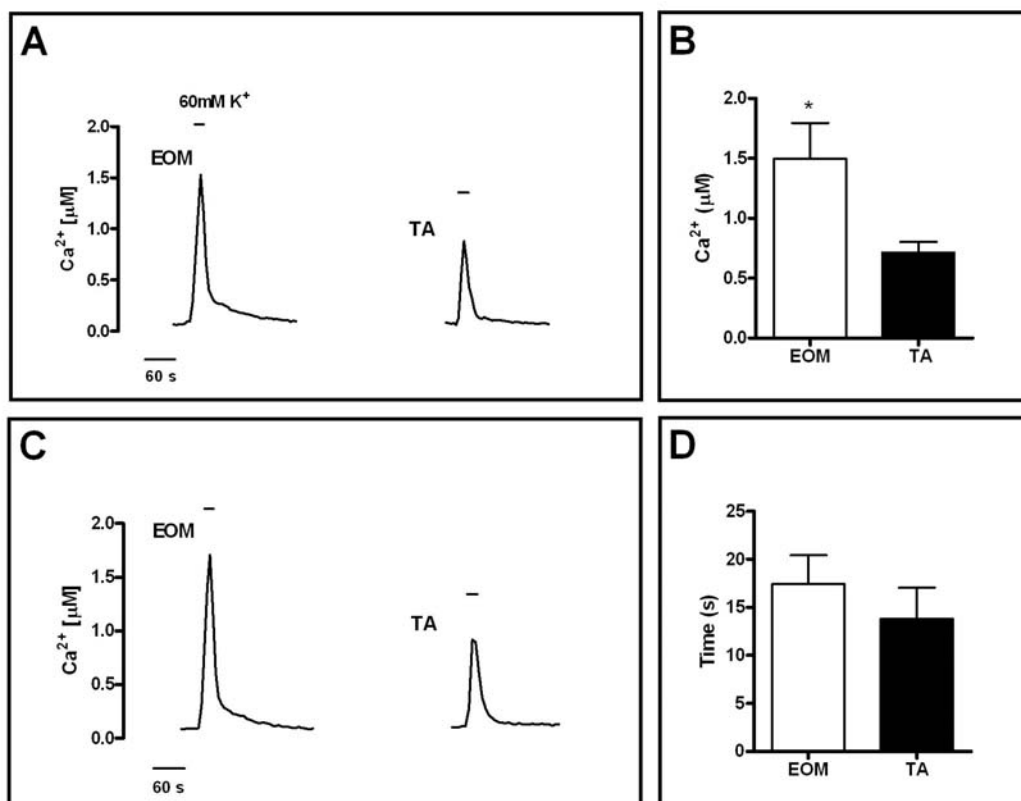


Fig. 3.5: High K⁺ induced Ca²⁺ transients in EOM myotubes. Representative Ca²⁺ traces are shown for perfusion experiments of Fura-2 loaded myotubes stimulated with high K⁺ (60 mM) solution. EOM myotubes showed a 1.9-fold larger maximum peak size than TA myotubes (A, B) and a similar average decay 0.5 time (C, D). Parameters were measured in the same way as illustrated in Fig. 3.3. (Mean ± SEM, * p < 0.05).

3.1.3 mRNA expression levels of calcium handling proteins in EOM

Having shown more efficient buffering of high Ca²⁺ levels in EOM myotubes compared to TA myotubes, expression levels of genes known to be involved in Ca²⁺ homeostasis were determined. qPCR was used to quantify mRNA levels of Ca²⁺ handling genes in the cultured myotubes. Candidate genes from five functionally distinct groups of Ca²⁺/SR proteins were investigated. As shown in Table 3.1, the first group contained genes of the sarcoplasmic and plasma membrane Ca²⁺ pumps (Serca1, Serca2, Pmca1 and Pmca4) and the Na⁺/Ca²⁺-exchanger (Ncx). The second group contained genes of proteins with regulatory functions on the Serca pumps (Pln, Sln and Rgn). The third group contained the major Ca²⁺ binding and

buffering proteins of the SR (Casq1, Casq2 and Srl). The fourth group of genes coded for cytosolic and sarcomeric Ca²⁺ binding proteins, predicted to buffer elevated intracellular Ca²⁺ (Parv, S100a1, Calm, Tnnc1 and Tnnc2). The final group of genes examined included the Ca²⁺ channels involved in E-C coupling, the ryanodine receptor (Ryr1) and the α 1S-subunit of the L-type Ca²⁺ channel (Cacna1s), also known as the DHPR receptor. mRNA levels of seven (Pln, Sln, Rgn, Casq2, Parv, S100a1 and Cacna1s) of the 18 genes quantified were expressed at significantly higher levels in EOM than in TA (Table 3.1 “Myotubes”). Most other genes were expressed at similar levels in EOM and TA myotubes.

To compare the values obtained from cultured myotubes, we also tested the gene expression of Ca²⁺/SR proteins in fully differentiated adult tissue. We found that eleven out of 18 quantified genes showed significantly higher expression in EOM compared with TA (Table 3.1 “Tissue”). The highest expression differences were detected for the Ca²⁺ pumps (Serca2, Pmca1, Pmca4 and Ncx), the regulatory proteins (Pln, Sln and Rgn) with changes of up to 75-fold difference (Pln) and the Ca²⁺ binding proteins Casq2 and Calm (29.9- and 10.1-fold, respectively). Only Serca1, Casq1, Cacna1s and Ryr1 were not differentially expressed in EOM vs. TA muscle tissue. Overall the expression differences observed in tissue were much more marked than in culture, where the differences were rather small. In addition, Cacna1s and Parv were not up-regulated in tissue as suggested by the expression in culture. The lower expression levels of the transcripts of Ca²⁺ handling proteins in myotubes suggest that the levels seen in culture may underestimate the amounts and hence activities in mature tissue.

Protein category	Protein Function	Gene	Myotubes		Tissue	
			Fold-change EOM vs TA	statistical significance	Fold-change EOM vs TA	statistical significance
Pumps	SR Ca ²⁺ -ATPase, fast-twitch	<i>Serca1</i>	1.0 ± 0.65	n.s.	1.1 ± 0.20	n.s.
	SR Ca ²⁺ -ATPase, slow-twitch	<i>Serca2</i>	1.2 ± 0.19	n.s.	13.2 ± 6.75	< 0.05
	Ca ²⁺ -ATPase 1, plasma membrane	<i>Pmca1/Atp2b1</i>	1.1 ± 0.20	n.s.	33.3 ± 7.77	< 0.05
	Ca ²⁺ -ATPase 4, plasma membrane	<i>Pmca4/Atp2b4</i>	1.1 ± 0.38	n.s.	30.0 ± 15.40	< 0.05
	Na ⁺ /Ca ²⁺ -exchanger, plasma membrane	<i>Ncx/Slc18a1</i>	1.4 ± 0.34	n.s.	15.8 ± 6.68	< 0.05
Regulatory proteins	SR, regulates SERCA2	<i>Phospholamban</i>	2.7 ± 0.42	< 0.05	74.7 ± 10.72	< 0.05
	SR, regulates SERCA1	<i>Sarcoplipin</i>	1.3 ± 0.16	< 0.05	20.6 ± 11.12	< 0.05
	cytosol, regulates SERCA s	<i>Regucalcin</i>	1.5 ± 0.33	< 0.05	12.7 ± 6.3	< 0.05
SR calcium binding proteins	SR, calcium binding protein, skeletal	<i>Calsequestrin 1</i>	0.9 ± 0.26	n.s.	1.5 ± 0.39	n.s.
	SR, calcium binding protein, cardiac	<i>Calsequestrin 2</i>	1.5 ± 0.27	< 0.05	29.9 ± 18.30	< 0.05
	SR, calcium binding protein	<i>Sarcalumenin</i>	1.4 ± 0.31	n.s.	2.6 ± 0.55	n.s.
Cytosolic calcium binding proteins	cytosol, calcium binding protein	<i>Parvalbumin</i>	2.0 ± 0.35	< 0.05	2.3 ± 0.54	n.s.
	cytosol, calcium binding protein	<i>S100a1</i>	2.3 ± 0.39	< 0.05	5.4 ± 0.68	< 0.05
	calcium binding protein	<i>Calmodulin</i>	0.9 ± 0.10	n.s.	10.1 ± 3.64	< 0.05
	calcium binding protein, slow-twitch/cardiac	<i>Troponin C 1</i>	1.0 ± 0.14	n.s.	5.1 ± 0.59	< 0.05
	calcium binding protein, fast-twitch	<i>Troponin C 2</i>	1.4 ± 0.29	n.s.	2.1 ± 0.49	n.s.
Calcium channels	calcium channel subunit	<i>Cacna1s</i>	1.5 ± 0.22	< 0.05	0.9 ± 0.12	n.s.
	calcium release channel, skeletal	<i>Ryanodine Receptor 1</i>	1.3 ± 0.25	n.s.	1.0 ± 0.16	n.s.

Table 3.1: Relative mRNA levels of genes encoding Ca²⁺ handling proteins in EOM myotubes and EOM tissue. Listed are relative mRNA levels of genes encoding Ca²⁺ handling proteins determined by SYBR Green qPCR in myotubes and muscle tissue. Expression differences (fold-changes) were calculated and statistically analyzed. p < 0.05 was considered statistically significant. (Mean ± SEM, n = 3).

3.1.4 Protein expression of calcium handling proteins in EOM

The proteins selected for western blot analysis were the major proteins for Ca²⁺ storage (CASQ1 and CASQ2) and reuptake in the SR (SERCA1, SERCA2 and PLN). The mean gray value of each western blot band was measured densitometrically in arbitrary units using ImageJ. Levels of the fast muscle isoform CASQ1 were lower in EOM but levels of the slow/cardiac isoform CASQ2 were much higher in EOM than in TA (Fig. 3.6 A). Total CASQ content was slightly higher in EOM but did not reach statistical significance (Fig. 3.6 A). Protein levels of the sarcoplasmic Ca²⁺ ATPase SERCA1 were reduced in EOM, while those for SERCA2 were considerably higher in EOM (Fig. 3.6 B). However, when considering relative band intensities of Serca1 and Serca2, Serca1 appears to be the dominant isoform in EOM.

PLN, a known regulator of SERCA, has frequently been found to be highly expressed at the mRNA level in EOM (Fischer et al., 2002; Khanna et al., 2003). To expand these data, the protein levels of PLN and the phosphorylation status of PLN was determined in EOM. Under non-reducing conditions, only monomeric PLN was detected in EOM, while in heart, which served as positive control, both monomeric and pentameric PLN were present. No PLN protein was detected in TA (Fig. 3.7 A). PLN regulates SERCA2 activity in the heart depending on its phosphorylation status and activates SERCA2 when phosphorylated on either or both of its phosphorylation sites: Ser16 is phosphorylated by protein kinase A (PKA) and Thr17 is phosphorylated by Ca²⁺/calmodulin dependent kinase II (CAMKII). Using phosphorylation site specific antibodies, only trace amounts of PKA dependent phosphorylation at Ser16 in PLN from EOM (Fig. 3.7 B) was detected. In vitro PKA treatment only slightly increased these levels in EOM, whereas in heart samples PKA treatment did increase endogenous levels of Ser16 phosphorylation (Fig. 3.7 B). On the other hand, EOM contained considerable amounts of endogenous CAMKII dependent phosphorylation of monomeric PLN at Thr17 (Fig. 3.7 C). Neither of the phospho-PLN specific antibodies detected a PLN pentamer in EOM. In both cases, heart samples served as positive control where endogenous phosphorylation at Ser16 and Thr17 was present in monomeric and pentameric PLN.

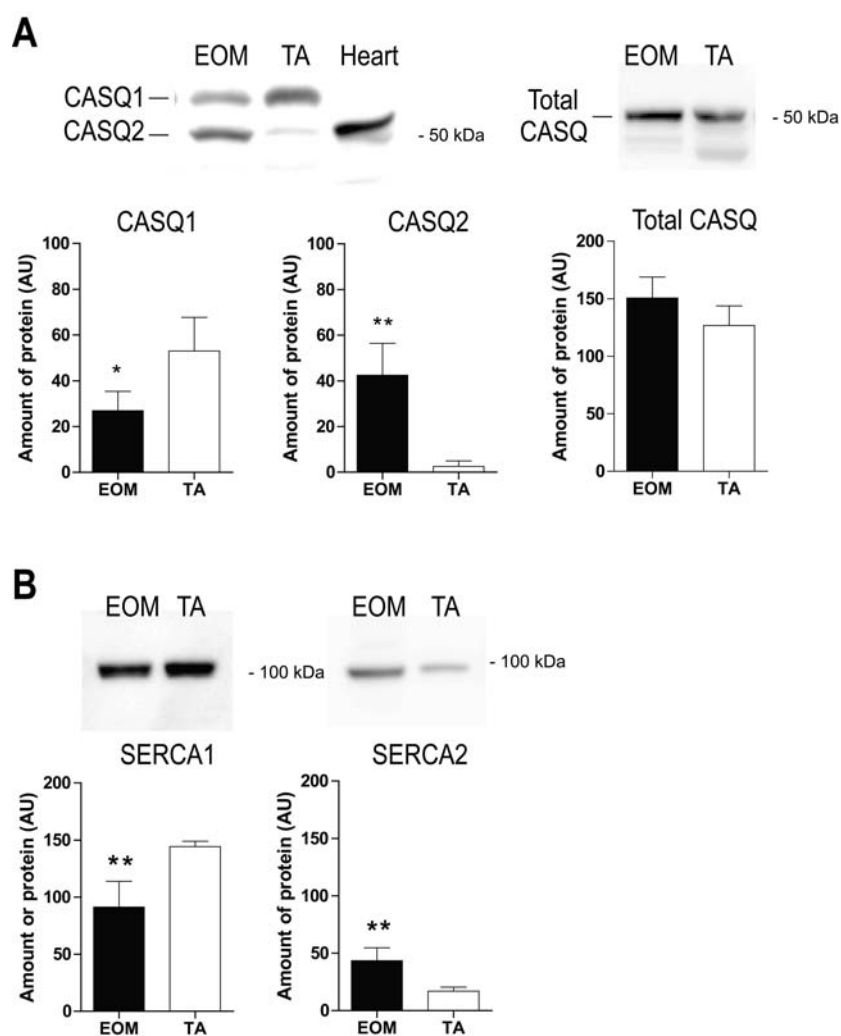


Fig. 3.6: Increased protein levels of SR Ca^{2+} handling proteins in EOM. Western blot analysis showing relative abundance of indicated proteins in EOM and TA. (A) CASQ1 and CASQ2 isoforms were resolved on a 7.5 % gel. Heart tissue indicates the molecular weight of CASQ2. In EOM, CASQ2 was more abundant than CASQ1 compared with TA. Total CASQ showed a tendency toward higher levels in EOM. (B) SERCA1 levels were less in EOM, whereas SERCA2 levels were significantly higher. SERCA1 was the predominant isoform in both tissues. Bands were quantified using densitometry and data were statistically analysed using an unpaired t-test. $p < 0.05$ was considered statistically significant. * $p < 0.05$, ** $p < 0.01$ ($n = 4$; Mean \pm SD; AU = arbitrary units).

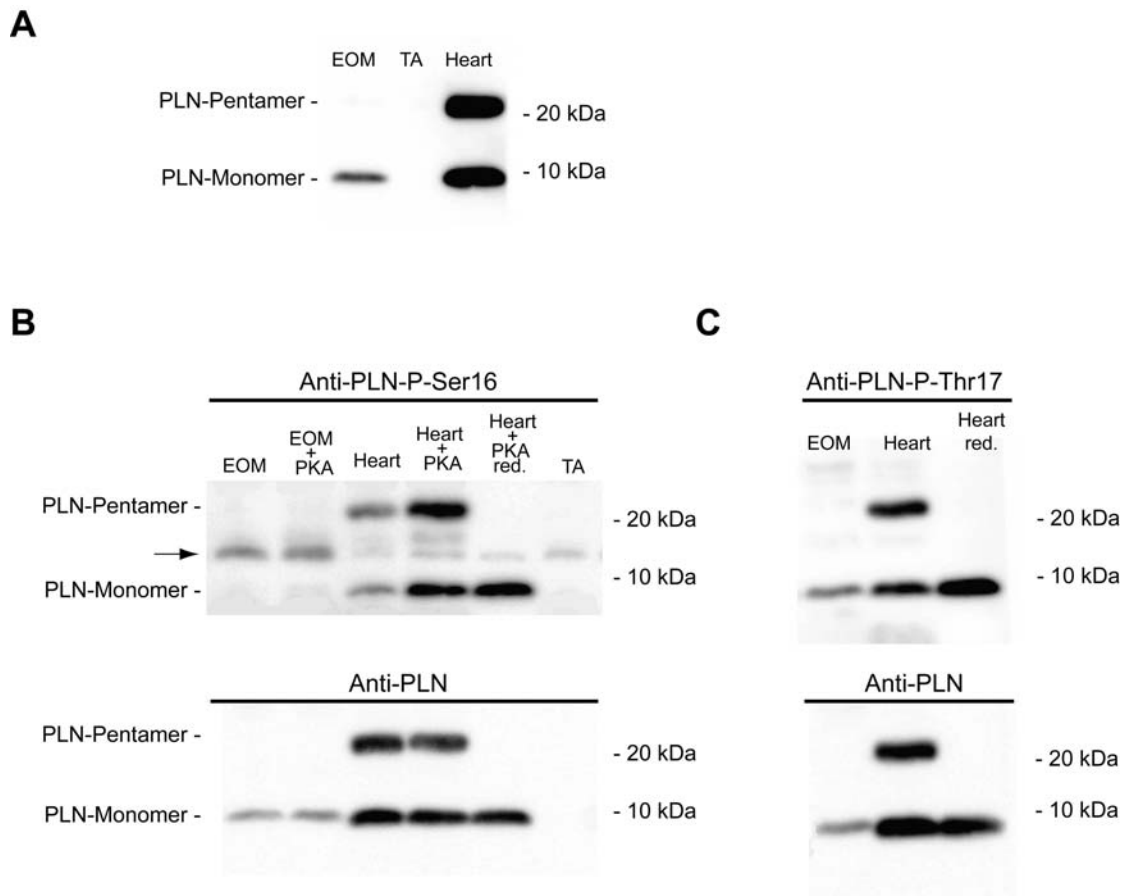


Fig. 3.7: Increased protein levels of PLN and PLN-phospho-Thr17 in EOM. Western blot analysis showing relative abundance of indicated proteins in EOM and TA. (A) Monomeric PLN is found in EOM but not in TA under non-reducing conditions. Under the same non-reducing conditions monomeric (~5 kDa) and pentameric PLN (~25 kDa) is present in heart. (B) In EOM PLN is phosphorylated in trace amounts at Ser16, which cannot be further induced by PKA treatment. In heart, serving as positive control, phosphorylation at Ser16 was increased after PKA treatment and only monomers were detected under reducing conditions. The arrow indicates binding of the antibody to phospholemman (see Fig. 3.8) (C) Phosphorylation of PLN at Thr17 in EOM is endogenously high. Heart tissue served as positive control demonstrating pentameric and monomeric forms under non-reducing and reducing conditions, respectively. Reprobing of blots with the Anti-PLN antibody (lower panels in B and C) showed relative abundance of total PLN versus the phosphorylated forms. red. = reducing.

The 14 kDa band detected by the PLN-phospho-Ser16 antibody was identified as phospholemman as described for this antibody (Fig. 3.8) (Drago and Colyer, 1994).

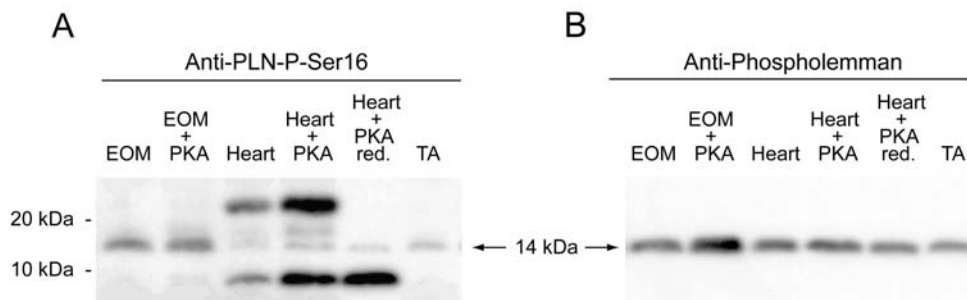


Fig. 3.8: Identification of the 14 kDa band detected by the phospho-Ser16-PLN antibody (A). By stripping and reprobing of the blot in Fig. 3.7 B the 14 kDa band indicated by the arrow could be identified as phospholemman (B).

Furthermore, in support of increased CAMKII activity significantly higher protein levels of CALM and CAMKII were detected in EOM (Fig. 3.9). This is in agreement with the finding of predominant Thr17 phosphorylation in EOM.

These results demonstrate differential expression of components underlying the unique signaling cascades modulating Ca^{2+} homeostasis of EOM, suggesting that regulation of SERCA activity in EOM by PLN relies mainly on CAMKII dependent phosphorylation.

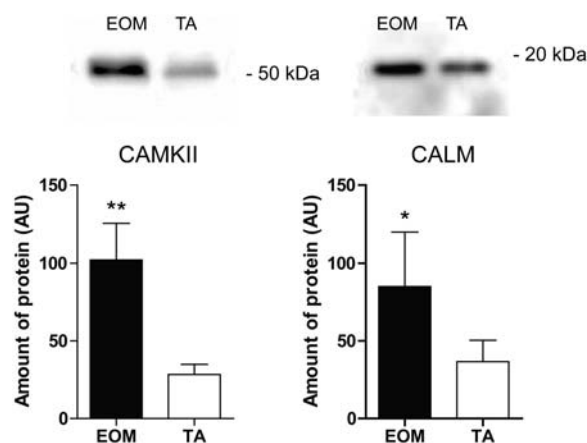
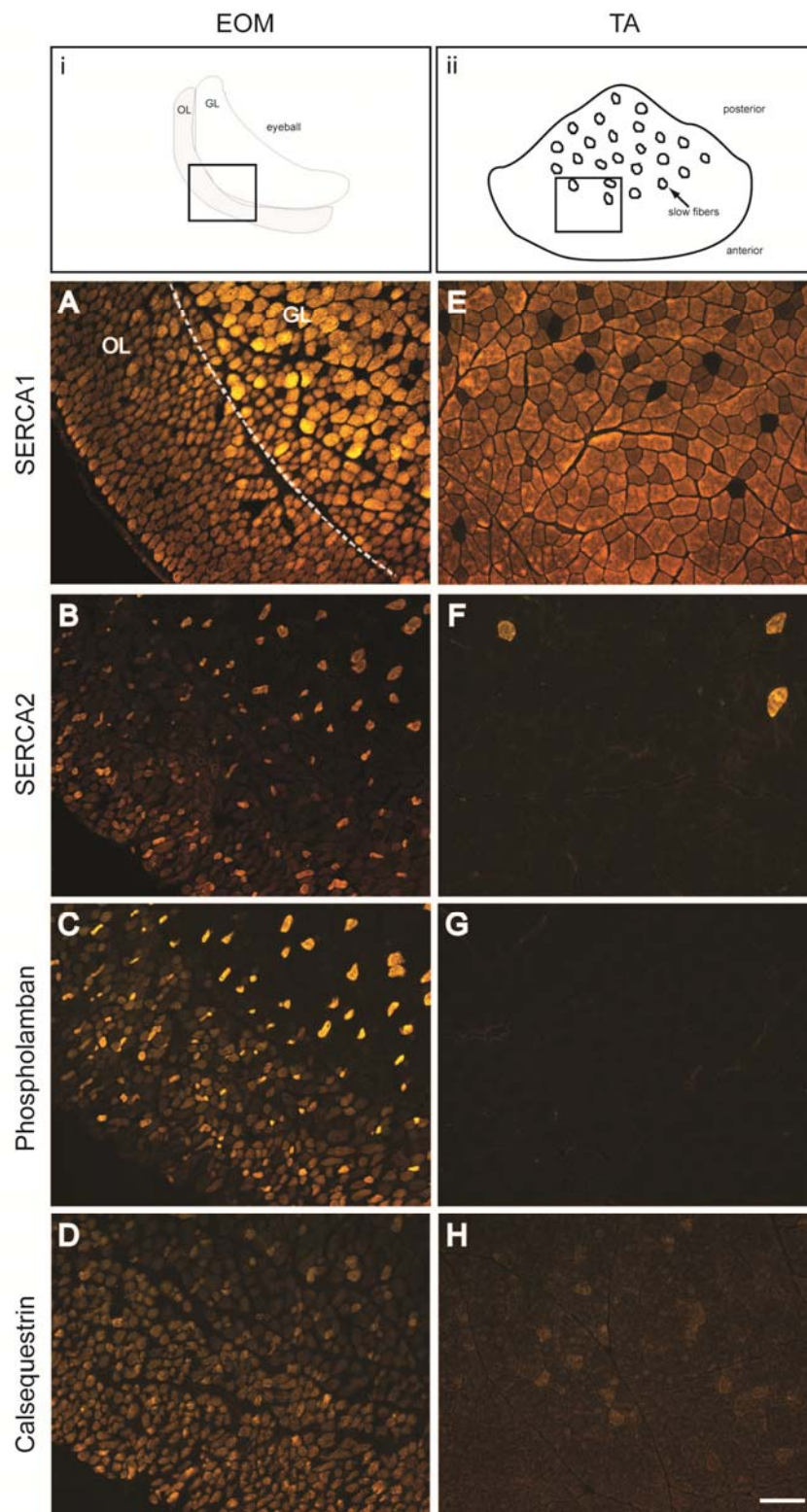


Fig. 3.9: Protein levels of CAMKII and CALM in EOM. CAMKII and CALM were more abundant in EOM compared with TA. Bands were quantified using densitometry and data were statistically analysed using an unpaired t-test. $p < 0.05$ was considered statistically significant. * $p < 0.05$, ** $p < 0.01$ ($n = 4$; Mean \pm SD; AU = arbitrary units).

3.1.5 Immunohistochemistry of calcium handling proteins

To address potential fiber-type dependent variations in the expression of Ca^{2+} handling proteins, the distribution of SERCA1, SERCA2, total CASQ and PLN was investigated by immunohistochemistry using semi-serial cryosections of EOM and TA muscle. The top panel in Fig. 3.10 shows a schematic of whole muscle sections of EOM and TA indicating the regions from where images were taken (Fig. 3.10 i and ii). As can be seen in Fig. 3.10, almost all fibers stained positively for SERCA1 in EOM and TA sections (Fig. 3.10 A, E). Overall, staining for SERCA2, PLN and total CASQ was more intense in EOM than in TA (Fig. 3.10 B - H). Regional differences were obvious. SERCA2 showed strong labeling of about one third of the fibers of the GL, whereas the remainder of the GL fibers showed weak or negative staining. Most OL fibers stained clearly for SERCA2 but the intensity varied (Fig. 3.10 B). Only a few TA fibers showed strong labeling with SERCA2 emanating from slow fibers based on their position (Fig. 3.10 F). In the GL of EOM, the pattern of staining for PLN was similar to that of SERCA2. Fiber labeling of the OL with anti-PLN was heterogeneous (Fig. 3.10 C). No TA fibers were positive for PLN (Fig. 3.10 G), consistent with the absence of bands on the western blots. The antibody against total CASQ showed strong staining of most EOM fibers with varying intensity among fibers (Fig. 3.10 D). The total CASQ labeling pattern of GL fibers appeared similar to the labeling by PLN and SERCA2, suggesting a possible co-regulation of expression. Staining for total CASQ was also observed for TA but with less overall intensity (Fig. 3.10 H).

Fig. 3.10: Localization of Ca^{2+} handling proteins in EOM. Immunohistochemistry showed tissue distribution of selected Ca^{2+} handling proteins. Semi-serial cryosections of EOM (left column) and TA (right column) were labeled with specific antibodies. Top panel shows the location on the section from where the images were taken (box): left top panel: schematic of an EOM section with GL and OL indicated; right top panel: schematic of a TA section with few slow-twitch fibers indicated. Dashed line in A marks border between OL and GL. Closely adjacent cryosections of EOM (left column) and TA (right column) were labeled with specific antibodies as marked. SERCA1 labeled in EOM and TA equally strong (A, E). SERCA2, PLN and CASQ were more intensely labeled in EOM (B, C, D). These antibodies showed a distinct staining pattern in the OL and GL. In EOM most fibers of the OL labeled positive but with varying intensity, whereas a set of ~30 % of the GL fibers labeled strongly with these antibodies. In TA, few fibers labeled strongly with SERCA2 (F), the antibody against total CASQ labeled all fibers weakly with varying intensity (H) and no fibers were positive for PLN (G). Scale bar = 100 μm .



3.2 Molecular components of the calcium homeostasis in normal and mdx mouse EOM

The previous chapter 3.1 demonstrated the superior Ca^{2+} homeostasis of normal EOMs. Due to the involvement of Ca^{2+} in the pathology of muscular dystrophy the Ca^{2+} homeostasis in EOMs of the mouse model of DMD, the mdx mouse was investigated. In the first set of experiments protein levels of key Ca^{2+} handling proteins were determined to test whether the expression of these proteins can be compared between rat and mouse in order to extrapolate the results obtained with rat EOM. At the same time the expression levels were compared to normal and mdx TA. Furthermore, because of recent interest in the potential role of TRP channels and SOCE in mediating increased Ca^{2+} influx in mdx muscle the expression of TRPC, TRPV and TRPM, as well as Orai and STIM proteins in EOM of normal and dystrophic mice was determined.

3.2.1 Protein expression of calcium handling proteins

Relative expression levels of the key components SERCA1, SERCA2, CASQ and PLN of the Ca^{2+} homeostasis were determined by western blot in normal and mdx mice. These data were compared with the findings in rat to determine whether mice and rat (see chapter 3.1) have comparable expression of Ca^{2+} handling proteins.

SERCA1 levels were similar in EOM and TA of normal and mdx mice (Fig. 3.11 A). SERCA2 levels were unchanged in normal and mdx EOM. SERCA2 levels were lower in normal TA and mdx TA. However, mdx TA showed increased SERCA2 levels compared with normal TA (Fig. 3.11 B).

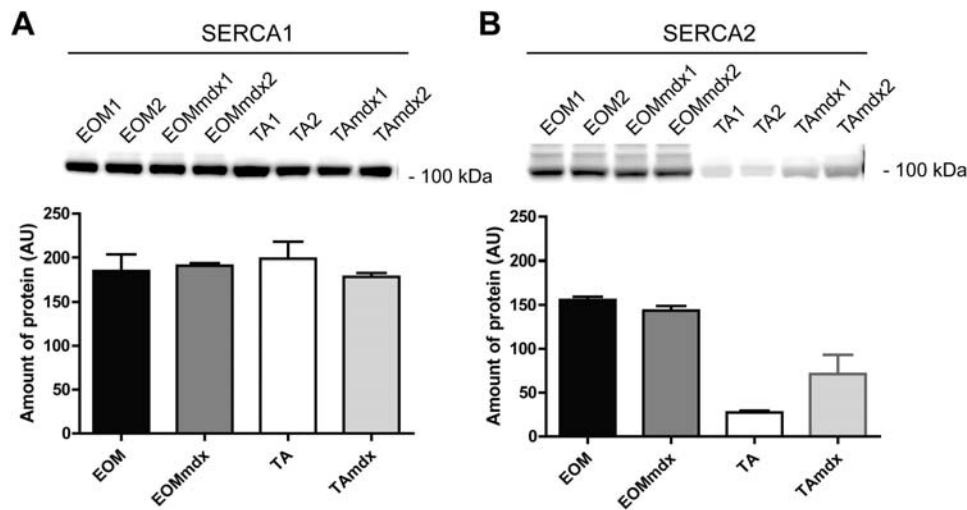


Fig. 3.11: Western blots of EOM and TA muscle from normal and mdx mice showing relative expression levels of SERCA1 (A) and SERCA2 (B). SERCA1 levels were similar in all muscles tested (A). SERCA2 levels were similar in EOM and mdx EOM, but higher in EOM compared with TA. mdx TA showed elevated levels compared with normal TA. Bands were quantified using densitometry but not statistically analysed because of $n = 2$ (Mean \pm SD, AU = arbitrary units).

Total CASQ (CASQ1 and CASQ2), the major SR buffering protein, was significantly higher expressed in EOM and mdx EOM compared with TA samples, in contrast to rat tissue where total CASQ levels were only slightly higher in EOM. Total CASQ levels were a little higher in mdx EOM but not statistically different from normal EOM (Fig. 3.12).

PLN protein expression in mouse tissue was similar to that in rat (Fig. 3.13, see also Fig. 3.7). Only monomeric PLN was detected under non-reducing conditions and no PLN was detected in normal or mdx TA tissue, while in mouse heart tissue monomeric and pentameric PLN was detected. There was no difference in PLN expression levels between normal and mdx EOM (Fig. 3.13).

These data suggest that normal rat and mouse show comparable expression patterns of the major Ca^{2+} handling proteins with the exception of CASQ, which showed significantly higher levels in EOM than TA.

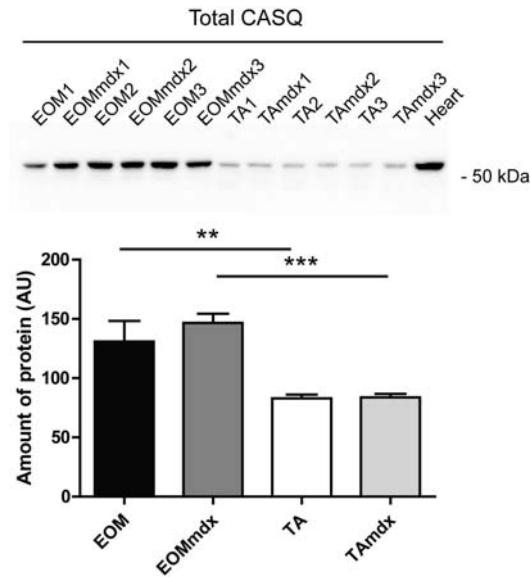


Fig. 3.12: Western blot of EOM and TA proteins from normal and mdx mice showing relative expression levels of total CASQ. Total CASQ levels in EOM and mdx EOM were similar but significantly higher than in TA and mdx TA. Total CASQ levels of TA and mdx TA were similar. Heart samples served as positive control. Bands were quantified using densitometry. Differences were established using an unpaired t-test with $p < 0.05$ considered statistically significant. ** $p < 0.01$, *** $p < 0.001$ ($n = 3$, mean \pm SD, AU = arbitrary units).

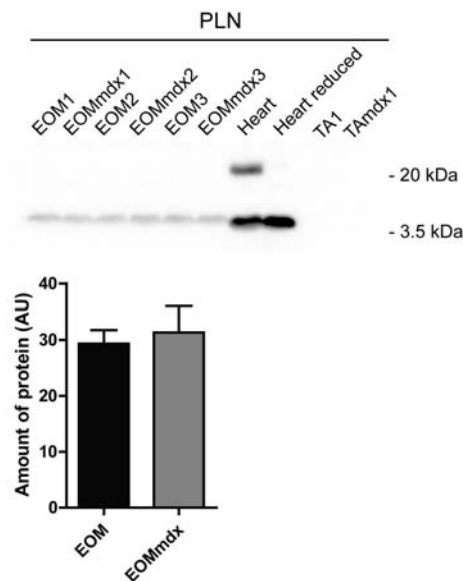


Fig. 3.13: Western blot of EOM and TA proteins from normal and mdx mice showing relative expression levels of PLN. Under non-reducing conditions equal levels of only monomeric PLN were detected in EOM and mdx EOM. No PLN was detected in TA or mdx TA. Heart tissue served as positive control. EOM bands were quantified using densitometry and statistically analyzed using an unpaired t-test. With $p > 0.05$ the difference was not statistically significant ($n = 3$, mean \pm SD, AU = arbitrary units).

3.2.2 Expression of TRP channel proteins in EOMs

TRP channels (e.g. TRPC1, TRPC3, TRPV2 and TRPV4) contribute to the Ca^{2+} homeostasis in muscle and have been shown to be differentially expressed in normal and dystrophic muscle (Gervasio et al., 2008; Iwata et al., 2009; Krüger et al., 2008; Kunert-Keil et al., 2006; Vandebrouck et al., 2002). To resolve expression patterns of the group 1 TRP channels, TRPC, TRPV and TRPM, in EOM, TaqMan assay based absolute quantification of copy numbers (qPCR) were conducted. Protein levels were assessed using western blotting. The mRNA expression of TRP channels with highest levels in EOM and mdx EOM was also determined in TA and mdx TA.

3.2.2.1 mRNA expression of TRPC channels

mRNA levels of the TRPC channels TRPC1 through TRPC7 were quantified. TRPC1, TRPC2, TRPC3, TRPC5 and TRPC6 were detected in EOM. TRPC3 levels, which have been reported as the predominant TRPC channel in muscle, showed uniformly high levels in EOM, TA, mdx EOM and mdx TA. Interestingly, TRPC1 levels in EOM and mdx EOM were equally high as the TRPC3 levels and significantly higher compared with TRPC1 levels of TA and mdx TA. Similarly, significantly higher levels of TRPC6 were noted in mdx EOM vs. mdx TA. TRPC2 and TRPC5 showed low expression levels in EOM and mdx EOM, whereas TRPC4 was not detected. TRPC7 showed negligible expression in EOM or mdx EOM (Fig. 3.14).

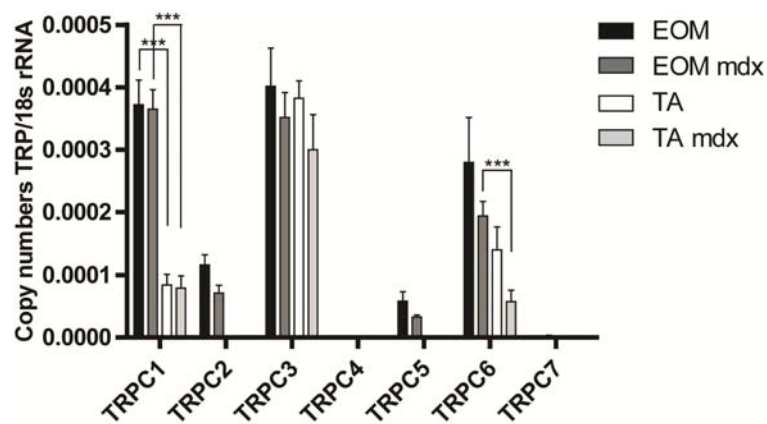


Fig. 3.14: mRNA quantification of the members of the TRPC channel subgroup. TRPC1, TRPC3 and TRPC6 were quantified in EOM, mdx EOM, TA and mdx TA. TRPC2, TRPC4, TRPC5 and TRPC7

were quantified only in EOM and mdx EOM due to low expression levels. Copy numbers were expressed relative to the reference gene 18s. Differences were established using an unpaired t-test with $p < 0.05$ considered statistically significant. ** $p < 0.01$, *** $p < 0.001$ ($n = 7-9$, mean \pm SEM).

3.2.2.2 Protein expression of TRPC1 and TRPC3

TRPC1 and TRPC3 showed the highest copy numbers in EOM tissue. Using western blotting the corresponding protein levels of these two channels were determined and quantified (Fig. 3.15 A). TRPC1 protein was equally abundant in EOM and mdx EOM. Both EOM tissues contained significantly higher TRPC1 protein levels compared with TA tissues. TA from mdx mice showed lower TRPC1 levels than normal TA. TRPC3 protein levels were similar between EOM and TA and between normal and mdx mice (Fig. 3.15 B). These data correspond well with the findings by TaqMan Assay. In both cases the double band detected by the antibodies possibly reflects phosphorylation or glycosylation of the TRPC1 and TRPC3 channel proteins in muscle (Cohen, 2006; Gervasio et al., 2008).

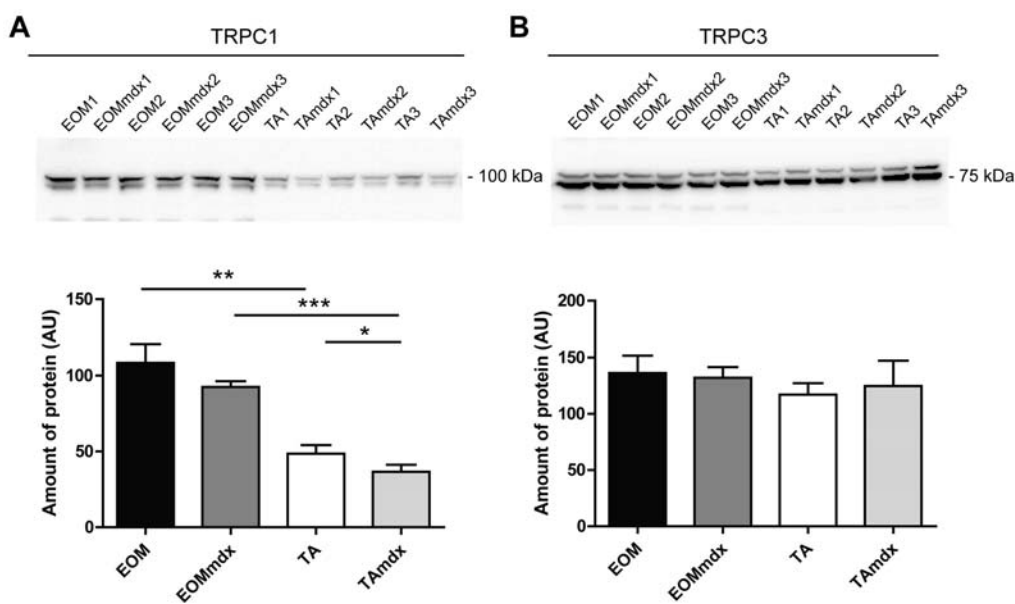


Fig. 3.15: Western Blot demonstrating protein levels of TRPC1 and TRPC3 in EOM, mdx EOM, TA and mdx TA. (A) TRPC1 was expressed at higher levels in EOM than in TA. TRPC1 was slightly reduced in TA mdx. (B) TRPC3 was expressed at equal levels in EOM and TA and was not changed in mdx tissue. (A, B) Statistical significance was determined using an unpaired t-test with $p < 0.05$ considered statistically significant. * $p < 0.05$, ** $p < 0.01$, * $p < 0.001$ ($n = 3$, mean \pm SD, AU = arbitrary units).**

3.2.2.3 mRNA expression of TRPV channels

mRNA copy numbers of the TRPV channels, TRPV1-TRPV6, were determined (Fig. 3.16). Out of the TRPV channel subgroup TRPV2 and TRPV4 were detected. TRPV1, TRPV3, TRPV5 and TRPV6 were not detectable in either EOM or TA. TRPV2 showed comparable expression levels in EOM, mdx EOM, TA and mdx TA. EOM showed significantly higher TRPV4 levels than TA, whereas no difference was seen in mdx EOM vs. mdx TA. The difference between EOM and mdx EOM did not reach significance. Overall, TRPV4 showed higher copy numbers than TRPV2 in EOM tissue. The expression levels of TRPV2 and TRPV4 were of comparable magnitude to TRPC1, TRPC3 and TRPC6.

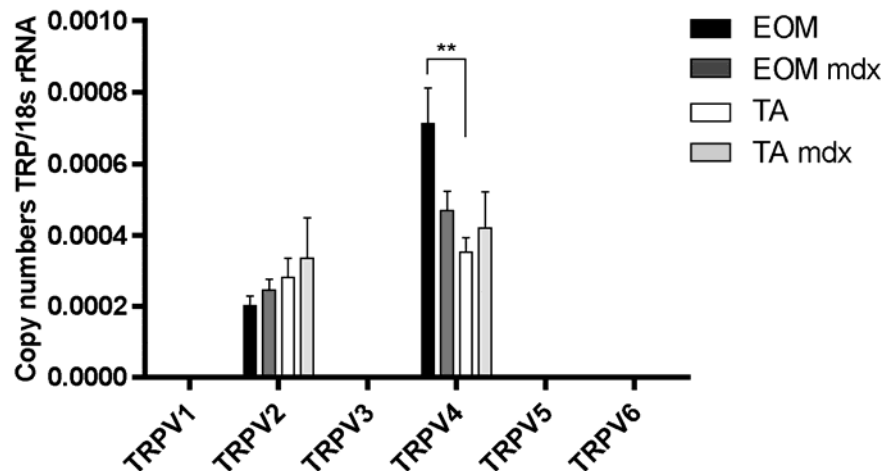


Fig. 3.16: mRNA quantification of the members of the TRPV channel subgroup. TRPV2 and TRPV4 were detected and were quantified in EOM, mdx EOM, TA and mdx TA. TRPV1, TRPV3, TRPV5 and TRPV6 were not detectable in either EOM or TA. Copy numbers were expressed relative to the reference gene 18s. Statistical significance was established using an unpaired t-test with $p < 0.05$ considered statistically significant. ** $p < 0.01$ ($n = 7-9$, mean \pm SEM).

3.2.2.4 Protein expression of TRPV4

To verify the findings on the mRNA level, western blotting was used to determine protein levels of the mechano-osmo-sensitive channel TRPV4 (Fig. 3.17). TRPV4 was detected as a double band, which is due to phosphorylation at about 98 kDa and 107 kDa as previously described (Xu et al., 2003). Brain tissue, which contains high levels of TRPV4, served as positive control. EOM and mdx EOM showed higher protein levels than TA and

mdx TA. In contrast to the mRNA levels a slight increase in protein levels in mdx EOM compared to normal EOM was noted.

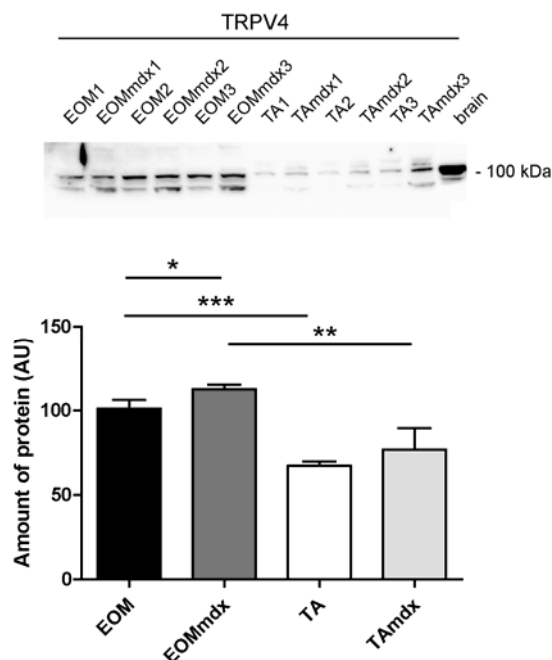


Fig. 3.17: Western blot demonstrating protein levels of TRPV4 in EOM, mdx EOM, TA and mdx TA. (A) TRPV4 was expressed at higher levels in EOM than in TA. Brain tissue served as control. Of note, 10 μ g of brain lysate and 30 μ g of muscle lysates were loaded. mdx EOM showed slightly higher TRPV4 levels compared with EOM. No difference was noted between normal and mdx tissue in TA. Statistical significance was determined using an unpaired t-test with $p < 0.05$ considered statistically significant. * $p < 0.05$, ** $p < 0.01$, *** $p < 0.001$. (n = 3, mean \pm SD, AU = arbitrary units).

3.2.2.5 mRNA expression of TRPM channels

mRNA expression levels of the TRPM channel subgroup members, TRPM1-TRPM8, were determined. TRPM3, TRPM4 and TRPM7 were expressed in EOM (Fig. 3.18). TRPM3 and TRPM7 levels were significantly decreased in mdx EOM. Consistent with previous reports and its ubiquitously high expression, TRPM7 was expressed at the highest level of all TRP channels in EOM tissue (Kunert-Keil et al., 2006). The expression of TRPM channels in TA tissue as well as protein expression was not further investigated.

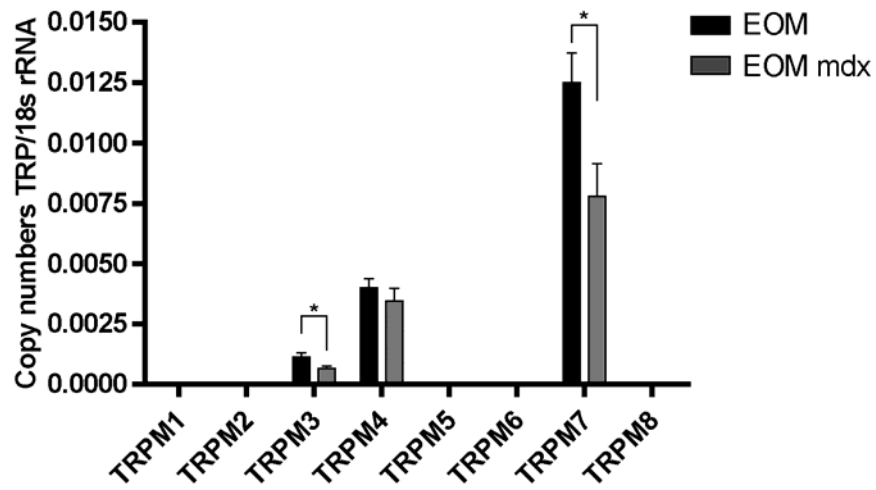


Fig. 3.18: mRNA quantification of TRPM1 through TRPM8. TRPM3, TRPM4 and TRPM7 were detected and were quantified in EOM and mdx EOM. TRPM1, TRPM2, TRPM5, TRPM6 and TRPM8 were not detectable in EOM. Copy numbers were expressed relative to the reference gene 18s. Statistical significance was determined using an unpaired t-test with * $p < 0.05$ considered statistically significant ($n = 7-9$, mean \pm SEM).

3.2.3 Expression of Orai1 and STIM1

3.2.3.1 mRNA expression of Orai1 and Stim1

Orai1 and Stim1 have recently been identified as the channel pore and the Ca^{2+} sensor of a Ca^{2+} selective SOCE (I_{CRAC}). For both genes, Orai1 and Stim1, mRNA levels were similar in EOM, mdx EOM and mdx TA. In addition, when comparing the copy numbers of Orai1 with Stim1 transcripts, they were found to be the same range. However, in TA, copy numbers of Orai1 and Stim1 were largely increased and significantly different compared with EOM and mdx TA (Fig. 3.19 A and B).

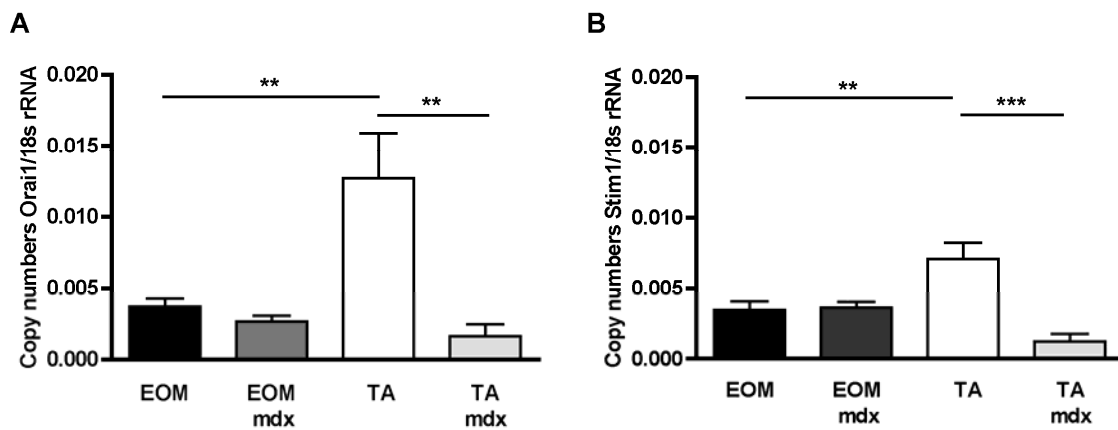


Fig. 3.19: mRNA quantification of Orai1 and Stim1. (A) Orai1 copy numbers were similar in EOM and mdx EOM. Copy numbers of TA were significantly higher in normal TA compared with EOM and mdx TA. (B) Similarly to Orai1, Stim1 copy numbers were similar in EOM and mdx EOM and TA copy numbers were significantly higher in normal TA compared with EOM and mdx TA. Copy numbers were expressed relative to the reference gene 18s. Differences were established using an unpaired t-test with $p < 0.05$ considered statistically significant. ** $p < 0.01$, *** $p < 0.001$ ($n = 7-9$, mean \pm SEM).

3.2.3.2 Protein expression of Orai1 and STIM1

Protein levels determined by western blotting confirmed the unchanged expression of Orai1 and STIM1 in EOM vs. mdx EOM as seen at the mRNA level (Fig. 3.20). However, STIM1 appeared to be more abundant in EOM and mdx EOM than Orai1 as estimated by the shorter exposure time and lower amount of protein lysate needed to detect STIM1 compared with Orai1 (Fig. 3.20 B). Higher expression of Orai1 or STIM1 in TA was not confirmed. Orai1 was expressed at similar levels in TA vs. mdx TA, while STIM1 was slightly increased

in mdx TA compared to TA (Fig. 3.20 B). This difference was only significant when only the lower band was quantified as described for this antibody by Edwards et al 2010 (Edwards et al., 2010b). Interestingly, levels of Orai1 protein were lower in EOM whereas STIM1 protein levels were higher compared with TA. There was no change between normal and mdx tissue. These results confirm the mRNA pattern in EOM and mdx EOM but not the large difference in mRNA levels between TA and mdx TA. A double band was detected for STIM1 in muscle, which may be due to glycosylation and/or phosphorylation of STIM1 (Manji et al., 2000). Quantification of the double band did not yield significant differences between normal and mdx tissues.

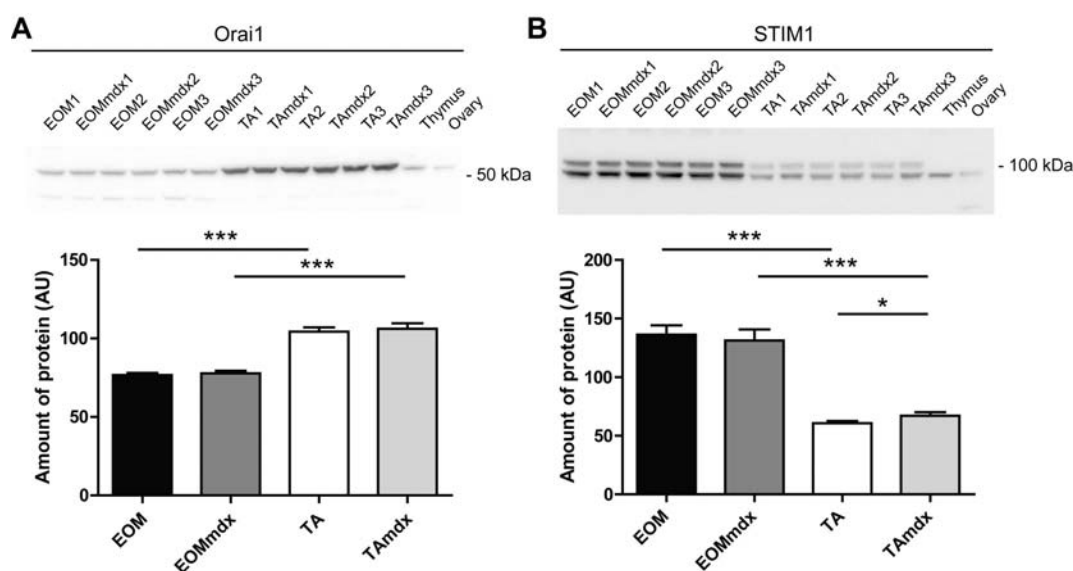


Fig. 3.20: Western blots demonstrating protein levels of Orai1 and STIM1 in EOM, mdx EOM, TA and mdx TA. (A) Orai1 was expressed at lower levels in EOM than in TA tissues. (B) STIM1 was expressed at higher levels in EOM than in TA. Thymus and ovary tissue served as positive control for Orai1 and STIM1. No difference was noted for either Orai1 or STIM1 between normal and mdx tissue in EOM. In TA a slight up-regulation was noted in mdx TA for STIM1, when only the lower band was quantified. Differences were established using an unpaired t-test with $p < 0.05$ considered statistically significant. * $p < 0.001$ ($n = 3$, mean \pm SD, AU = arbitrary units).**

4. Discussion

In this thesis it was shown that EOMs possess a superior Ca^{2+} homeostasis compared with TA. A combination of physiological, molecular and biochemical methods were used to demonstrate clear differences in the mechanisms used by EOM and TA to regulate cytoplasmic Ca^{2+} and in the ability of these cell types to buffer excess Ca^{2+} . Intracellular measurement of cytoplasmic Ca^{2+} levels demonstrated more effective buffering of excessive Ca^{2+} in EOM (Fig. 3.3 and 3.5). Molecular and biochemical methods revealed increased expression of mRNAs and proteins encoding numerous Ca^{2+} handling proteins, in particular CASQ2, SERCA2 and PLN (Table 3.1 & Fig. 3.6). Studies on protein phosphorylation suggested differential signaling and modulation cascades involving PLN-mediated Ca^{2+} regulation in EOM (Fig. 3.7). Combined, these data suggest that EOM may be better able to prevent prolonged elevations of cytoplasmic Ca^{2+} levels. To extend these data, molecular and biochemical expression analysis of the TRP and Orai channels and the regulatory protein STIM1 in EOM and TA provided clues toward the important role these channels may play in the Ca^{2+} homeostasis of EOM. Parallel expression analyses of these proteins in addition to the key Ca^{2+} handling proteins, SERCA1, SERCA2, CASQ and PLN, in EOM and TA of the mdx mouse model of DMD provided further details on potential alterations in the Ca^{2+} homeostasis in mdx EOM. These results offer further understanding of the physiology of EOM and of potential protective mechanisms that may be in place in the spared EOMs.

4.1 Calcium buffering in rat EOM

Ca^{2+} is a critical mediator of E-C coupling in muscles. Depolarization triggers the release of Ca^{2+} from the intracellular SR Ca^{2+} stores leading to transiently elevated Ca^{2+} levels in the cytoplasm, which results in muscle contraction (Melzer et al., 1995). This action is terminated when Ca^{2+} is cleared from the cytoplasm by pumps situated in the SR, the plasma membrane and by mitochondrial Ca^{2+} uptake (Rossi et al., 2009b; Rossi and Dirksen, 2006). EOM are superfast muscles with very fast contraction cycles depending on rapid Ca^{2+} turnover, including both the quick release of Ca^{2+} from intracellular stores for contraction and the prompt sequestering of Ca^{2+} to terminate the contraction and to allow muscle relaxation (Asmussen and Gaunitz, 1981; Bach-y-Rita and Ito, 1966; Close and Luff, 1974).

Measurements of cytoplasmic Ca^{2+} levels in EOM and TA myotubes suggested rapid depletion of Ca^{2+} from the SR in the cultured cells. This is supported by the fact that the Ca^{2+} peaks surpassed the 300 nM Ca^{2+} contained in the perfusion solution. EOM myotubes released larger amounts of Ca^{2+} from the SR, which was subsequently removed from the cytoplasm more efficiently than in TA myotubes. The larger Ca^{2+} peak in EOM cells stimulated with ionomycin or high K^+ suggests that the SR contains and can release more Ca^{2+} into the cytoplasm as compared to the TA. However, the peaks triggered with high K^+ were only a little more than half as high as those triggered by ionomycin, possibly reflecting the differences in physiological vs. pharmacological approaches used experimentally, such as the shorter stimulation time with high K^+ and the differences in receptor and channel involvement rather than membrane perforation achieved using ionophores.

Interestingly, EOM cultured myotubes reduced the higher cytoplasmic levels of Ca^{2+} more efficiently than TA; indeed EOM were nearly twice as effective as TA in terms of the time required to reduce the increased Ca^{2+} by 50% after ionomycin stimulation. The Ca^{2+} cycle observed in the cultured EOM myotubes, may have been facilitated by the increased levels of Casq2 in the SR and Pln stimulating Serca mediated Ca^{2+} uptake. However, only moderately elevated mRNA levels of Ca^{2+} handling proteins were found in the cultured myotubes, compared to muscle tissue (Table 3.1 “Myotubes”). This may be related to the fact that the cultured cells only partially recapitulate the physiological characteristics of fully differentiated muscle (Barjot et al., 1995; Rubinstein and Holtzer, 1979). The slight up-regulation of Cacna1s and Parv seen in EOM myotubes in contrast to adult EOM (Table 3.1 “Tissue”) compared to TA may also be due to a relative immaturity of myotubes (Schwartz and Kay, 1988). The similar morphology of EOM and TA myotubes (as opposed to the dissimilar morphology of EOM and TA muscle) further suggests that allotype-specific expression in cultured cells is partially rather than fully maintained. Indeed, this has been demonstrated in cell lines made from EOM and limb muscles and studied at the level of the transcriptome (Porter et al., 2006). For instance, this cell line does not express the eom-specific MyHC, which is known to be expressed rather late in the developing muscle (Brueckner et al., 1996). This suggests that the cell culture results likely underestimated the ability of EOM to buffer Ca^{2+} , and that even more dramatic differences may exist in vivo. The expression of Ca^{2+} handling proteins was further investigated using western blotting and immunohistochemistry. Due to the limited amount of primary myotubes available for western

blotting, mature muscle tissue for biochemical assays was used showing confirming clearly elevated levels of Ca²⁺ handling proteins in EOM.

The larger Ca²⁺ release from the EOM myotubes is in accord with an abundant SR in EOM containing potentially more releasable Ca²⁺ than TA limb muscles (Mayr, 1971). This is also consistent with the elevated levels of CASQ isoforms observed in EOM. CASQ as the major Ca²⁺ storage protein in the SR is believed to act as a luminal Ca²⁺ sensor regulating Ca²⁺ release by direct interaction with the RYR receptor (Beard et al., 2004). CASQ2, normally found in slow-twitch fibers and cardiac muscle, shares about 65% homology with CASQ1, the skeletal muscle isoform and has a slightly lower Ca²⁺ binding capacity (Park et al., 2004). Interestingly, CASQ2 was the predominant isoform in EOM; although the majority of EOM fibers are fast muscle fibers of which most have an abundant SR (Mayr, 1971; Porter et al., 1995). In fast EOM fibers, CASQ2 may also be present and co-expressed with the fast fiber isoform CASQ1 in at least some EOM fiber-types as has been suggested for SERCA1 and SERCA2 in human EOM (Kjellgren et al., 2003). This suggests functional differences in terms of Ca²⁺ storage and turnover in EOM.

The fast removal of elevated intracellular Ca²⁺ in muscle fibers is mainly carried out by the SR Ca²⁺ pumps (Rossi and Dirksen, 2006). SERCA2 was expressed at considerably higher levels in rat EOM than in TA; nevertheless SERCA1 was still the predominant isoform over SERCA2 in rat EOM in contrast to human EOM (Kjellgren et al., 2003). SERCA1 and SERCA2 are widely co-expressed in human EOM and in rabbit EOMs SERCA1 expression does not seem to be strictly co-regulated with fast myosin heavy chain as normally seen in fast muscle (Jacoby and Ko, 1993; Kjellgren et al., 2003). SERCA2 has a lower apparent Ca²⁺ affinity in cardiac SR than SERCA1 in skeletal muscle SR, but SERCA2 pump activity can be dynamically regulated by PLN (see below) (Lytton et al., 1992; Slack et al., 1997; Traaseth et al., 2008). This suggests, in analogy to the co-expression of CASQ2 and CASQ1, that co-expression of SERCA1 and SERCA2 in rat EOM may occur resulting in functional variance and unique kinetic of Ca²⁺ resquestration into the SR (Porter et al., 1995). In addition, the SR of fast vs. slow fibers of limb muscles differ regarding their Ca²⁺ load and release kinetics (Fryer and Stephenson, 1996), which would add to a unique SR function and Ca²⁺ handling in EOM fibers. Therefore, co-existence of both fast and slow characteristics in EOM fibers, in addition to the varying abundance of SR, would increase the complexity of Ca²⁺ homeostasis in EOM in respect to different fiber-types (Mayr, 1971;

Spencer and Porter, 2005). More detailed studies would help to elucidate fiber-type specific expression of Ca²⁺ binding proteins.

Indeed, initial immunohistochemical analysis supported the notion of complex fiber-type variation. Normally, SERCA2 and PLN are only found in cardiac and slow skeletal muscle (Reggiani and te Kronnie, 2006). Although, EOM are not thought to have classic slow fibers (Close and Luff, 1974), yet some fibers express slow myosin and have slow tonic contraction properties (Bormioli et al., 1980). SERCA2, PLN and CASQ-labeling was found at varying strengths in different fibers throughout the EOM sections. Further co-expression analysis would be of interest to identify those fibers along with investigating the SR content of individual fiber-types. Together, these results support the concept that EOM uniquely combine features of fast, slow and cardiac protein isoforms to facilitate constant activity including fast contraction cycles and high endurance.

Both SERCA1 and SERCA2 activity can be regulated by the homologous proteins PLN and SLN depending on their phosphorylation status, a process that is well understood for PLN but much less for SLN (Babu et al., 2005; Gramolini et al., 2006; Slack et al., 1997; Traaseth et al., 2008). While PLN was not expressed in TA, the high levels of PLN (mRNA and protein) and Sln (mRNA) could play a major role in regulating SERCA activity in EOM (Morita et al., 2008). SERCA activity is inhibited by PLN, but this inhibition is relieved upon phosphorylation of PLN (Traaseth et al., 2008). In EOM, PLN was predominantly endogenously phosphorylated at Thr17 and at trace levels at Ser16. Furthermore, phosphorylation at Ser16 could not be increased in vitro suggesting that the PLN-Ser16 site in EOM is not subject to significant functional regulation (Drago and Colyer, 1994; Simmerman et al., 1986). This is consistent with results in rabbit soleus muscle, a slow and high endurance skeletal muscle, where endogenous phosphorylation at Thr17 predominates over phosphorylation at Ser16 (Damiani et al., 2000). Phosphorylation at Thr17 is mediated by the SR bound CAMKII, which is activated by increased Ca²⁺ levels and CALM (Simmerman et al., 1986). Previously and in this study it was demonstrated that CAMKII expression is increased in rat EOM (Fraterman et al., 2007b). This is in accordance with the increased levels of CALM and the predominance of endogenous phosphorylation at Thr17 in EOM.

In addition, it has been proposed that CAMKII activity and the resulting phosphorylation of PLN at Thr17 have a predominant role in skeletal muscle endurance exercise, which is consistent with the constant activity of EOMs (Damiani et al., 2000; Rose et al., 2007; Rose et al., 2006). Only monomeric PLN was found in rat EOM, which is believed to be the active form (MacLennan and Kranias, 2003). This suggests that PLN is mainly present in its active form stimulating SERCA activity. CAMKII dependent phosphorylation of PLN has been shown to predominate at the terminal cisternae in close proximity to the Ca^{2+} release site (Gasser et al., 1988), which further supports efficient removal of Ca^{2+} in EOM. CAMKII is also able to phosphorylate SERCA2 directly and increase its activity (Toyofuku et al., 1993; Xu et al., 1993). These results suggest that in contrast to limb muscle, SERCA2 and possibly SERCA1 take advantage of an extra level of regulation in EOM, which may be modulated dependent on the activity of the fibers.

In addition to Ca^{2+} turnover mediated by the SR, the increased levels of cytoplasmic buffers, such as Parv, S100a and Tnnc observed in EOM may also help to quickly reduce the cytoplasmic concentration of free Ca^{2+} (Heizmann et al., 1982; Rome, 2006). Moreover, mitochondria are known to contribute significantly to the Ca^{2+} homeostasis in muscle (Pozzan and Rizzuto, 2000; Rossi et al., 2009b). The greater amount of mitochondria in EOM (Fischer et al., 2002; Mayr, 1971) has been implicated in playing a substantial role in taking up free Ca^{2+} increasing the dynamic response range of EOM (Andrade et al., 2005). Overall, the greater release and more rapid buffering of excess cytoplasmic Ca^{2+} that was observed provides direct support for the hypothesis that differences in Ca^{2+} handling dynamics contribute to the fast contraction cycles in EOM. Furthermore, this capacity to handle Ca^{2+} may act protective in dystrophin deficient fibers.

4.2 Calcium buffering in mouse EOM

Divergence in the expression of Ca^{2+} handling proteins in between species has been described. For instance, human fast muscle does not express PARV, whereas in small animals like the mouse, PARV plays an important role for relaxation in fast muscles (Celio and Heizmann, 1982; Heizmann et al., 1982). These expression differences have been correlated with the contraction-relaxation speed of the individual muscle and the size of the animal, where the ratio of fast vs. intermediate/slow muscle decreases with increasing size of the

individual (Heizmann et al., 1982). Even between rodents, muscle PARV levels were 2-fold higher in mouse compared with rat (Heizmann et al., 1982). To further compare key components of the Ca^{2+} homeostasis of rat and mouse, the protein levels of SERCA1, SERCA2, PLN and total CASQ were analyzed in mouse as well. The expression patterns of these proteins were largely similar in mouse tissue compared with rat. These data suggest that key components of the Ca^{2+} homeostasis in rat and mouse EOM are expressed at comparable proportions. Though, the relative expression level of total CASQ showed a more significant difference between mouse EOM and TA than between rat EOM and TA. This illustrates that variations in the magnitude of expression differences exist between rat and mouse suggesting that direct comparison between the two species should be done with caution. In conclusion, these results support the hypothesis and demonstrate that rodent EOMs are endowed with an extraordinary capacity to regulate their Ca^{2+} homeostasis.

4.3 Model of the superior calcium homeostasis in EOM

The model in Fig. 4.1 illustrates the Ca^{2+} homeostasis in EOM compared with TA. It schematically depicts general differences between EOM and TA in terms of SR size and number of Ca^{2+} handling proteins. The superior Ca^{2+} homeostasis is consistent with the functional demands of very fast and constantly active muscles (Asmussen and Gaunitz, 1981; Bach-y-Rita and Ito, 1966; Close and Luff, 1974; Fuchs and Binder, 1983). This model does not take into account the different fiber-types of EOM, which are predicted to differ in their Ca^{2+} homeostatic properties (Jacoby and Ko, 1993; Kjellgren et al., 2003). Nevertheless, distinct regulatory mechanisms, such as the role of PLN, involved in the Ca^{2+} homeostasis of EOMs is demonstrated. Revealing the molecular components of the Ca^{2+} homeostasis underlying the extraordinary physiological properties of EOMs would help explain the lack of Ca^{2+} -mediated damage in DMD and mdx EOM (Khurana et al., 1995). In the future, it will be of interest to map out the expression of Ca^{2+} buffering and Ca^{2+} handling proteins with respect to the different EOM fiber-types in more detail as well as functional differences in Ca^{2+} buffering properties of these fibers.

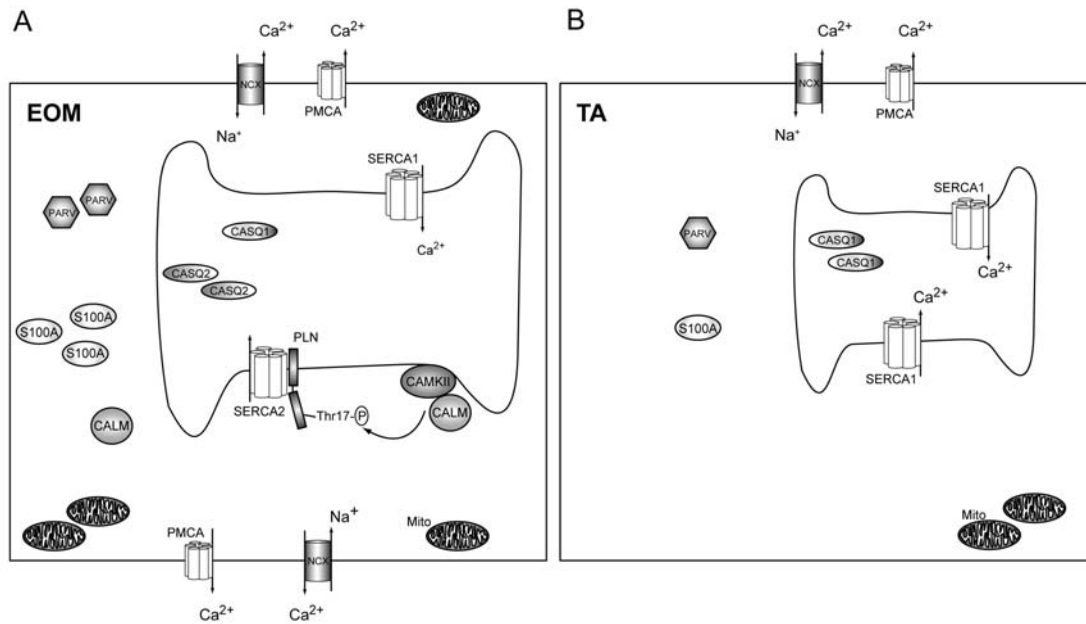


Fig. 4.1: Model of superior Ca^{2+} homeostasis in EOM. Schematic (A) shows an EOM muscle cell with a larger SR, numerous pumps and transporters in both the sarcolemma and the sarcoplasmic membrane and many Ca^{2+} binding proteins in the cytoplasm (e.g. S100a, PARV) and SR (CASQ1 and CASQ2), as well as numerous mitochondria. SERCA2 is regulated by PLN phosphorylated by CAMKII/CALM at Thr17. This regulation is missing in TA (B). Schematic (B) represents a TA muscle cell containing a smaller SR, fewer pumps and transporters and less Ca^{2+} binding proteins in the cytoplasm and SR compared with EOM. Excess Ca^{2+} ions entering the cell can be bound and/or removed more effectively in EOM than TA, leading to a faster return to resting Ca^{2+} levels. It is proposed that the extensive Ca^{2+} handling capacity of EOM reflects their functional properties and may help to protect this muscle group from Ca^{2+} mediated damage in DMD. (Symbols: SERCA: sarcoplasmic reticulum Ca^{2+} ATPase, CASQ: calsequestrin, PLN: phospholamban, PMCA: plasmamembrane Ca^{2+} ATPase, PARV: parvalbumin, CAMKII: Ca^{2+} /calmodulin dependent kinase II, CALM: calmodulin, Mito: mitochondria).

4.3 Expression of TRP channels, Orai and STIM in normal mouse muscle including EOM

To address the potential functional role of SOCE and other Ca^{2+} influx pathways in the Ca^{2+} homeostasis of EOMs the expression patterns of TRP channels and Orai and STIM proteins were studied. The extreme activity patterns of EOMs suggest that a high activity of SOCE plays a critical part to replenish Ca^{2+} for rapid and continuous cycles of contraction (Edwards et al., 2010b; Fuchs and Binder, 1983). Members of the TRPC channel subfamily

and the proteins Orai1 and STIM1 have been implicated with SOCE (Edwards et al., 2010b; Lyfenko and Dirksen, 2008; Stiber et al., 2008a; Vandebrouck et al., 2002).

The role of TRP channels (e.g. TRPC1, TRPC3, TRPV2 and TRPV4) in muscle has become increasingly evident (Gervasio et al., 2008; Iwata et al., 2009; Vandebrouck et al., 2002). Various muscles of wildtype mice and dystrophic muscles of mdx mice showed differential expression of TRP channels (Krüger et al., 2008; Kunert-Keil et al., 2006). The analysis of the expression pattern of TRPC channels in mouse EOM and TA muscle revealed high expression of TRPC1, TRPC3 and TRPC6. TRPC1 showed the highest levels in EOM as opposed to other skeletal muscles that showed predominant expression of TRPC3 and little TRPC1 expression at least in fast muscles (Kunert-Keil et al., 2006; Zanou et al., 2010). Moreover, differential expression was evident between EOM and TA. TRPC1 and TRPC6 showed higher expression in EOM compared with TA, while TRPC3 was expressed at similar levels in all muscle samples investigated. These results suggest a more dominant role for TRPC1 and TRPC6 in EOM and an equal importance of TRPC3 in EOM compared with TA. TRPC1 and TRPC3 protein expression was also confirmed by western blotting. Bands of the expected molecular weight (~100 kDa for TRPC1 and ~75 kDa for TRPC3) were frequently detected as indicated by the manufacturer of the antibodies. The specificity of these antibodies has been demonstrated before (Jorgensen et al., 2011). However, specificity issues with a number of TRP antibodies have been raised in the past (Flockerzi et al., 2005; Tajeddine et al., 2010), and testing tissue of the respective knockout mice in parallel would be helpful to support the expression results in this work.

TRPC channels can function as homo- or heteromers (Venkatachalam and Montell, 2007). In HEK293 cells, TRPC3 can heteromultimerize with TRPC1, while TRPC6 can heteromultimerize with TRPC4 to generate SOCE activated by Stim1 (Yuan et al., 2007). Since TRPC4 was hardly detectable and TRPC1 and TRPC3 were robustly expressed at the mRNA and protein level, TRPC1/TRPC3 heteromultimers may play a role in EOM SOCE, even though, the role of such heteromultimers has not yet been established in skeletal muscle (Lee et al., 2006). In addition, several studies in muscle showed an involvement of TRPC1 in increased Ca^{2+} entry after store depletion. In muscle fibers TRPC1 was localized at the sarcolemma and increased TRPC1 levels were associated with increased Ca^{2+} influx in mdx fibers (Vandebrouck et al., 2002). Recently, a role of TRPC1 in muscle fatigue by modulating

Ca²⁺ entry into muscle fibers during repeated contractions has been implicated (Zanou et al., 2010).

There is evidence that the main components of SOCE in muscle are Orai and STIM (Lyfenko and Dirksen, 2008). SOCE in muscle fibers is rapidly activated and inactivated to adapt to the rapid Ca²⁺ turnover in muscle (Edwards et al., 2010b; Lyfenko and Dirksen, 2008). In EOM lower Orai1 levels and higher STIM1 levels were found by western blotting compared with TA. The low levels of Orai1 may point toward less I_{CRAC} mediated by Orai1 or a relative increased importance of Orai2 or Orai3 in EOM. However, preliminary mRNA expression data on Orai2 and Orai3 showed that Orai2 and Orai3 expression levels were much less than Orai1 (data not shown). Another explanation for this result may be a lack of specificity of the used Orai1-CT antibody (ProSci Incorporated, see Materials), which has been questioned by a recent study (Edwards et al., 2010b). This antibody detected a protein of about 50 kDa that did not shift after de-glycosylation as suggested by the supplier. The detected band did also not correspond to a specific band of about 33 kDa detected by another well characterized antibody (Edwards et al., 2010b). Therefore, the Orai1 data in this thesis should be interpreted with caution. An additional argument against lower Orai1 levels in EOM is that the absolute quantification of mRNA by qPCR suggested equal expression levels of Orai1 and STIM1 (Fig. 3.19). Unfortunately, the qPCR data do not allow a final interpretation either because there seems to be a trend in the TA data that could not be confirmed on the protein level by western blotting. The STIM1 antibody from ProSci Incorporated has also been tested by the same group and was considered suitable for western blotting. However, they suggested that the specific band for STIM1 was only a single band and not the double band. Since STIM1 has been described as a phosphoprotein that can be glycosylated (Manji et al., 2000), it is possible that the double band is representative of total STIM1 in muscle. Therefore, the double band and the single band were quantified separately. Quantification of the single band resulted in a slight but significant up-regulation of STIM1 in TA mdx, whereas quantification of the double band showed no difference between EOM and EOM mdx or TA and TA mdx. In both cases EOM showed much higher expression levels of STIM1 than TA, which points toward high importance of SOCE regulation in EOM (Liou et al., 2005; Soboloff et al., 2006b). High STIM1 levels are also in accord with the abundant SR of EOM (Mayr, 1971; Porter et al., 1995).

Besides interacting with Orai1, STIM1 can activate SOCE mediated by TRPC1 (and other TRPC channels) and has been suggested to be a universal regulator of SOCE (Stiber et al., 2008a; Yuan et al., 2007). Due to its high expression levels, STIM1 might play an important role in sensing SR Ca^{2+} depletion and the regulation of SOCE in EOM. Accordingly, the high levels of TRPC1 in EOM compared with TA could further be associated with increased SOCE (Vandebrouck et al., 2002). Moreover, in non-muscle cells it has been described that TRPC1 can form a complex with Orai1 and STIM1 to conduct store-operated Ca^{2+} influx (Ambudkar et al., 2007; Ong et al., 2007). It remains to be elucidated, whether this complex formation exists in muscle and how each component contributes to its properties (Liao et al., 2007; Ong et al., 2007). However, it could be speculated that a muscle-type specific stoichiometry of TRPC1-Orai1-STIM1 or TRPC channel complexes may serve the Ca^{2+} needs of individual muscle- and allotypes (Ambudkar et al., 2007; Kunert-Keil et al., 2006; Yuan et al., 2007). To this point these results suggest SOCE may play an important component of the Ca^{2+} homeostasis in EOM consistent with the high requirements of the fast and highly adaptable Ca^{2+} turnover cycles in these muscles (Asmussen and Gaunitz, 1981; Bach-y-Rita and Ito, 1966; Close and Luff, 1974; Fuchs and Binder, 1983).

Of the TRPV channels, TRPV2 and TRPV4 were both expressed at similar levels in EOM and TA. Both channels can be activated by various stimuli, such as changes in temperature or osmolarity or by arachidonic acid (TRPV4) or growth-factors, such as IGF1 (TRPV2) (Kanzaki et al., 1999; Venkatachalam and Montell, 2007). Their roles in muscle are starting to be elucidated (Iwata et al., 2003; Pritschow et al., 2010). TRPV2 has been characterized as a stretch-activated channel (formerly growth-factor regulated channel), which may contribute to increased Ca^{2+} influx in mdx muscle (Iwata et al., 2003; Iwata et al., 2009).

TRPV4 channels have recently been implicated with muscle fatigue (Pritschow et al., 2010). Fatigue, due to repeated muscle activity is a multifactorial process that results in less efficient Ca^{2+} handling in the muscle, such as ionic/metabolic changes that reduce the Ca^{2+} sensitivity of myofilaments or impairment of SR Ca^{2+} release (Allen et al., 2008).

Recently, Ca^{2+} influx through TRPC1 and TRPV4 has been implicated with increased fatigue resistance in skeletal muscle fibers. Zanou and co-workers reported that TRPC1 showed the highest expression in the oxidative soleus muscle. Soleus of TRPC1^{-/-} mice

subjected to a fatigue protocol showed a much faster force loss than soleus from TRPC^{+/+} mice (Zanou et al., 2010). Pritschow and co-workers reported involvement of Ca²⁺ influx through TRPV4 in modulating fatigue (Pritschow et al., 2010). The TRPV4 activator α -PDD attenuated fatigue in normal soleus muscle. This effect was not seen in TRPV4^{-/-} mice (Pritschow et al., 2010). TRPV4 was found to be expressed at higher levels in EOM compared with TA. This was also confirmed on the protein level. However, because of potential specificity issues of certain batches of the TRPV4 antibody that have been suggested (personal communication Prof. Brinkmeier), a more stringent approach, such as testing tissue of knockout mice and the usage of additional TRPV4 antibodies would be helpful to confirm specificity.

The high fatigue resistance of EOM previously has been attributed mainly to their high oxidative activity (Frueh et al., 1994). The TRPV4 and TRPC1 expression patterns suggest that, besides SOCE, EOM benefit from additional pathways of Ca²⁺ influx to sustain continuous and fast activity. This, particularly the high levels of TRPC1, is also in accord with the characteristic expression of proteins in EOM usually seen in slow-oxidative muscles (Rossi et al., 2009a; Zanou et al., 2010; Zeiger et al., 2010). Another contributing factor may be the high STIM1 levels, which have been correlated with efficient refilling of Ca²⁺ stores, thereby imparting fatigue resistance (Stiber et al., 2008a). In summary, high levels of TRPC1, TRPV4 and STIM1 suggest that these proteins contribute to enhanced Ca²⁺ influx necessary to confer the high fatigue resistance of EOM (Frueh et al., 1994; Fuchs and Binder, 1983).

Besides their apparent functional importance in E-C coupling and Ca²⁺ homeostasis in muscle, several TRP channels and STIM1 have been suggested to be involved in myogenesis (Lee et al., 2006; Louis et al., 2008; Woo et al., 2010). EOMs continue to express embryonic protein isoforms and differentiation markers, such as embryonic MyHC, fetal acetylcholine receptor, neural cell adhesion molecule (NCAM) or insulin-growth factor (IGF) (Kaminski et al., 1996; McLoon and Wirtschafter, 1996). This phenomenon may be explained with a form of developmental arrest or continued cell division and myofiber remodeling (McLoon and Wirtschafter, 1996). SOCE via TRPCs, Orai and STIM may be involved in these processes in EOM as SOCE and other Ca²⁺ entry pathways have been associated with myoblast proliferation, differentiation and migration (Formigli et al., 2009; Lee et al., 2006; Louis et al., 2008; Stiber et al., 2008a; Woo et al., 2010). During myotube differentiation TRPC3 channels are sharply up-regulated and remain elevated in the mature myotubes (Lee et al.,

2006). Equal levels of TRPC3 in normal and mdx EOM and TA suggests that in these muscles TRPC3 expression and function are similar. In contrast to TRPC3, TRPC1 is highly expressed in immature myoblasts and together with a concomitant Ca^{2+} influx TRPC1 is only transiently up-regulated in muscle differentiation and fusion in skeletal myotubes (Formigli et al., 2009; Louis et al., 2008). The high TRPC1 levels might therefore also be a result of developmental arrest or myofiber remodeling in EOM. In addition, SOCE mediated by Orai/STIM has been shown to regulate myoblast differentiation and skeletal muscle development (Darbellay et al., 2009). Silencing of Orai1 or STIM1 reduced SOCE and myoblast differentiation (Darbellay et al., 2009) and mice lacking STIM1 develop a perinatally lethal skeletal myopathy suggesting involvement of STIM1 in early muscle development (Stiber et al., 2008a). EOM express high levels of STIM1, which has been suggested to correlate with greater SOCE and refilling of Ca^{2+} stores (Stiber et al., 2008a). These results suggest that Ca^{2+} influx mediated by TRPC channels (especially TRPC1) or Orai1/STIM1 may be part of the continued expression of developmental isoforms of the EOM muscle allotype (Fraterman et al., 2006; McLoon and Wirtschafter, 1996; Wieczorek et al., 1985).

The high levels of CALM noted in EOMs could offer additional regulatory control of TRPC channels, TRPV4 and TRPM4 (Strotmann et al., 2003; Zhu, 2005). TRP channels contain several putative CALM binding sites that confer varying levels of inhibition, e.g. for TRPC3, or in some cases activation, e.g. for TRPV4 (Zhu, 2005). TRPV4 channels have a C-terminal CALM binding site, where CALM binds and controls TRPV4 activity in a Ca^{2+} dependent manner in HEK293 cells (Strotmann et al., 2003). However, the functional role of modulatory CALM binding sites as Ca^{2+} mediated feedback mechanisms is only starting to be understood (Zhu, 2005).

Of the TRPM channels TRPM3, TRPM4 and TRPM7 were expressed in EOM. Interestingly, after TRPM7, TRPM4 showed the highest expression in contrast to previous reports about TRPM3 being the second most abundant TRPM channel after TRPM7 in muscle (Kunert-Keil et al., 2006). TRPM7 is ubiquitously expressed and is involved in Mg^{2+} homeostasis. TRPM3 is regulated by hypotonicity in kidney and sphingosines in brain (Harteneck, 2005). TRPM4 is a Ca^{2+} activated non-selective monovalent channel (Guinamard et al., 2010). The qPCR data showed reduced levels of TRPM3 and TRPM7 in EOM mdx, while TRPM4 expression did not change in EOM mdx. In another study, only TRPM4 was reduced in mdx muscle (Krüger et al., 2008). The relative abundance of TRPM channels in

muscle and their reduction in mdx mice hint toward a significant role in muscle (Krüger et al., 2008; Kunert-Keil et al., 2006). Although, not much is known about the function of TRPM channels in skeletal muscle the homeostasis of mono- and divalent cations besides the homeostasis of Ca^{2+} may be of as yet underappreciated importance in muscle pathophysiology.

4.4 Expression of calcium handling proteins and channels in mdx muscle: Implications for DMD

The physiological qualities of EOM may provide clues toward their enigmatic sparing in DMD. The EOMs ability to undergo rapid twitch contractions for extended periods of time endows them with enhanced Ca^{2+} buffering properties that may act protective in DMD. When the expression of key Ca^{2+} handling proteins, such as SERCA1, SERCA2, CASQ and PLN was tested in EOM from mdx mouse, no difference was found compared with normal mouse EOM. In addition, the expression of most tested TRP channels and the Orai1 and STIM1 proteins were unchanged between normal and mdx EOM. Exceptions were small increases in the TRPV4 protein and decreases in TRPM3 and TRPM7 in mdx EOM. These changes in mdx EOM could point to subtle compensatory changes due to the disease. In agreement with this, Pertille and co-workers reported increased levels of CALM and CASQ in mdx EOM suggesting some adaptive changes regarding Ca^{2+} homeostasis (Pertille et al., 2010). However, an increase in CASQ expression in mdx EOM could not be confirmed in this study. Previous, mRNA expression profiling in mdx EOM also revealed very few changes in global transcript expression that could not be correlated with the course of the disease (Porter et al., 2003b). This suggested that EOM are rather constitutively protected and do not actively adapt to compensate disease processes (Porter et al., 2003b). However, the findings of this work and the study by Pertille and co-workers concerning Ca^{2+} handling proteins suggest that some slight adaptive changes may occur in mdx EOM due to the loss of dystrophin (Pertille et al., 2010).

As expected the affected TA from mdx mice showed differential expression of Ca^{2+} handling proteins. Levels of the slow-muscle isoform SERCA2 were found to be increased in TA mdx tissue. This is consistent with previous reports, where increased or unchanged

SERCA2 levels in the fast EDL muscle of mdx mice were associated with altered SR Ca^{2+} uptake (Divet et al., 2005; Kargacin and Kargacin, 1996; Khammari et al., 1998; Plant and Lynch, 2003). Several studies reported decreased expression of Ca^{2+} handling proteins in mdx tissue. Ca^{2+} buffers like CASQ-like proteins, CASQ and SLN were decreased in mdx muscle tissue (Culligan et al., 2002; Doran et al., 2004; Dowling et al., 2004). In this thesis the proteomic findings of reduced CASQ levels reported by Dowling and co-workers could not be confirmed suggesting that western blotting with the antibody used may not be sensitive enough to detect subtle changes (Doran et al., 2004). This reduction of Ca^{2+} handling proteins, in combination with decreased SR Ca^{2+} uptake via SERCA2, would impair Ca^{2+} resequestration and storage, a critical part of excitation-contraction coupling (Hollingworth et al., 2008; Woods et al., 2004). Increased intracellular Ca^{2+} levels and dysregulated Ca^{2+} homeostasis in mdx muscle are followed by necrotic processes damaging the muscle (Turner et al., 1988). As outlined before, EOM have an enhanced Ca^{2+} buffering capacity to handle potentially increased Ca^{2+} levels in mdx EOM effectively, which may protect the muscle from Ca^{2+} induced damage.

Recently, pathways that may cause increased Ca^{2+} influx in mdx muscle have been investigated in more detail. These potential pathways have been narrowed down to be stretch-activated or store-operated channels. Several channel proteins or channel regulators have been implicated with this role, such as TRPC1, Orai1/ STIM1, TRPV2 or PLA2-metabolite regulated channels (Boittin et al., 2006; Edwards et al., 2010a; Iwata et al., 2003; Venkatachalam et al., 2002). In this work TRPC1 protein was found at slightly decreased levels in TA mdx, while there was no change at the mRNA level compared with normal TA. Others have reported increased TRPC1 levels in mdx limb muscle and suggested increased Ca^{2+} influx upon fiber stretch or store depletion (SOCE) (Gervasio et al., 2008; Vandebrouck et al., 2002). The quantitative discrepancy between the data may stem from the usage of different antibodies. In addition, in this work the results of TRPC1 channel expression have not been supported by functional data. However, since EOM are not affected, it suggests that high levels of TRPC1 alone do not confer pathology. Dysfunctional regulatory mechanisms might be in place in mdx muscle. Indeed, while TRPC1 is expressed and localized normally in Homer^{-/-} mice, the loss of Homer 1, a scaffolding protein of TRPC1 results in increased Ca^{2+} influx (Stiber et al., 2008b). Furthermore, Gervasio and co-workers suggested enhanced activation of TRPC1 by elevated reactive oxygen species (ROS) in mdx that could be blocked

by specific inhibitors (Gervasio et al., 2008). The high ROS scavenging capacity of EOM might act protective in this pathway in mdx mice (Ragusa et al., 1996).

The proteins Orai1 and STIM1 have been identified as the molecular components of highly Ca^{2+} selective SOCE in muscle (Edwards et al., 2010b; Lyfenko and Dirksen, 2008). No change in the expression of Orai1 and STIM1 between control EOM and mdx EOM was detected. However, a small increase of STIM1 in TA mdx tissue was noted, when quantifying only the single STIM1 band. This is in accord with a recent finding (Edwards et al., 2010a). Edwards and co-workers reported increased SOCE in mdx fibers accompanied by three-fold elevated Orai1 and STIM1 levels compared to normal muscle suggesting that Ca^{2+} influx is increased in mdx mice via the Ca^{2+} selective SOCE pathway (Edwards et al., 2010a). Interestingly, EOM showed high levels of STIM1, while Orai1 levels might be reduced or equally high compared to TA. Functionally, this could hint toward a high degree of regulative communication between the SR and SOCE in EOM because STIM1 regulates Orai1 and other SOCE capable TRPC channels, including TRPC1 (Liao et al., 2007; Soboloff et al., 2006b; Yuan et al., 2007). This suggests that in analogy to TRPC1 high STIM1 levels alone may not result in pathology and that additional dysregulation is occurring in mdx muscle. On the other hand functional demands may require enhanced SOCE activity in EOM, which in turn could be detrimental in a “slower” muscle like TA.

Krüger and co-workers examined differential expression of TRP channels in mdx tissue and found TRPC6 and TRPM4 to be decreased in mdx. Consistent with that report TRPC6 was found to be down-regulated in mdx TA (Krüger et al., 2008). Although not much is known about the function of TRPC6 in muscle, it could be speculated that involvement of TRPC6 in dystrophic muscle may be regulated through a putative CALM binding site which is common to all TRPC isoforms (Zhu, 2005). Ca^{2+} /calmodulin signaling plays a role in muscle remodeling and up-regulation of utrophin in DMD/mdx (Chakkalakal et al., 2006).

The analysis of TRPM channel expression in EOM showed that TRPM4 expression was unchanged in EOM mdx on the mRNA level, while TRPM3 and TRPM7 were down-regulated. The TRPM channels were not further investigated in TA as too little is known about their function in muscle, although they are among the most abundant TRP channels in muscle (Krüger et al., 2008; Kunert-Keil et al., 2006). They are not likely to be involved in increased Ca^{2+} influx in mdx muscle, though their role may extend to the regulation of a

larger range of mono- and divalent cations, including Mg^{2+} , Na^+ and K^+ . For instance, TRPM7 regulates the Mg^{2+} homeostasis, while TRPM4 conducts mainly Na^+ and K^+ (Guinamard et al., 2010). However, TRPM4 is a Ca^{2+} activated channel and its down-regulation in mdx mice might be secondary to increased Ca^{2+} in mdx fibers (Krüger et al., 2008).

In addition to a potential role in SOCE, there is strong evidence supporting the implication of a stretch-activated or mechanosensitive channels in the pathology of mdx. Overly active stretch-activated channels in mdx muscle can be blocked by streptomycin and spider venom improving functional and histological parameters (Yeung et al., 2005). A likely candidate for a dysregulated stretch-activated channel in mdx fibers is TRPV2. TRPV2 normally resides in intracellular compartments and translocates to the sarcolemma upon stimulation by stretch, increases in intracellular Ca^{2+} or stimulation by growth-factors, such as IGF-1 (Ducret et al., 2006; Iwata et al., 2003). In mdx mice, TRPV2 is concentrated at the sarcolemma rather than intracellularly (Iwata et al., 2009). Dominant negative expression of a TRPV2 mutant can decrease Ca^{2+} influx and ameliorate membrane damage and improve functional properties as well as histological changes of the muscle (Iwata et al., 2009; Zanou et al., 2009). By qPCR similar levels of mRNA were detected in EOM and TA and mdx muscle suggesting that TRPV2 channels have similar importance in EOM and TA. However, functional and regulatory differences may apply and are yet to be explored in EOM. Based on the previous studies regulation and localization of TRPV2 is critical rather than overall concentration highlighting the importance of functional studies.

Another aspect in the dysregulation of Ca^{2+} in mdx may be an increase in intracellular Na^+ levels. TRPC1 and TRPV2 are non-selective channels that conduct Na^+ as well as Ca^{2+} (Venkatachalam and Montell, 2007). Increased Na^+ influx through these channels have been suggested to contribute to the pathogenesis of muscular dystrophy. High intracellular Na^+ levels can inhibit Ca^{2+} extrusion by NCX or enhance the Ca^{2+} influx by reverse mode of NCX aggravating the dysregulation of Ca^{2+} concentrations in DMD/mdx (Iwata et al., 2007). In addition, augmented activity of Na^+/H^+ exchangers in dystrophic myotubes increases Na^+ further (Dunn et al., 1995). Yeung et al demonstrated that increased Na^+ levels after ECCs could be reduced by Gd^{3+} , a blocker of stretch-activated channels (Yeung et al., 2003). In EOM, NCX, Na^+/K^+ ATPase and its regulator phospholemman were expressed at higher levels (Fig. 3.8 and personal observation), which could account for more tightly regulated

Na⁺ levels in normal EOM and better compensation for increases in Na⁺ in dystrophic EOM compared with TA.

None of the channels suggested to be involved in increased Ca²⁺ influx in mdx muscle were differentially expressed in EOM mdx. This again suggests that EOM are inherently protected toward the loss of dystrophin rather than gaining resistance by adaptation (Porter et al., 2003a).

4.5 Therapeutic interventions targeting calcium homeostasis in DMD

The findings concerning the Ca²⁺ homeostasis of EOM can aid in developing new therapeutic targets for DMD. In previous studies several therapeutic interventions to protect the muscle from elevated Ca²⁺ levels have been tested. In clinical trials using Ca²⁺ antagonists such as diltiazem, verapamil or nifedipine no beneficial effects regarding muscle function were noted in DMD patients (Phillips and Quinlivan, 2008). Additional approaches were tested in mdx mice with varying results. Inhibition of the Ca²⁺ activated protease calpain by leupeptin or calpastatin showed some or no beneficial effect in mdx mice (Badalamente and Stracher, 2000; Briguet et al., 2008). Ca²⁺-independent phospholipase A2 has been shown to be overexpressed exhibiting enhanced activity in dystrophic muscle fibers leading to increased store-operated Ca²⁺ entry. Phospholipase-inhibitors were able to completely abolish the exaggerated Ca²⁺ influx (Boittin et al., 2006). Moreover, prednisone, the only drug with some beneficial effect in DMD patients may exert part of its effect via improvement of the Ca²⁺ homeostasis in dystrophic muscle (Leijendekker et al., 1996; Metzinger et al., 1995).

The results in this work suggested that EOMs seem to benefit from high levels of SERCA pumps and its regulator PLN in dealing with frequent and high Ca²⁺ transients. Therefore, overexpression of SERCA may be beneficial to remove excess Ca²⁺ from the cytosol in mdx/DMD muscle. Indeed, Morine et al reported that overexpression of SERCA1 improved histology and function of the mdx diaphragm (Morine et al., 2010). Another recent study confirmed and extended these data showing that overexpression of SERCA1 and SERCA2 almost completely rescued the dystrophic phenotype in two mouse models of muscular dystrophy, mdx and δ -sarcoglycan-null mice (*Sgcd*^{-/-}) (Goonasekera et al., 2011).

Transgenic overexpression reduced central nucleation in myofibers, tissue fibrosis and serum kinase levels in both mouse models and improved exercise capacity in *Sgcd*^{-/-} mice. In addition, over-expression of SERCA2a by adeno-associated virus gene therapy ameliorated dystrophic pathology in *Sgcd*^{-/-} mice. Further, Ca²⁺ mediated damage, such as swollen mitochondria and calpain activation was reduced by SERCA1 over-expression. These results showed that SERCA over-expression removed Ca²⁺ effectively from the cytoplasm suggesting a novel therapeutic approach for muscular dystrophies with altered Ca²⁺ homeostasis (Goonasekera et al., 2011).

Furthermore, differential expression and regulation of TRP channels in EOM may help to counteract potential dysregulation of Ca²⁺ homeostasis in EOM of mdx mice and DMD patients. Targeting TRP channels to reduce Ca²⁺ seems to be promising in mdx mice as a number of studies showed improvement of mdx pathology using inhibitors that act on TRP channels. ROS and SRC inhibitors reduced stretch-activated Ca²⁺ influx, possibly mediated by TRPC1, in mdx fibers (Gervasio et al., 2008). Streptomycin blocked stretch-activated channels and has been used to investigate Ca²⁺ influx in mdx fibers. In one study, streptomycin decreased stretch-activated Ca²⁺ influx ameliorating mdx pathology (Whitehead et al., 2006). Another recent study showed that long-term treatment with streptomycin improved limb muscle pathology but worsened heart histology (Jorgensen et al., 2011). Interestingly, among the few dysregulated proteins in mdx EOM a slight dysregulation of three TRP channels was noted. TRPV4 was slightly increased, while TRPM3 and TRPM7 were decreased in EOM mdx. However, not much is known about the function of these channels in muscle. As mentioned in the previous chapter, increased activation and Ca²⁺ influx through TRPV4 has been implicated with fatigue resistance and neither TRPM3 nor TRPM7 are associated with Ca²⁺ influx. Owing to the diversity and the relative lack of knowledge about TRP channel function in muscle and EOM, it is difficult to draw conclusions or derive potential therapeutic targets as yet from the TRP channel data in EOM.

Overall, EOM seem to show only very subtle adaptation to the disease. Concerning the involvement of EOM in the disease process, it can be concluded that regarding their Ca²⁺ homeostasis EOM are largely constitutively protected. In conclusion, the data in this thesis have improved the understanding of the Ca²⁺ homeostasis in the spared EOMs and may help to design new therapeutic approaches to ameliorate muscular dystrophy. Particularly, better understanding of the function and role of TRP channels in normal and dystrophic muscle will

provide new avenues for therapeutic approaches. Future studies should investigate the expression of different channels in more detail, as well as explore functional and regulatory aspects of the channels to understand their role in different muscle types including spared muscle allotypes, such as the EOMs.

5. Summary

The six extraocular muscles (EOMs) are arranged around the eyeball as agonist-antagonist pairs performing the eye movements. The EOMs comprise a distinct muscle group that is fundamentally different from other skeletal muscle, which is reflected on many levels, such as functionality, anatomy as well as in their molecular make-up. EOMs are compartmentalized into two distinct layers that are thought to be functionally different. Within those two layers at least six muscle fiber types can be distinguished, instead of the four classical fiber types found in other skeletal muscles. Physiologically EOMs are considered superfast, high endurance muscles that are continuously active. In addition, EOMs contain unusual slow-tonic fibers that share features with amphibian and avian slow-tonic fibers. EOMs also express slow/cardiac isoforms of proteins and genes along with the typical isoforms of fast muscle fibers. The EOM muscle fibers also continue to express embryonic protein isoforms, such as the fetal isoform of the acetylcholine receptor in adult muscle and embryonic myosin heavy chain. Another striking hallmark of EOM is their differential involvement in a number of diseases. For instance, EOMs are preferentially spared in Duchenne Muscular Dystrophy (DMD). DMD is the most common fatal, genetic disease in males clinically characterized by progressive muscle wasting. Mutations in the dystrophin gene result in a destabilization of the muscle membrane causing muscle fiber damage. While all other skeletal muscles deteriorate the EOMs remain morphologically and functionally healthy. In the pathogenesis of DMD elevated Ca^{2+} levels are believed to be an early event and it has been shown that EOMs are protected from pharmacologically induced Ca^{2+} damage. In addition, previous expression studies suggested that transcripts of several Ca^{2+} handling proteins were elevated in EOMs.

The goal of this study was to characterize the spared EOMs, in particular their Ca^{2+} homeostasis, in the context of DMD pathology to reveal new potential therapeutic targets for the disease.

A combination of physiological, molecular and biochemical methods was used to investigate the Ca^{2+} homeostasis of EOMs to demonstrate clear differences compared with the fast limb muscle tibialis anterior (TA). Ca^{2+} handling of stimulated cultured EOM myotubes suggested more efficient Ca^{2+} removal from the cytoplasm after induced Ca^{2+} influx compared with cultured myoblasts from TA. Subsequent mRNA and protein

expression analyses of myoblasts and adult muscle tissue using qPCR and Western blotting revealed high expression levels of many key Ca^{2+} regulating and buffering proteins in rodent EOMs compared with TA. Among these Ca^{2+} proteins were slow/cardiac proteins, which normally are not found in fast muscles. For instance, the sarcoplasmic Ca^{2+} ATPase SERCA2 was elevated along with its regulator phospholamban (PLN). Further, PLN was preferentially endogenously phosphorylated at Thr17 suggesting continuous activation of SERCA2 and possibly the fast isoform SERCA1, the main Ca^{2+} pumps responsible for removing Ca^{2+} from the cytoplasm after muscle contraction. Furthermore, Ca^{2+} buffers, such as calsequestrin (CASQ2) in the SR and parvalbumin (PARV) in the cytoplasm were elevated.

These results suggest that EOMs are endowed with a unique and superior Ca^{2+} homeostasis that facilitates efficient Ca^{2+} buffering and removal from the cytoplasm. This is in agreement with their continuous and fast activation cycles, as well as with a potential protective mechanism in prevention of Ca^{2+} overload in DMD.

The extreme activity patterns of EOM suggested that a high activity of store-operated Ca^{2+} entry (SOCE) plays a critical part to replenish Ca^{2+} for rapid and continuous cycles of contractions. To extend the data on general Ca^{2+} homeostasis and because of possible implications of store-operated Ca^{2+} influx and other Ca^{2+} influx pathways in DMD, the expression patterns of group 1 transient receptor potential (TRP) channels and the proteins Orail and STIM1 were studied. Out of the group 1 TRP channels, TRPC1, TRPC6 and TRPV4 channel proteins in addition to STIM1 showed higher expression in EOM compared with TA. High TRPC1, TRPV4 and STIM1 levels could play a significant role in the high fatigue resistance, muscle differentiation and SOCE in EOM. To investigate expression changes of Ca^{2+} handling proteins and channels in dystrophic muscle, tissue from the mdx mouse model of DMD, was used. The only channels differentially expressed in mdx EOM compared with normal EOM were TRPM4 and TRPM7 (decreased in mdx EOM) and TRPV4 (increased in mdx EOM). Although, these changes in mdx EOM were of small magnitude, they could point toward subtle compensatory changes related to the disease process. In general, EOMs seem to be unaffected by the disease and inherently protected. In conclusion, the results in this thesis have improved the understanding of the Ca^{2+} homeostasis in EOMs and suggest that EOM may be better able to prevent prolonged elevation of cytoplasmic Ca^{2+} levels. These data may help to design new therapeutic approaches targeting Ca^{2+} handling proteins to ameliorate muscular dystrophy.

6. References

- Aartsma-Rus, A., J.T. den Dunnen, and G.J. van Ommen. 2010. New insights in gene-derived therapy: the example of Duchenne muscular dystrophy. *Ann N Y Acad Sci.* 1214:199-212.
- Alderton, J.M., and R.A. Steinhardt. 2000. Calcium influx through calcium leak channels is responsible for the elevated levels of calcium-dependent proteolysis in dystrophic myotubes. *J Biol Chem.* 275:9452-60.
- Allamand, V., and K.P. Campbell. 2000. Animal models for muscular dystrophy: valuable tools for the development of therapies. *Hum Mol Genet.* 9:2459-67.
- Allen, D.G., G.D. Lamb, and H. Westerblad. 2008. Skeletal muscle fatigue: cellular mechanisms. *Physiol Rev.* 88:287-332.
- Ambros, V. 2004. The functions of animal microRNAs. *Nature.* 431:350-5.
- Ambudkar, I.S., H.L. Ong, X. Liu, B.C. Bandyopadhyay, and K.T. Cheng. 2007. TRPC1: the link between functionally distinct store-operated calcium channels. *Cell Calcium.* 42:213-23.
- Andrade, F.H., C.A. McMullen, and R.E. Rumbaut. 2005. Mitochondria are fast Ca²⁺ sinks in rat extraocular muscles: a novel regulatory influence on contractile function and metabolism. *Invest Ophthalmol Vis Sci.* 46:4541-7.
- Andrade, F.H., J.D. Porter, and H.J. Kaminski. 2000. Eye muscle sparing by the muscular dystrophies: lessons to be learned? *Microsc Res Tech.* 48:192-203.
- Asmussen, G. 1978. The properties of the extraocular muscles of the frog. I. Mechanical properties of the isolated superior oblique and superior rectus muscles. *Acta Biol Med Ger.* 37:301-12.
- Asmussen, G., and U. Gaunitz. 1981. Mechanical properties of the isolated inferior oblique muscle of the rabbit. *Pflügers Arch.* 392:183-90.
- Ausubel, F.M., B. Roger, R.E. Kingston, D.D. Moore 1999. Short protocols in molecular biology. John Wiley & Sons.
- Babu, G.J., Z. Zheng, P. Natarajan, D. Wheeler, P.M. Janssen, and M. Periasamy. 2005. Overexpression of sarcolipin decreases myocyte contractility and calcium transient. *Cardiovasc Res.* 65:177-86.
- Bach-y-Rita, P., and F. Ito. 1966. In vivo studies on fast and slow muscle fibers in cat extraocular muscles. *J Gen Physiol.* 49:1177-98.
- Badalamente, M.A., and A. Stracher. 2000. Delay of muscle degeneration and necrosis in mdx mice by calpain inhibition. *Muscle Nerve.* 23:106-11.

-
- Bahn, R.S., and A.E. Heufelder. 1993. Pathogenesis of Graves' ophthalmopathy. *N Engl J Med.* 329:1468-75.
- Barjot, C., M.L. Cotten, C. Goblet, R.G. Whalen, and F. Bacou. 1995. Expression of myosin heavy chain and of myogenic regulatory factor genes in fast or slow rabbit muscle satellite cell cultures. *J Muscle Res Cell Motil.* 16:619-28.
- Bartel, D.P. 2004. MicroRNAs: genomics, biogenesis, mechanism, and function. *Cell.* 116:281-97.
- Beard, N.A., D.R. Laver, and A.F. Dulhunty. 2004. Calsequestrin and the calcium release channel of skeletal and cardiac muscle. *Prog Biophys Mol Biol.* 85:33-69.
- Beech, D.J., K. Muraki, and R. Flemming. 2004. Non-selective cationic channels of smooth muscle and the mammalian homologues of *Drosophila* TRP. *J Physiol.* 559:685-706.
- Berbey, C., N. Weiss, C. Legrand, and B. Allard. 2009. Transient receptor potential canonical type 1 (TRPC1) operates as a sarcoplasmic reticulum calcium leak channel in skeletal muscle. *J Biol Chem.* 284:36387-94.
- Bodensteiner, J.B., and A.G. Engel. 1978. Intracellular calcium accumulation in Duchenne dystrophy and other myopathies: a study of 567,000 muscle fibers in 114 biopsies. *Neurology.* 28:439-46.
- Boittin, F.X., O. Petermann, C. Hirn, P. Mittaud, O.M. Dorchies, E. Roulet, and U.T. Rüegg. 2006. Ca²⁺-independent phospholipase A2 enhances store-operated Ca²⁺ entry in dystrophic skeletal muscle fibers. *J Cell Sci.* 119:3733-42.
- Bormioli, S.P., S. Sartore, M. Vitadello, and S. Schiaffino. 1980. "Slow" myosins in vertebrae skeletal muscle. An immunofluorescence study. *J Cell Biol.* 85:672-681.
- Brandman, O., J. Liou, W.S. Park, and T. Meyer. 2007. STIM2 is a feedback regulator that stabilizes basal cytosolic and endoplasmic reticulum Ca²⁺ levels. *Cell.* 131:1327-39.
- Brenman, J.E., D.S. Chao, H. Xia, K. Aldape, and D.S. Bredt. 1995. Nitric oxide synthase complexed with dystrophin and absent from skeletal muscle sarcolemma in Duchenne muscular dystrophy. *Cell.* 82:743-52.
- Brennecke, J., A. Stark, R.B. Russell, and S.M. Cohen. 2005. Principles of microRNA-target recognition. *PLoS Biol.* 3:e85.
- Briguet, A., M. Erb, I. Courdier-Fruh, P. Barzaghi, G. Santos, H. Herzner, C. Lescop, H. Siendt, M. Henneboehle, P. Weyermann, J.P. Magyar, J. Dubach-Powell, G. Metz, and T. Meier. 2008. Effect of calpain and proteasome inhibition on Ca²⁺-dependent proteolysis and muscle histopathology in the mdx mouse. *Faseb J.* 22:4190-200.
- Bron, A.J., R.C. Tripathi, and B.J. Tripathi. 1997. Wolff's Anatomy of the eye and the orbit. Chapman & Hall Medical, London.

-
- Brooke, M.H., and K.K. Kaiser. 1970. Muscle fiber types: how many and what kind? *Arch Neurol.* 23:369-79.
- Brueckner, J.K., O. Itkis, and J.D. Porter. 1996. Spatial and temporal patterns of myosin heavy chain expression in developing rat extraocular muscle. *J Muscle Res Cell Motil.* 17:297-312.
- Budak, M.T., S. Bogdanovich, M.H. Wiesen, O. Lozynska, T.S. Khurana, and N.A. Rubinstein. 2004. Layer-specific differences of gene expression in extraocular muscles identified by laser-capture microscopy. *Physiol Genomics.* 20:55-65.
- Bulfield, G., W.G. Siller, P.A. Wight, and K.J. Moore. 1984. X chromosome-linked muscular dystrophy (mdx) in the mouse. *Proc Natl Acad Sci U S A.* 81:1189-92.
- Burke, R.E. 1981. Motor units: anatomy, physiology, and functional organization. *American Physiological Society, Bethesda.*
- Campbell, K.P., and S.D. Kahl. 1989. Association of dystrophin and an integral membrane glycoprotein. *Nature.* 338:259-62.
- Caress, J.B., M.J. Kothari, S.B. Bauer, and J.M. Shefner. 1996. Urinary dysfunction in Duchenne muscular dystrophy. *Muscle Nerve.* 19:819-22.
- Celio, M.R., and C.W. Heizmann. 1982. Calcium-binding protein parvalbumin is associated with fast contracting muscle fibres. *Nature.* 297:504-6.
- Chakkalakal, J.V., S.A. Michel, E.R. Chin, R.N. Michel, and B.J. Jasmin. 2006. Targeted inhibition of Ca²⁺/calmodulin signaling exacerbates the dystrophic phenotype in mdx mouse muscle. *Hum Mol Genet.* 15:1423-35.
- Chomczynski, P., and N. Sacchi. 1987. Single-step method of RNA isolation by acid guanidinium thiocyanate-phenol-chloroform extraction. *Analytical Biochemistry.* 162:156-159.
- Clapham, D.E. 2003. TRP channels as cellular sensors. *Nature.* 426:517-24.
- Clapham, D.E., L.W. Runnels, and C. Strubing. 2001. The TRP ion channel family. *Nat Rev Neurosci.* 2:387-96.
- Close, R.I., and A.R. Luff. 1974. Dynamic properties of inferior rectus muscle of the rat. *J Physiol.* 236:259-270.
- Cohen, D.M. 2006. Regulation of TRP channels by N-linked glycosylation. *Semin Cell Dev Biol.* 17:630-7.
- Collet, C., B. Allard, Y. Tourneur, and V. Jacquemond. 1999. Intracellular calcium signals measured with indo-1 in isolated skeletal muscle fibres from control and mdx mice. *J Physiol.* 520:417-29.

- Cooper, B.J., N.J. Winand, H. Stedman, B.A. Valentine, E.P. Hoffman, L.M. Kunkel, M.O. Scott, K.H. Fischbeck, J.N. Kornegay, R.J. Avery, and et al. 1988. The homologue of the Duchenne locus is defective in X-linked muscular dystrophy of dogs. *Nature*. 334:154-6.
- Coulton, G.R., J.E. Morgan, T.A. Partridge, and J.C. Sloper. 1988. The mdx mouse skeletal muscle myopathy: I. A histological, morphometric and biochemical investigation. *Neuropathol Appl Neurobiol*. 14:53-70.
- Culligan, K., N. Banville, P. Dowling, and K. Ohlendieck. 2002. Drastic reduction of calsequestrin-like proteins and impaired calcium binding in dystrophic mdx muscle. *J Appl Physiol*. 92:435-45.
- Damiani, E., R. Sacchetto, and A. Margreth. 2000. Variation of phospholamban in slow-twitch muscle sarcoplasmic reticulum between mammalian species and a link to the substrate specificity of endogenous Ca²⁺-calmodulin-dependent protein kinase. *Biochim Biophys Acta*. 1464:231-41.
- Darbellay, B., S. Arnaudeau, D. Ceroni, C.R. Bader, S. Konig, and L. Bernheim. 2010. Human muscle economy myoblast differentiation and excitation-contraction coupling use the same molecular partners, STIM1 and STIM2. *J Biol Chem*. 285:22437-47.
- Darbellay, B., S. Arnaudeau, S. Konig, H. Jousset, C. Bader, N. Demaurex, and L. Bernheim. 2009. STIM1- and Orai1-dependent store-operated calcium entry regulates human myoblast differentiation. *J Biol Chem*. 284:5370-80.
- Deconinck, N., and B. Dan. 2007. Pathophysiology of duchenne muscular dystrophy: current hypotheses. *Pediatr Neurol*. 36:1-7.
- Deconinck, N., J. Tinsley, F. De Backer, R. Fisher, D. Kahn, S. Phelps, K. Davies, and J.M. Gillis. 1997. Expression of truncated utrophin leads to major functional improvements in dystrophin-deficient muscles of mice. *Nat Med*. 3:1216-21.
- Demer, J.L. 2002. The orbital pulley system: a revolution in concepts of orbital anatomy. *Ann N Y Acad Sci*. 956:17-32.
- Demer, J.L., S.Y. Oh, and V. Poukens. 2000. Evidence for active control of rectus extraocular muscle pulleys. *Invest Ophthalmol Vis Sci*. 41:1280-90.
- Deng, X., Y. Wang, Y. Zhou, J. Soboloff, and D.L. Gill. 2009. STIM and Orai: dynamic intermembrane coupling to control cellular calcium signals. *J Biol Chem*. 284:22501-5.
- Divet, A., A.M. Lompre, and C. Huchet-Cadiou. 2005. Effect of cyclopiazonic acid, an inhibitor of the sarcoplasmic reticulum Ca²⁺-ATPase, on skeletal muscles from normal and mdx mice. *Acta Physiol Scand*. 184:173-86.
- Doran, P., P. Dowling, P. Donoghue, M. Buffini, and K. Ohlendieck. 2006. Reduced expression of regucalcin in young and aged mdx diaphragm indicates abnormal cytosolic calcium handling in dystrophin-deficient muscle. *Biochim Biophys Acta*. 1764:773-85.

- Doran, P., P. Dowling, J. Lohan, K. McDonnell, S. Poetsch, and K. Ohlendieck. 2004. Subproteomics analysis of Ca²⁺-binding proteins demonstrates decreased calsequestrin expression in dystrophic mouse skeletal muscle. *Eur J Biochem.* 271:3943-52.
- Dowling, P., P. Doran, and K. Ohlendieck. 2004. Drastic reduction of sarcalumenin in Dp427 (dystrophin of 427 kDa)-deficient fibres indicates that abnormal calcium handling plays a key role in muscular dystrophy. *Biochem J.* 379:479-88.
- Drago, G.A., and J. Colyer. 1994. Discrimination between two sites of phosphorylation on adjacent amino acids by phosphorylation site-specific antibodies to phospholamban. *J Biol Chem.* 269:25073-7.
- Ducret, T., C. Vandebrouck, M.L. Cao, J. Lebacq, and P. Gailly. 2006. Functional role of store-operated and stretch-activated channels in murine adult skeletal muscle fibres. *J Physiol.* 575:913-24.
- Dunn, J.F., K.A. Burton, and M.J. Dauncey. 1995. Ouabain sensitive Na⁺/K⁺-ATPase content is elevated in mdx mice: implications for the regulation of ions in dystrophic muscle. *J Neurol Sci.* 133:11-5.
- Edwards, J.N., O. Friedrich, T.R. Cully, F. von Wegner, R.M. Murphy, and B.S. Launikonis. 2010a. Upregulation of store-operated Ca²⁺ entry in dystrophic mdx mouse muscle. *Am J Physiol Cell Physiol.* 299:C42-50.
- Edwards, J.N., R.M. Murphy, T.R. Cully, F. von Wegner, O. Friedrich, and B.S. Launikonis. 2010b. Ultra-rapid activation and deactivation of store-operated Ca²⁺ entry in skeletal muscle. *Cell Calcium.* 47:458-67.
- Eisenberg, I., A. Eran, I. Nishino, M. Moggio, C. Lamperti, A.A. Amato, H.G. Lidov, P.B. Kang, K.N. North, S. Mitrani-Rosenbaum, K.M. Flanigan, L.A. Neely, D. Whitney, A.H. Beggs, I.S. Kohane, and L.M. Kunkel. 2007. Distinctive patterns of microRNA expression in primary muscular disorders. *Proc Natl Acad Sci U S A.* 104:17016-21.
- Emery, A.E., and D. Burt. 1980. Intracellular calcium and pathogenesis and antenatal diagnosis of Duchenne muscular dystrophy. *Br Med J.* 280:355-7.
- Emery, A.E.H., and F. Muntoni. 2003. Duchenne muscular dystrophy. Oxford University Press, Oxford; New York. 270 p. pp.
- Ervasti, J.M., K. Ohlendieck, S.D. Kahl, M.G. Gaver, and K.P. Campbell. 1990. Deficiency of a glycoprotein component of the dystrophin complex in dystrophic muscle. *Nature.* 345:315-9.
- Ervasti, J.M., and K.J. Sonnemann. 2008. Biology of the striated muscle dystrophin-glycoprotein complex. *Int Rev Cytol.* 265:191-225.
- Farh, K.K., A. Grimson, C. Jan, B.P. Lewis, W.K. Johnston, L.P. Lim, C.B. Burge, and D.P. Bartel. 2005. The widespread impact of mammalian MicroRNAs on mRNA repression and evolution. *Science.* 310:1817-21.

- Felder, E., S. Bogdanovich, N.A. Rubinstein, and T.S. Khurana. 2005. Structural details of rat extraocular muscles and three-dimensional reconstruction of the rat inferior rectus muscle and muscle-pulley interface. *Vision Res.* 45:1945-55.
- Fischer, M.D., M.T. Budak, M. Bakay, J.R. Gorospe, D. Kjellgren, F. Pedrosa-Domellof, E.P. Hoffman, and T.S. Khurana. 2005. Definition of the unique human extraocular muscle allotype by expression profiling. *Physiol Genomics.* 22:283-91.
- Fischer, M.D., J.R. Gorospe, E. Felder, S. Bogdanovich, F. Pedrosa-Domellof, R.S. Ahima, N.A. Rubinstein, E.P. Hoffman, and T.S. Khurana. 2002. Expression profiling reveals metabolic and structural components of extraocular muscles. *Physiol Genomics.* 9:71-84.
- Fleig, A., and R. Penner. 2004. The TRPM ion channel subfamily: molecular, biophysical and functional features. *Trends Pharmacol Sci.* 25:633-9.
- Flockerzi, V., C. Jung, T. Aberle, M. Meissner, M. Freichel, S.E. Philipp, W. Nastainczyk, P. Maurer, and R. Zimmermann. 2005. Specific detection and semi-quantitative analysis of TRPC4 protein expression by antibodies. *Pflügers Arch.* 451:81-6.
- Formigli, L., C. Sassoli, R. Squecco, F. Bini, M. Martinesi, F. Chellini, G. Luciani, F. Sbrana, S. Zecchi-Orlandini, F. Francini, and E. Meacci. 2009. Regulation of transient receptor potential canonical channel 1 (TRPC1) by sphingosine 1-phosphate in C2C12 myoblasts and its relevance for a role of mechanotransduction in skeletal muscle differentiation. *J Cell Sci.* 122:1322-33.
- Franco-Obregon, A., and J.B. Lansman. 1994. Mechanosensitive ion channels in skeletal muscle from normal and dystrophic mice. *J Physiol.* 481:299-309.
- Franco, A., Jr., and J.B. Lansman. 1990. Calcium entry through stretch-inactivated ion channels in mdx myotubes. *Nature.* 344:670-3.
- Fraterman, S., T.S. Khurana, and N.A. Rubinstein. 2006. Identification of acetylcholine receptor subunits differentially expressed in singly and multiply innervated fibers of extraocular muscles. *Invest Ophthalmol Vis Sci.* 47:3828-34.
- Fraterman, S., U. Zeiger, T.S. Khurana, N.A. Rubinstein, and M. Wilm. 2007a. Combination of peptide OFFGEL fractionation and label-free quantitation facilitated proteomics profiling of extraocular muscle. *Proteomics.* 7:3404-16.
- Fraterman, S., U. Zeiger, T.S. Khurana, M. Wilm, and N.A. Rubinstein. 2007b. Quantitative proteomics profiling of sarcomere associated proteins in limb and extraocular muscle allotypes. *Mol Cell Proteomics.* 6:728-37.
- Frueh, B.R., A. Hayes, G.S. Lynch, and D.A. Williams. 1994. Contractile properties and temperature sensitivity of the extraocular muscles, the levator and superior rectus, of the rabbit. *J Physiol.* 475:327-36.
- Fryer, M.W., and D.G. Stephenson. 1996. Total and sarcoplasmic reticulum calcium contents of skinned fibres from rat skeletal muscle. *J Physiol.* 493:357-70.

-
- Fuchs, A.F., and M.D. Binder. 1983. Fatigue resistance of human extraocular muscles. *J Neurophysiol.* 49:28-34.
- Gailly, P., B. Boland, B. Himpens, R. Casteels, and J.M. Gillis. 1993a. Critical evaluation of cytosolic calcium determination in resting muscle fibres from normal and dystrophic (mdx) mice. *Cell Calcium.* 14:473-83.
- Gailly, P., E. Hermans, J.N. Octave, and J.M. Gillis. 1993b. Specific increase of genetic expression of parvalbumin in fast skeletal muscles of mdx mice. *FEBS Lett.* 326:272-274.
- Gasser, J., P. Paganetti, E. Carafoli, and M. Chiesi. 1988. Heterogeneous distribution of calmodulin- and cAMP-dependent regulation of Ca^{2+} uptake in cardiac sarcoplasmic reticulum subfractions. *Eur J Biochem.* 176:535-41.
- Gervasio, O.L., N.P. Whitehead, E.W. Yeung, W.D. Phillips, and D.G. Allen. 2008. TRPC1 binds to caveolin-3 and is regulated by Src kinase - role in Duchenne muscular dystrophy. *J Cell Sci.* 121:2246-55.
- Gibson, B. 2001. Long-term ventilation for patients with Duchenne muscular dystrophy : physicians' beliefs and practices. *Chest.* 119:940-6.
- Gillis, J.M. 1999. Understanding dystrophinopathies: an inventory of the structural and functional consequences of the absence of dystrophin in muscles of the mdx mouse. *J Muscle Res Cell Motil.* 20:605-25.
- Goonasekera, S.A., C.K. Lam, D.P. Millay, M.A. Sargent, R.J. Hajjar, E.G. Kranias, and J.D. Molkenstin. 2011. Mitigation of muscular dystrophy in mice by SERCA overexpression in skeletal muscle. *J Clin Invest.* in press.
- Gorospe, J.R., M.D. Tharp, J. Hinckley, J.N. Kornegay, and E.P. Hoffman. 1994. A role for mast cells in the progression of Duchenne muscular dystrophy? Correlations in dystrophin-deficient humans, dogs, and mice. *J Neurol Sci.* 122:44-56.
- Gramolini, A.O., M.G. Trivieri, G.Y. Oudit, T. Kislinger, W. Li, M.M. Patel, A. Emili, E.G. Kranias, P.H. Backx, and D.H. MacLennan. 2006. Cardiac-specific overexpression of sarcolipin in phospholamban null mice impairs myocyte function that is restored by phosphorylation. *Proc Natl Acad Sci U S A.* 103:2446-51.
- Grynkiewicz, G., M. Poenie, and R.Y. Tsien. 1985. A new generation of Ca^{2+} indicators with greatly improved fluorescence properties. *J Biol Chem.* 260:3440-50.
- Guinamard, R., M. Demion, and P. Launay. 2010. Physiological Roles of the TRPM4 Channel Extracted from Background Currents. *Physiology.* 25:155-164.
- Han, R., M.D. Grounds, and A.J. Bakker. 2006. Measurement of sub-membrane $[\text{Ca}^{2+}]$ in adult myofibers and cytosolic $[\text{Ca}^{2+}]$ in myotubes from normal and mdx mice using the Ca^{2+} indicator FFP-18. *Cell Calcium.* 40:299-307.

-
- Harteneck, C. 2005. Function and pharmacology of TRPM cation channels. *Naunyn Schmiedebergs Arch Pharmacol.* 371:307-14.
- Head, S.I. 1993. Membrane potential, resting calcium and calcium transients in isolated muscle fibres from normal and dystrophic mice. *J Physiol.* 469:11-9.
- Heizmann, C.W., M.W. Berchtold, and A.M. Rowlerson. 1982. Correlation of parvalbumin concentration with relaxation speed in mammalian muscles. *Proc Natl Acad Sci U S A.* 79:7243-7.
- Hess, A., and G. Pilar. 1963. Slow Fibres in the Extraocular Muscles of the Cat. *J Physiol.* 169:780-98.
- Hoh, J.F., and S. Hughes. 1988. Myogenic and neurogenic regulation of myosin gene expression in cat jaw-closing muscles regenerating in fast and slow limb muscle beds. *J Muscle Res Cell Motil.* 9:59-72.
- Hoh, J.F.Y., Hughes, S., Hugh, G. and Pozgaj, I. 1989. Three hierarchies in skeletal muscle fibre classification: Allotype, isotype, and phenotype. *In Cellular and Molecular Biology of Muscle Development.* Alan R. Liss, New York. 15-26.
- Hollingworth, S., U. Zeiger, and S.M. Baylor. 2008. Comparison of the myoplasmic calcium transient elicited by an action potential in intact fibres of mdx and normal mice. *J Physiol.* 586:5063-75.
- Hopf, F.W., P.R. Turner, W.F. Denetclaw, Jr., P. Reddy, and R.A. Steinhardt. 1996. A critical evaluation of resting intracellular free calcium regulation in dystrophic mdx muscle. *Am J Physiol.* 271:C1325-39.
- Hunter, M.I., and J.B. Mohamed. 1986. Plasma antioxidants and lipid peroxidation products in Duchenne muscular dystrophy. *Clin Chim Acta.* 155:123-31.
- Imbert, N., C. Cognard, G. Duport, C. Guillou, and G. Raymond. 1995. Abnormal calcium homeostasis in Duchenne muscular dystrophy myotubes contracting in vitro. *Cell Calcium.* 18:177-86.
- Imbert, N., C. Vandebrouck, B. Constantin, G. Duport, C. Guillou, C. Cognard, and G. Raymond. 1996. Hypoosmotic shocks induce elevation of resting calcium level in Duchenne muscular dystrophy myotubes contracting in vitro. *Neuromuscul Disord.* 6:351-60.
- Iwata, Y., Y. Katanosaka, Y. Arai, K. Komamura, K. Miyatake, and M. Shigekawa. 2003. A novel mechanism of myocyte degeneration involving the Ca²⁺-permeable growth factor-regulated channel. *J Cell Biol.* 161:957-67.
- Iwata, Y., Y. Katanosaka, Y. Arai, M. Shigekawa, and S. Wakabayashi. 2009. Dominant-negative inhibition of Ca²⁺ influx via TRPV2 ameliorates muscular dystrophy in animal models. *Hum Mol Genet.* 18:824-34.
-

- Iwata, Y., Y. Katanosaka, T. Hisamitsu, and S. Wakabayashi. 2007. Enhanced Na^+/H^+ exchange activity contributes to the pathogenesis of muscular dystrophy via involvement of P2 receptors. *Am J Pathol.* 171:1576-87.
- Jacoby, J., and K. Ko. 1993. Sarcoplasmic reticulum fast Ca^{2+} -pump and myosin heavy chain expression in extraocular muscles. *Invest Ophthalmol Vis Sci.* 34:2848-58.
- Jacoby, J., K. Ko, C. Weiss, and J.I. Rushbrook. 1990. Systematic variation in myosin expression along extraocular muscle fibres of the adult rat. *J Muscle Res Cell Motil.* 11:25-40.
- Johnstone, L.S., S.J. Graham, and M.A. Dziadek. 2010. STIM proteins: integrators of signalling pathways in development, differentiation and disease. *J Cell Mol Med.* 14:1890-903.
- Jorgensen, L.H., A. Blain, E. Grealley, S.H. Laval, A.M. Blamire, B.J. Davison, H. Brinkmeier, G.A. MacGowan, H.D. Schroder, K. Bushby, V. Straub, and H. Lochmuller. 2011. Long-term blocking of calcium channels in mdx mice results in differential effects on heart and skeletal muscle. *Am J Pathol.* 178:273-83.
- Kaminski, H.J., M. al-Hakim, R.J. Leigh, M.B. Katirji, and R.L. Ruff. 1992. Extraocular muscles are spared in advanced Duchenne dystrophy. *Ann Neurol.* 32:586-8.
- Kaminski, H.J., L.L. Kusner, and C.H. Block. 1996. Expression of acetylcholine receptor isoforms at extraocular muscle endplates. *Invest Ophthalmol Vis Sci.* 37:345-51.
- Kaminski, H.J., C.R. Richmonds, L.L. Kusner, and H. Mitsumoto. 2002. Differential susceptibility of the ocular motor system to disease. *Ann N Y Acad Sci.* 956:42-54.
- Kaminski, H.J., and R.L. Ruff. 1997. Ocular muscle involvement by myasthenia gravis. *Ann Neurol.* 41:419-20.
- Kanzaki, M., Y.Q. Zhang, H. Mashima, L. Li, H. Shibata, and I. Kojima. 1999. Translocation of a calcium-permeable cation channel induced by insulin-like growth factor-I. *Nat Cell Biol.* 1:165-70.
- Kargacin, M.E., and G.J. Kargacin. 1996. The sarcoplasmic reticulum calcium pump is functionally altered in dystrophic muscle. *Biochim Biophys Acta.* 1290:4-8.
- Karpati, G., and S. Carpenter. 1986. Small-caliber skeletal muscle fibers do not suffer deleterious consequences of dystrophic gene expression. *Am J Med Genet.* 25:653-8.
- Karpati, G., S. Carpenter, and S. Prescott. 1988. Small-caliber skeletal muscle fibers do not suffer necrosis in mdx mouse dystrophy. *Muscle Nerve.* 11:795-803.
- Kato, T. 1938. Über die histologischen Untersuchungen der Augenmuskeln von Menschen und Säugetieren. *Okajimas Folia Anat Jpn.* 16:14.

- Khammari, A., Y. Pereon, S. Baudet, and J. Noireaud. 1998. In situ study of the sarcoplasmic reticulum function in control and mdx mouse diaphragm muscle. *Can J Physiol Pharmacol.* 76:1161-5.
- Khanna, S., G. Cheng, B. Gong, M.J. Mustari, and J.D. Porter. 2004. Genome-wide transcriptional profiles are consistent with functional specialization of the extraocular muscle layers. *Invest Ophthalmol Vis Sci.* 45:3055-66.
- Khanna, S., A.P. Merriam, B. Gong, P. Leahy, and J.D. Porter. 2003. Comprehensive expression profiling by muscle tissue class and identification of the molecular niche of extraocular muscle. *Faseb J.* 17:1370-2.
- Khurana, T.S., and K.E. Davies. 2003. Pharmacological strategies for muscular dystrophy. *Nat Rev Drug Discov.* 2:379-90.
- Khurana, T.S., R.A. Prendergast, H.S. Alameddine, F.M. Tome, M. Fardeau, K. Arahata, H. Sugita, and L.M. Kunkel. 1995. Absence of extraocular muscle pathology in Duchenne's muscular dystrophy: role for calcium homeostasis in extraocular muscle sparing. *J Exp Med.* 182:467-75.
- Kinali, M., V. Arechavala-Gomez, L. Feng, S. Cirak, D. Hunt, C. Adkin, M. Guglieri, E. Ashton, S. Abbs, P. Nihoyannopoulos, M.E. Garralda, M. Rutherford, C. McCulley, L. Popplewell, I.R. Graham, G. Dickson, M.J. Wood, D.J. Wells, S.D. Wilton, R. Kole, V. Straub, K. Bushby, C. Sewry, J.E. Morgan, and F. Muntoni. 2009. Local restoration of dystrophin expression with the morpholino oligomer AVI-4658 in Duchenne muscular dystrophy: a single-blind, placebo-controlled, dose-escalation, proof-of-concept study. *Lancet Neurol.* 8:918-28.
- Kjellgren, D., M. Ryan, K. Ohlendieck, L.E. Thornell, and F. Pedrosa-Domellof. 2003. Sarco(endo)plasmic reticulum Ca^{2+} ATPases (SERCA1 and -2) in human extraocular muscles. *Invest Ophthalmol Vis Sci.* 44:5057-62.
- Krüger, J., C. Kunert-Keil, F. Bisping, and H. Brinkmeier. 2008. Transient receptor potential cation channels in normal and dystrophic mdx muscle. *Neuromuscul Disord.* 18:501-13.
- Kunert-Keil, C., F. Bisping, J. Krüger, and H. Brinkmeier. 2006. Tissue-specific expression of TRP channel genes in the mouse and its variation in three different mouse strains. *BMC Genomics.* 7:159.
- Kurebayashi, N., and Y. Ogawa. 2001. Depletion of Ca^{2+} in the sarcoplasmic reticulum stimulates Ca^{2+} entry into mouse skeletal muscle fibres. *J Physiol.* 533:185-99.
- Kuznetsov, A.V., K. Winkler, F.R. Wiedemann, P. von Bossanyi, K. Dietzmann, and W.S. Kunz. 1998. Impaired mitochondrial oxidative phosphorylation in skeletal muscle of the dystrophin-deficient mdx mouse. *Mol Cell Biochem.* 183:87-96.
- Laemmli, U.K. 1970. Cleavage of structural proteins during the assembly of the head of bacteriophage T4. *Nature.* 227:680-5.

-
- Launikonis, B.S., R.M. Murphy, and J.N. Edwards. 2010. Toward the roles of store-operated Ca^{2+} entry in skeletal muscle. *Pflügers Arch.* 460:813-23.
- Launikonis, B.S., and E. Rios. 2007. Store-operated Ca^{2+} entry during intracellular Ca^{2+} release in mammalian skeletal muscle. *J Physiol.* 583:81-97.
- Leberer, E., J.H. Charuk, N.M. Green, and D.H. MacLennan. 1989. Molecular cloning and expression of cDNA encoding a luminal calcium binding glycoprotein from sarcoplasmic reticulum. *Proc Natl Acad Sci U S A.* 86:6047-51.
- Lee, E.H., G. Cherednichenko, I.N. Pessah, and P.D. Allen. 2006. Functional coupling between TRPC3 and RyR1 regulates the expressions of key triadic proteins. *J Biol Chem.* 281:10042-8.
- Leijendekker, W.J., A.C. Passaquin, L. Metzinger, and U.T. Rüegg. 1996. Regulation of cytosolic calcium in skeletal muscle cells of the mdx mouse under conditions of stress. *Br J Pharmacol.* 118:611-6.
- Lewis, C., and K. Ohlendieck. 2010. Proteomic profiling of naturally protected extraocular muscles from the dystrophin-deficient mdx mouse. *Biochem Biophys Res Commun.* 396:1024-9.
- Liao, Y., C. Erxleben, E. Yildirim, J. Abramowitz, D.L. Armstrong, and L. Birnbaumer. 2007. Orai proteins interact with TRPC channels and confer responsiveness to store depletion. *Proc Natl Acad Sci U S A.* 104:4682-7.
- Liedtke, W. 2007. Role of TRPV ion channels in sensory transduction of osmotic stimuli in mammals. *Exp Physiol.* 92:507-12.
- Liou, J., M. Fivaz, T. Inoue, and T. Meyer. 2007. Live-cell imaging reveals sequential oligomerization and local plasma membrane targeting of stromal interaction molecule 1 after Ca^{2+} store depletion. *Proc Natl Acad Sci U S A.* 104:9301-6.
- Liou, J., M.L. Kim, W.D. Heo, J.T. Jones, J.W. Myers, J.E. Ferrell, Jr., and T. Meyer. 2005. STIM is a Ca^{2+} sensor essential for Ca^{2+} -store-depletion-triggered Ca^{2+} influx. *Curr Biol.* 15:1235-41.
- Louis, M., N. Zanou, M. Van Schoor, and P. Gailly. 2008. TRPC1 regulates skeletal myoblast migration and differentiation. *J Cell Sci.* 121:3951-9.
- Lowry, O.H., N.J. Rosebrough, A.L. Farr, and R.J. Randall. 1951. Protein measurement with the Folin phenol reagent. *J Biol Chem.* 193:265-75.
- Lyfenko, A.D., and R.T. Dirksen. 2008. Differential dependence of store-operated and excitation-coupled Ca^{2+} entry in skeletal muscle on STIM1 and Orai1. *J Physiol.* 586:4815-24.

- Lynch, G.S., B.R. Frueh, and D.A. Williams. 1994. Contractile properties of single skinned fibres from the extraocular muscles, the levator and superior rectus, of the rabbit. *J Physiol.* 475:337-46.
- Lytton, J., M. Westlin, S.E. Burk, G.E. Shull, and D.H. MacLennan. 1992. Functional comparisons between isoforms of the sarcoplasmic or endoplasmic reticulum family of calcium pumps. *J Biol Chem.* 267:14483-9.
- MacLennan, D.H., and E.G. Kranias. 2003. Phospholamban: a crucial regulator of cardiac contractility. *Nat Rev Mol Cell Biol.* 4:566-77.
- MacLennan, D.H., and P.T. Wong. 1971. Isolation of a calcium-sequestering protein from sarcoplasmic reticulum. *Proc Natl Acad Sci U S A.* 68:1231-5.
- Mallouk, N., V. Jacquemond, and B. Allard. 2000. Elevated subsarcolemmal Ca^{2+} in mdx mouse skeletal muscle fibers detected with Ca^{2+} -activated K^+ channels. *Proc Natl Acad Sci U S A.* 97:4950-5.
- Manji, S.S., N.J. Parker, R.T. Williams, L. van Stekelenburg, R.B. Pearson, M. Dziadek, and P.J. Smith. 2000. STIM1: a novel phosphoprotein located at the cell surface. *Biochim Biophys Acta.* 1481:147-55.
- Manzur, A.Y., T. Kuntzer, M. Pike, and A. Swan. 2008. Glucocorticoid corticosteroids for Duchenne muscular dystrophy. *Cochrane Database Syst Rev*:CD003725.
- Maroto, R., A. Raso, T.G. Wood, A. Kurosky, B. Martinac, and O.P. Hamill. 2005. TRPC1 forms the stretch-activated cation channel in vertebrate cells. *Nat Cell Biol.* 7:179-85.
- Marques, M.J., R. Ferretti, V.U. Vomero, E. Minatel, and H.S. Neto. 2007. Intrinsic laryngeal muscles are spared from myonecrosis in the mdx mouse model of Duchenne muscular dystrophy. *Muscle Nerve.* 35:349-53.
- Matsuda, R., A. Nishikawa, and H. Tanaka. 1995. Visualization of dystrophic muscle fibers in mdx mouse by vital staining with Evans blue: evidence of apoptosis in dystrophin-deficient muscle. *J Biochem.* 118:959-64.
- Matsumura, K., and K.P. Campbell. 1994. Dystrophin-glycoprotein complex: its role in the molecular pathogenesis of muscular dystrophies. *Muscle Nerve.* 17:2-15.
- Matsumura, K., J.M. Ervasti, K. Ohlendieck, S.D. Kahl, and K.P. Campbell. 1992. Association of dystrophin-related protein with dystrophin-associated proteins in mdx mouse muscle. *Nature.* 360:588-91.
- Mayr, R. 1971. Structure and distribution of fiber types in the external eye muscles of the rat. *Tissue Cell.* 3:433-462.
- McCarl, C.A., C. Picard, S. Khalil, T. Kawasaki, J. Rother, A. Papolos, J. Kutok, C. Hivroz, F. Ledeist, K. Plogmann, S. Ehl, G. Notheis, M.H. Albert, B.H. Belohradsky, J. Kirschner, A. Rao, A. Fischer, and S. Feske. 2009. ORAI1 deficiency and lack of store-operated Ca^{2+} entry

- cause immunodeficiency, myopathy, and ectodermal dysplasia. *J Allergy Clin Immunol.* 124:1311-1318.
- McDouall, R.M., M.J. Dunn, and V. Dubowitz. 1990. Nature of the mononuclear infiltrate and the mechanism of muscle damage in juvenile dermatomyositis and Duchenne muscular dystrophy. *J Neurol Sci.* 99:199-217.
- McKeon, T.A., and M.L. Lyman. 1991. Calcium ion improves electrophoretic transfer of calmodulin and other small proteins. *Anal Biochem.* 193:125-30.
- McLoon, L.K., and J. Wirtschafter. 2003. Activated satellite cells in extraocular muscles of normal adult monkeys and humans. *Invest Ophthalmol Vis Sci.* 44:1927-32.
- McLoon, L.K., and J.D. Wirtschafter. 1996. N-CAM is expressed in mature extraocular muscles in a pattern conserved among three species. *Invest Ophthalmol Vis Sci.* 37:318-27.
- McLoon, L.K., and J.D. Wirtschafter. 2002. Continuous myonuclear addition to single extraocular myofibers in uninjured adult rabbits. *Muscle Nerve.* 25:348-58.
- Mechler, F., S. Imre, and P. Dioszeghy. 1984. Lipid peroxidation and superoxide dismutase activity in muscle and erythrocytes in Duchenne muscular dystrophy. *J Neurol Sci.* 63:279-83.
- Melzer, W., A. Herrmann-Frank, and H.C. Lüttgau. 1995. The role of Ca²⁺ ions in excitation-contraction coupling of skeletal muscle fibres. *Biochim Biophys Acta.* 1241:59-116.
- Metzinger, L., A.C. Passaquin, W.J. Leijendekker, P. Poindron, and U.T. Rüegg. 1995. Modulation by prednisolone of calcium handling in skeletal muscle cells. *Br J Pharmacol.* 116:2811-6.
- Millay, D.P., S.A. Goonasekera, M.A. Sargent, M. Maillet, B.J. Aronow, and J.D. Molkenin. 2009. Calcium influx is sufficient to induce muscular dystrophy through a TRPC-dependent mechanism. *Proc Natl Acad Sci U S A.* 106:19023-8.
- Minetti, C., E. Ricci, and E. Bonilla. 1991. Progressive depletion of fast alpha-actinin-positive muscle fibers in Duchenne muscular dystrophy. *Neurology.* 41:1977-81.
- Moens, P., P.H. Baatsen, and G. Marechal. 1993. Increased susceptibility of EDL muscles from mdx mice to damage induced by contractions with stretch. *J Muscle Res Cell Motil.* 14:446-51.
- Montell, C. 2005. The TRP superfamily of cation channels. *Sci STKE.* 2005:re3.
- Montell, C., L. Birnbaumer, and V. Flockerzi. 2002. The TRP channels, a remarkably functional family. *Cell.* 108:595-8.
- Morine, K.J., M.M. Sleeper, E.R. Barton, and H.L. Sweeney. 2010. Overexpression of SERCA1a in the mdx diaphragm reduces susceptibility to contraction-induced damage. *Hum Gene Ther.* 21:1735-9.

- Morita, T., D. Hussain, M. Asahi, T. Tsuda, K. Kurzydowski, C. Toyoshima, and D.H. MacLennan. 2008. Interaction sites among phospholamban, sarcolipin, and the sarco(endo)plasmic reticulum Ca^{2+} -ATPase. *Biochem Biophys Res Commun.* 369:188-194.
- Murphy, R.M., N.T. Larkins, J.P. Mollica, N.A. Beard, and G.D. Lamb. 2008. Calsequestrin content and SERCA determine normal and maximal Ca^{2+} storage levels in sarcoplasmic reticulum of fast- and slow-twitch fibres of rat. *J Physiol.* 587:443-460.
- Oh, S.Y., V. Poukens, M.S. Cohen, and J.L. Demer. 2001. Structure-function correlation of laminar vascularity in human rectus extraocular muscles. *Invest Ophthalmol Vis Sci.* 42:17-22.
- Ohlendieck, K., and K.P. Campbell. 1991. Dystrophin-associated proteins are greatly reduced in skeletal muscle from mdx mice. *J Cell Biol.* 115:1685-94.
- Ong, H.L., K.T. Cheng, X. Liu, B.C. Bandyopadhyay, B.C. Paria, J. Soboloff, B. Pani, Y. Gwack, S. Srikanth, B.B. Singh, D.L. Gill, and I.S. Ambudkar. 2007. Dynamic assembly of TRPC1-STIM1-Orail ternary complex is involved in store-operated calcium influx. Evidence for similarities in store-operated and calcium release-activated calcium channel components. *J Biol Chem.* 282:9105-16.
- Pacheco-Pinedo, E.C., M.T. Budak, U. Zeiger, L.H. Jorgensen, S. Bogdanovich, H.D. Schroder, N.A. Rubinstein, and T.S. Khurana. 2009. Transcriptional and functional differences in stem cell populations isolated from extraocular and limb muscles. *Physiol Genomics.* 37:35-42.
- Parekh, A.B., and J.W. Putney, Jr. 2005. Store-operated calcium channels. *Physiol Rev.* 85:757-810.
- Park, H., I.Y. Park, E. Kim, B. Youn, K. Fields, A.K. Dunker, and C. Kang. 2004. Comparing skeletal and cardiac calsequestrin structures and their calcium binding: a proposed mechanism for coupled calcium binding and protein polymerization. *J Biol Chem.* 279:18026-33.
- Parvez, S., A. Beck, C. Peinelt, J. Soboloff, A. Lis, M. Monteilh-Zoller, D.L. Gill, A. Fleig, and R. Penner. 2008. STIM2 protein mediates distinct store-dependent and store-independent modes of CRAC channel activation. *Faseb J.* 22:752-61.
- Penna, A., A. Demuro, A.V. Yeromin, S.L. Zhang, O. Safrina, I. Parker, and M.D. Cahalan. 2008. The CRAC channel consists of a tetramer formed by Stim-induced dimerization of Orail dimers. *Nature.* 456:116-20.
- Pertille, A., C.L. de Carvalho, C.Y. Matsumura, H.S. Neto, and M.J. Marques. 2010. Calcium-binding proteins in skeletal muscles of the mdx mice: potential role in the pathogenesis of Duchenne muscular dystrophy. *Int J Exp Pathol.* 91:63-71.
- Petrof, B.J., J.B. Shrager, H.H. Stedman, A.M. Kelly, and H.L. Sweeney. 1993. Dystrophin protects the sarcolemma from stresses developed during muscle contraction. *Proc Natl Acad Sci U S A.* 90:3710-4.

-
- Phillips, M.F., and R. Quinlivan. 2008. Calcium antagonists for Duchenne muscular dystrophy. *Cochrane Database Syst Rev*:CD004571.
- Plant, D.R., and G.S. Lynch. 2003. Depolarization-induced contraction and SR function in mechanically skinned muscle fibers from dystrophic mdx mice. *Am J Physiol Cell Physiol*. 285:C522-8.
- Porter, J.D., and R.S. Baker. 1996. Muscles of a different 'color': the unusual properties of the extraocular muscles may predispose or protect them in neurogenic and myogenic disease. *Neurology*. 46:30-7.
- Porter, J.D., R.S. Baker, R.J. Ragusa, and J.K. Brueckner. 1995. Extraocular muscles: basic and clinical aspects of structure and function. *Surv Ophthalmol*. 39:451-84.
- Porter, J.D., D.P. Edney, E.J. McMahon, and L.A. Burns. 1988. Extraocular myotoxicity of the retrobulbar anesthetic bupivacaine hydrochloride. *Invest Ophthalmol Vis Sci*. 29:163-74.
- Porter, J.D., S. Israel, B. Gong, A.P. Merriam, J. Feuerman, S. Khanna, and H.J. Kaminski. 2006. Distinctive morphological and gene/protein expression signatures during myogenesis in novel cell lines from extraocular and hindlimb muscle. *Physiol Genomics*. 24:264-75.
- Porter, J.D., and P. Karathanasis. 1998. Extraocular muscle in merosin-deficient muscular dystrophy: cation homeostasis is maintained but is not mechanistic in muscle sparing. *Cell Tissue Res*. 292:495-501.
- Porter, J.D., S. Khanna, H.J. Kaminski, J.S. Rao, A.P. Merriam, C.R. Richmonds, P. Leahy, J. Li, and F.H. Andrade. 2001a. Extraocular muscle is defined by a fundamentally distinct gene expression profile. *Proc Natl Acad Sci U S A*. 98:12062-7.
- Porter, J.D., A.P. Merriam, A.A. Hack, F.H. Andrade, and E.M. McNally. 2001b. Extraocular muscle is spared despite the absence of an intact sarcoglycan complex in gamma- or delta-sarcoglycan-deficient mice. *Neuromuscul Disord*. 11:197-207.
- Porter, J.D., A.P. Merriam, S. Khanna, F.H. Andrade, C.R. Richmonds, P. Leahy, G. Cheng, P. Karathanasis, X. Zhou, L.L. Kusner, M.E. Adams, M. Willem, U. Mayer, and H.J. Kaminski. 2003a. Constitutive properties, not molecular adaptations, mediate extraocular muscle sparing in dystrophic mdx mice. *Faseb J*. 17:893-5.
- Porter, J.D., A.P. Merriam, P. Leahy, B. Gong, and S. Khanna. 2003b. Dissection of temporal gene expression signatures of affected and spared muscle groups in dystrophin-deficient (mdx) mice. *Hum Mol Genet*. 12:1813-21.
- Porter, J.D., J.A. Rafael, R.J. Ragusa, J.K. Brueckner, J.I. Trickett, and K.E. Davies. 1998. The sparing of extraocular muscle in dystrophinopathy is lost in mice lacking utrophin and dystrophin. *J Cell Sci*. 111:1801-11.
- Pozzan, T., and R. Rizzuto. 2000. The renaissance of mitochondrial calcium transport. *Eur J Biochem*. 267:5269-73.
-

- Pressmar, J., H. Brinkmeier, M.J. Seewald, T. Naumann, and R. Rudel. 1994. Intracellular Ca^{2+} concentrations are not elevated in resting cultured muscle from Duchenne (DMD) patients and in MDX mouse muscle fibres. *Pflügers Arch.* 426:499-505.
- Pritschow, B.W., T. Lange, J. Kasch, C. Kunert-Keil, W. Liedtke, and H. Brinkmeier. 2010. Functional TRPV4 channels are expressed in mouse skeletal muscle and can modulate resting Ca^{2+} influx and muscle fatigue. *Pflügers Arch.* 461:115-122.
- Ragusa, R.J., C.K. Chow, and J.D. Porter. 1997. Oxidative stress as a potential pathogenic mechanism in an animal model of Duchenne muscular dystrophy. *Neuromuscul Disord.* 7:379-86.
- Ragusa, R.J., C.K. Chow, D.K. St Clair, and J.D. Porter. 1996. Extraocular, limb and diaphragm muscle group-specific antioxidant enzyme activity patterns in control and mdx mice. *J Neurol Sci.* 139:180-6.
- Rando, T.A., and H.M. Blau. 1994. Primary mouse myoblast purification, characterization, and transplantation for cell-mediated gene therapy. *J Cell Biol.* 125:1275-87.
- Reggiani, C., and T. te Kronnie. 2006. RyR isoforms and fibre type-specific expression of proteins controlling intracellular calcium concentration in skeletal muscles. *J Muscle Res Cell Motil.* 27:327-35.
- Robert, V., M.L. Massimino, V. Tosello, R. Marsault, M. Cantini, V. Sorrentino, and T. Pozzan. 2001. Alteration in calcium handling at the subcellular level in mdx myotubes. *J Biol Chem.* 276:4647-51.
- Roberts-Thomson, S.J., A.A. Peters, D.M. Grice, and G.R. Monteith. 2010. ORAI-mediated calcium entry: mechanism and roles, diseases and pharmacology. *Pharmacol Ther.* 127:121-30.
- Rome, L.C. 2006. Design and function of superfast muscles: new insights into the physiology of skeletal muscle. *Annu Rev Physiol.* 68:193-221.
- Rose, A.J., C. Froisig, B. Kiens, J.F. Wojtaszewski, and E.A. Richter. 2007. Effect of endurance exercise training on Ca^{2+} calmodulin-dependent protein kinase II expression and signalling in skeletal muscle of humans. *J Physiol.* 583:785-95.
- Rose, A.J., B. Kiens, and E.A. Richter. 2006. Ca^{2+} -calmodulin-dependent protein kinase expression and signalling in skeletal muscle during exercise. *J Physiol.* 574:889-903.
- Rosenberg, P., A. Hawkins, J. Stiber, J.M. Shelton, K. Hutcheson, R. Bassel-Duby, D.M. Shin, Z. Yan, and R.S. Williams. 2004. TRPC3 channels confer cellular memory of recent neuromuscular activity. *Proc Natl Acad Sci U S A.* 101:9387-92.
- Rossi, A.C., C. Mammucari, C. Argentini, C. Reggiani, and S. Schiaffino. 2009a. Two novel/ancient myosins in mammalian skeletal muscles: MYH14 and MYH15 are expressed in extraocular muscles and muscle spindles. *J Physiol.* 588:352-364.

- Rossi, A.E., S. Boncompagni, and R.T. Dirksen. 2009b. Sarcoplasmic reticulum-mitochondrial symbiosis: bidirectional signaling in skeletal muscle. *Exerc Sport Sci Rev.* 37:29-35.
- Rossi, A.E., and R.T. Dirksen. 2006. Sarcoplasmic reticulum: the dynamic calcium governor of muscle. *Muscle Nerve.* 33:715-31.
- Rouger, K., M. Le Cunff, M. Steenman, M.C. Potier, N. Gibelin, C.A. Dechesne, and J.J. Leger. 2002. Global/temporal gene expression in diaphragm and hindlimb muscles of dystrophin-deficient (mdx) mice. *Am J Physiol Cell Physiol.* 283:C773-84.
- Rubinstein, N.A., and H. Holtzer. 1979. Fast and slow muscles in tissue culture synthesise only fast myosin. *Nature.* 280:323-5.
- Rubinstein, N.A., J.D. Porter, and J.F. Hoh. 2004. The development of longitudinal variation of Myosin isoforms in the orbital fibers of extraocular muscles of rats. *Invest Ophthalmol Vis Sci.* 45:3067-72.
- Sabourin, J., C. Lamiche, A. Vandebrouck, C. Magaud, J. Rivet, C. Cognard, N. Bourmeyster, and B. Constantin. 2009. Regulation of TRPC1 and TRPC4 Cation Channels Requires an alpha1-Syntrophin-dependent Complex in Skeletal Mouse Myotubes. 284:36248-36261.
- Saiki, R.K., S. Scharf, F. Faloona, K.B. Mullis, G.T. Horn, H.A. Erlich, and N. Arnheim. 1985. Enzymatic amplification of beta-globin genomic sequences and restriction site analysis for diagnosis of sickle cell anemia. *Science.* 230:1350-4.
- Salido, G.M., S.O. Sage, and J.A. Rosado. 2009. Biochemical and functional properties of the store-operated Ca²⁺ channels. *Cell Signal.* 21:457-61.
- Sambrook, J., T. Maniatis. 1989. *Molecular Cloning: A Laboratory Manual.* Cold Spring Harbor Laboratory Press.
- Santillan, G., S. Katz, C. Buitrago, and R. Boland. 2004. 1alpha,25(OH)2D3 induces capacitative calcium entry involving a TRPC3 protein in skeletal muscle and osteoblastic cells. *Biol Res.* 37:647-51.
- Schiaffino, S., M. Sandri, and M. Murgia. 2007. Activity-dependent signaling pathways controlling muscle diversity and plasticity. *Physiology (Bethesda).* 22:269-78.
- Schmalbruch, H. 1984. Regenerated muscle fibers in Duchenne muscular dystrophy: a serial section study. *Neurology.* 34:60-5.
- Schwartz, L.M., and B.K. Kay. 1988. Differential expression of the Ca²⁺-binding protein parvalbumin during myogenesis in *Xenopus laevis*. *Dev Biol.* 128:441-52.
- Scott, A.B., and C.C. Collins. 1973. Division of labor in human extraocular muscle. *Arch Ophthalmol.* 90:319-22.

-
- Sicinski, P., Y. Geng, A.S. Ryder-Cook, E.A. Barnard, M.G. Darlison, and P.J. Barnard. 1989. The Molecular Basis of Muscular Dystrophy in the mdx Mouse: A Point Mutation. *Science*. 244:1578-1580.
- Simmerman, H.K., J.H. Collins, J.L. Theibert, A.D. Wegener, and L.R. Jones. 1986. Sequence analysis of phospholamban. Identification of phosphorylation sites and two major structural domains. *J Biol Chem*. 261:13333-41.
- Slack, J.P., I.L. Grupp, D.G. Ferguson, N. Rosenthal, and E.G. Kranias. 1997. Ectopic expression of phospholamban in fast-twitch skeletal muscle alters sarcoplasmic reticulum Ca²⁺ transport and muscle relaxation. *J Biol Chem*. 272:18862-8.
- Smythe, G.M. 2009. Dystrophic pathology in the intrinsic and extrinsic laryngeal muscles in the mdx mouse. *J Otolaryngol Head Neck Surg*. 38:323-36.
- Soboloff, J., M.A. Spassova, T. Hewavitharana, L.P. He, W. Xu, L.S. Johnstone, M.A. Dziadek, and D.L. Gill. 2006a. STIM2 is an inhibitor of STIM1-mediated store-operated Ca²⁺ entry. *Curr Biol*. 16:1465-70.
- Soboloff, J., M.A. Spassova, X.D. Tang, T. Hewavitharana, W. Xu, and D.L. Gill. 2006b. Orai1 and STIM reconstitute store-operated calcium channel function. *J Biol Chem*. 281:20661-5.
- Spencer, M.J., D.E. Croall, and J.G. Tidball. 1995. Calpains are activated in necrotic fibers from mdx dystrophic mice. *J Biol Chem*. 270:10909-14.
- Spencer, R.F., and J.D. Porter. 2005. Biological organization of the extraocular muscles. *Prog Brain Res*. 151:43-80.
- Stedman, H.H., H.L. Sweeney, J.B. Shrager, H.C. Maguire, R.A. Panettieri, B. Petrof, M. Narusawa, J.M. Lefterovich, J.T. Sladky, and A.M. Kelly. 1991. The mdx mouse diaphragm reproduces the degenerative changes of Duchenne muscular dystrophy. *Nature*. 352:536-9.
- Stiber, J., A. Hawkins, Z.S. Zhang, S. Wang, J. Burch, V. Graham, C.C. Ward, M. Seth, E. Finch, N. Malouf, R.S. Williams, J.P. Eu, and P. Rosenberg. 2008a. STIM1 signalling controls store-operated calcium entry required for development and contractile function in skeletal muscle. *Nat Cell Biol*. 10:688-97.
- Stiber, J.A., Z.S. Zhang, J. Burch, J.P. Eu, S. Zhang, G.A. Truskey, M. Seth, N. Yamaguchi, G. Meissner, R. Shah, P.F. Worley, R.S. Williams, and P.B. Rosenberg. 2008b. Mice lacking Homer 1 exhibit a skeletal myopathy characterized by abnormal transient receptor potential channel activity. *Mol Cell Biol*. 28:2637-47.
- Strotmann, R., G. Schultz, and T.D. Plant. 2003. Ca²⁺-dependent potentiation of the nonselective cation channel TRPV4 is mediated by a C-terminal calmodulin binding site. *J Biol Chem*. 278:26541-9.
- Tajeddine, N., N.g. Zanou, M. Van Schoor, J. Lebacq, and P. Gailly. 2010. TRPC1: Subcellular Localization? *J Biol Chem*. 285:1e1.
-

- Tidball, J.G., and M. Wehling-Henricks. 2004. Expression of a NOS transgene in dystrophin-deficient muscle reduces muscle membrane damage without increasing the expression of membrane-associated cytoskeletal proteins. *Mol Genet Metab.* 82:312-20.
- Tinsley, J.M., A.C. Potter, S.R. Phelps, R. Fisher, J.I. Trickett, and K.E. Davies. 1996. Amelioration of the dystrophic phenotype of mdx mice using a truncated utrophin transgene. *Nature.* 384:349-53.
- Torres, L.F., and L.W. Duchen. 1987. The mutant mdx: inherited myopathy in the mouse. Morphological studies of nerves, muscles and end-plates. *Brain.* 110:269-99.
- Toyofuku, T., K. Kurzydowski, M. Tada, and D.H. MacLennan. 1993. Identification of regions in the Ca²⁺-ATPase of sarcoplasmic reticulum that affect functional association with phospholamban. *J Biol Chem.* 268:2809-15.
- Traaseth, N.J., K.N. Ha, R. Verardi, L. Shi, J.J. Buffy, L.R. Masterson, and G. Veglia. 2008. Structural and dynamic basis of phospholamban and sarcolipin inhibition of Ca²⁺-ATPase. *Biochemistry.* 47:3-13.
- Turner, P.R., P.Y. Fong, W.F. Denetclaw, and R.A. Steinhardt. 1991. Increased calcium influx in dystrophic muscle. *J Cell Biol.* 115:1701-12.
- Turner, P.R., R. Schultz, B. Ganguly, and R.A. Steinhardt. 1993. Proteolysis results in altered leak channel kinetics and elevated free calcium in mdx muscle. *J Membr Biol.* 133:243-51.
- Turner, P.R., T. Westwood, C.M. Regen, and R.A. Steinhardt. 1988. Increased protein degradation results from elevated free calcium levels found in muscle from mdx mice. *Nature.* 335:735-8.
- Tutdibi, O., H. Brinkmeier, R. Rudel, and K.J. Fohr. 1999. Increased calcium entry into dystrophin-deficient muscle fibres of MDX and ADR-MDX mice is reduced by ion channel blockers. *J Physiol.* 515 (Pt 3):859-68.
- van Deutekom, J.C., A.A. Janson, I.B. Ginjaar, W.S. Frankhuizen, A. Aartsma-Rus, M. Bremmer-Bout, J.T. den Dunnen, K. Koop, A.J. van der Kooi, N.M. Goemans, S.J. de Kimpe, P.F. Ekhart, E.H. Venneker, G.J. Platenburg, J.J. Verschuuren, and G.J. van Ommen. 2007. Local dystrophin restoration with antisense oligonucleotide PRO051. *N Engl J Med.* 357:2677-86.
- Vandebrouck, A., J. Sabourin, J. Rivet, H. Balghi, S. Sebille, A. Kitzis, G. Raymond, C. Cognard, N. Bourmeyster, and B. Constantin. 2007. Regulation of capacitative calcium entries by alpha1-syntrophin: association of TRPC1 with dystrophin complex and the PDZ domain of alpha1-syntrophin. *Faseb J.* 21:608-17.
- Vandebrouck, C., D. Martin, M. Colson-Van Schoor, H. Debaix, and P. Gailly. 2002. Involvement of TRPC in the abnormal calcium influx observed in dystrophic (mdx) mouse skeletal muscle fibers. *J Cell Biol.* 158:1089-96.

- Varnai, P., L. Hunyady, and T. Balla. 2009. STIM and Orai: the long-awaited constituents of store-operated calcium entry. *Trends Pharmacol Sci.* 30:118-28.
- Venkatachalam, K., and C. Montell. 2007. TRP channels. *Annu Rev Biochem.* 76:387-417.
- Venkatachalam, K., D.B. van Rossum, R.L. Patterson, H.T. Ma, and D.L. Gill. 2002. The cellular and molecular basis of store-operated calcium entry. *Nat Cell Biol.* 4:E263-72.
- Vennekens, R., and B. Nilius. 2007. Insights into TRPM4 function, regulation and physiological role. *In Handb Exp Pharmacol.* Springer. 269-85.
- Vig, M., C. Peinelt, A. Beck, D.L. Koomoa, D. Rabah, M. Koblan-Huberson, S. Kraft, H. Turner, A. Fleig, R. Penner, and J.P. Kinet. 2006. CRACM1 is a plasma membrane protein essential for store-operated Ca²⁺ entry. *Science.* 312:1220-3.
- von Scheven, G., L.c.E. Alvares, R.C. Mootosamy, and S. Dietrich. 2006. Neural tube derived signals and Fgf8 act antagonistically to specify eye versus mandibular arch muscles. *Development.* 133:2731-2745.
- Webster, C., L. Silberstein, A.P. Hays, and H.M. Blau. 1988. Fast muscle fibers are preferentially affected in Duchenne muscular dystrophy. *Cell.* 52:503-13.
- Wehling, M., J.T. Stull, T.J. McCabe, and J.G. Tidball. 1998. Sparing of mdx extraocular muscles from dystrophic pathology is not attributable to normalized concentration or distribution of neuronal nitric oxide synthase. *Neuromuscul Disord.* 8:22-9.
- Welch, E.M., E.R. Barton, J. Zhuo, Y. Tomizawa, W.J. Friesen, P. Trifillis, S. Paushkin, M. Patel, C.R. Trotta, S. Hwang, R.G. Wilde, G. Karp, J. Takasugi, G. Chen, S. Jones, H. Ren, Y.C. Moon, D. Corson, A.A. Turpoff, J.A. Campbell, M.M. Conn, A. Khan, N.G. Almstead, J. Hedrick, A. Mollin, N. Risher, M. Weetall, S. Yeh, A.A. Branstrom, J.M. Colacino, J. Babiak, W.D. Ju, S. Hirawat, V.J. Northcutt, L.L. Miller, P. Spatrack, F. He, M. Kawana, H. Feng, A. Jacobson, S.W. Peltz, and H.L. Sweeney. 2007. PTC124 targets genetic disorders caused by nonsense mutations. *Nature.* 447:87-91.
- Weller, B., G. Karpati, and S. Carpenter. 1990. Dystrophin-deficient mdx muscle fibers are preferentially vulnerable to necrosis induced by experimental lengthening contractions. *J Neurol Sci.* 100:9-13.
- Whitehead, N.P., M. Streamer, L.I. Lusambili, F. Sachs, and D.G. Allen. 2006. Streptomycin reduces stretch-induced membrane permeability in muscles from mdx mice. *Neuromuscul Disord.* 16:845-54.
- Wieczorek, D.F., M. Periasamy, G.S. Butler-Browne, R.G. Whalen, and B. Nadal-Ginard. 1985. Co-expression of multiple myosin heavy chain genes, in addition to a tissue-specific one, in extraocular musculature. *J Cell Biol.* 101:618-29.
- Woo, J.S., C.H. Cho, H. Kim do, and E.H. Lee. 2010. TRPC3 cation channel plays an important role in proliferation and differentiation of skeletal muscle myoblasts. *Exp Mol Med.* 42:614-27.

- Woo, J.S., H. Kim do, P.D. Allen, and E.H. Lee. 2008. TRPC3-interacting triadic proteins in skeletal muscle. *Biochem J.* 411:399-405.
- Woods, C.E., D. Novo, M. DiFranco, and J.L. Vergara. 2004. The action potential-evoked sarcoplasmic reticulum calcium release is impaired in mdx mouse muscle fibres. *J Physiol.* 557:59-75.
- Worley, P.F., W. Zeng, G.N. Huang, J.P. Yuan, J.Y. Kim, M.G. Lee, and S. Muallem. 2007. TRPC channels as STIM1-regulated store-operated channels. *Cell Calcium.* 42:205-11.
- Xu, A., C. Hawkins, and N. Narayanan. 1993. Phosphorylation and activation of the Ca^{2+} -pumping ATPase of cardiac sarcoplasmic reticulum by Ca^{2+} /calmodulin-dependent protein kinase. *J Biol Chem.* 268:8394-7.
- Xu, H., H. Zhao, W. Tian, K. Yoshida, J.B. Roullet, and D.M. Cohen. 2003. Regulation of a transient receptor potential (TRP) channel by tyrosine phosphorylation. SRC family kinase-dependent tyrosine phosphorylation of TRPV4 on TYR-253 mediates its response to hypotonic stress. *J Biol Chem.* 278:11520-7.
- Yeung, E.W., H.J. Ballard, J.P. Bourreau, and D.G. Allen. 2003. Intracellular sodium in mammalian muscle fibers after eccentric contractions. *J Appl Physiol.* 94:2475-82.
- Yeung, E.W., N.P. Whitehead, T.M. Suchyna, P.A. Gottlieb, F. Sachs, and D.G. Allen. 2005. Effects of stretch-activated channel blockers on $[\text{Ca}^{2+}]_i$ and muscle damage in the mdx mouse. *J Physiol.* 562:367-80.
- Yuan, J.P., W. Zeng, G.N. Huang, P.F. Worley, and S. Muallem. 2007. STIM1 heteromultimerizes TRPC channels to determine their function as store-operated channels. *Nat Cell Biol.* 9:636-45.
- Zanou, N., Y. Iwata, O. Schakman, J. Lebacqz, S. Wakabayashi, and P. Gailly. 2009. Essential role of TRPV2 ion channel in the sensitivity of dystrophic muscle to eccentric contractions. *FEBS Lett.* 583:3600-3604.
- Zanou, N., G. Shapovalov, M. Louis, N. Tajeddine, C. Gallo, M. Van Schoor, I. Anguish, M.L. Cao, O. Schakman, A. Dietrich, J. Lebacqz, U. Ruegg, E. Roulet, L. Birnbaumer, and P. Gailly. 2010. Role of TRPC1 channel in skeletal muscle function. *Am J Physiol Cell Physiol.* 298:C149-62.
- Zeiger, U., and T.S. Khurana. 2010. Distinctive Patterns of MicroRNA Expression in Extraocular Muscles. *Physiol Genomics.*
- Zeiger, U., C.H. Mitchell, and T.S. Khurana. 2010. Superior calcium homeostasis of extraocular muscles. *Exp Eye Res.* 91:613-22.
- Zhang, S.L., Y. Yu, J. Roos, J.A. Kozak, T.J. Deerinck, M.H. Ellisman, K.A. Stauderman, and M.D. Cahalan. 2005a. STIM1 is a Ca^{2+} sensor that activates CRAC channels and migrates from the Ca^{2+} store to the plasma membrane. *Nature.* 437:902-5.

Zhang, X., M. Zhang, A.M. Laties, and C.H. Mitchell. 2005b. Stimulation of P2X7 receptors elevates Ca^{2+} and kills retinal ganglion cells. *Invest Ophthalmol Vis Sci.* 46:2183-91.

Zhu, M.X. 2005. Multiple roles of calmodulin and other Ca^{2+} -binding proteins in the functional regulation of TRP channels. *Pflügers Arch.* 451:105-15.

Acknowledgements

I would like to thank Dr. Tejvir Khurana for the opportunity to work in his laboratory, the training I received and for his great support and encouragement through all the years especially to pursue the doctorate degree.

I am also grateful to all the members of the Khurana- and Rubinstein labs who were part of our group throughout my stay for their scientific advice, help, and training and for being great colleagues and friends and lastly simply for a lot of fun times making these years a wonderful experience.

I also would like to thank Dr. Claire Mitchell to collaborate with us and to provide equipment and expertise in calcium imaging and for always having an open ear to discuss data helping to move on with the project.

I am further indebted to Prof. Brinkmeier for taking me on as a grad student giving me the opportunity to obtain my doctorate from the University of Greifswald. I am very grateful for his always available advice and help and for the opportunity to use his laboratory resources to carry out experiments as part of this thesis. In this regard I would also like to thank the members of his laboratory, especially Dr. Christiane Kunert-Keil and Ms. Dietlind Schulz, for their expertise, guidance and help.

Many thanks and appreciation also goes to my parents for their endless patience and support.

Finally, I am deeply grateful to Matias for his patience and help, especially for his scientific advice on my work and efforts on proof-reading the manuscript.